Multivariate Effects of Brain Micro-environmental Constituents on Amyloid Proteins

Inaugural dissertation

zur
Erlangung der Würde eines Doktors der Philosophie
vorgelegt der
Philosophisch-Naturwissenschaftlichen Fakultät
der Universität Basel

von

Hongzhi Wang

Basel, Schweiz, 2022

Genehmigt von der Philosophisch-Naturwissenschaftlichen Fakultät
auf Antrag von

Dr. Jinghui Luo
Prof. Dr. Jan Pieter Abrahams
Prof. Dr. Roderick Lim
Prof. Dr. Raffaele Mezzenga

Basel, 19. Oktober 2021

Prof. Dr. Marcel Mayor

Contents

Chapter 1

General introduction

1.1 Amyloid proteins and protein misfolding diseases

Aberrant folding of proteins has been linked to a cluster of disorders called **protein misfolding diseases**, among which neurodegenerative diseases and type II diabetes (T2D) are included (1, 2). Neurodegenerative diseases predominantly affect neurons in central nervous system (CNS) or peripheral nervous system (3, 4), leading to the progressive loss of structures and functions of neurons (5). Besides aging (6), other factors like genetic mutation and environmental pollution contribute to the initiation and progression of neurodegenerative disorders. The disorders are pathologically manifested by the abnormal deposition of amyloid proteins in cells, tissues or organs (7). Amyloid proteins are a group of proteins that can convert stepwise from normally soluble monomers into toxic aggregates (8, 9). The general aggregation of amyloid proteins usually proceeds via the typical lag-, elongation-, and plateau- phases, in which the secondary structure transition and hydrophobic interactions are involved (10, 11). These aggregates of amyloid proteins are associated with disease development. For instance, amyloid oligomers are toxic due to their ability to permeabilize cellular membranes and cause cellular dysfunctions like mitochondrial dysfunction (12-14). Among 30 different types of amyloid related diseases that can be classified into localized and systemic forms (15, 16), **Alzheimer's Disease (AD)** is the most prevalent one that approximately takes up 65% of Dementia (17), followed by **Parkinson's Disease (PD)**. Other less common ones include amyotrophic lateral sclerosis (ALS), Huntington's Disease (HD), T2D, and Transmissible Spongiform Encephalopathies (TSEs), etc. (18). AD is pathogenically manifested by extracellular Aβ senile plaques (19) and intracellular tau neurofibrillary tangles (20) that result from the abnormal aggregation of the amyloid beta (Aβ) peptides and the tau protein, respectively. In spite of the extracellular Aβ

deposits, the intracellular accumulation of Aβ (21) contributes to the development of AD and down-regulates various normal functions including autophagy and apoptosis (22, 23). The major hallmark of PD is the intracellular Lewy bodies formed mainly by the α-synuclein (α-Syn) protein, an intrinsically unfolded protein participating in neurotransmitter release from presynaptic terminals (24). In addition to the roles in the diseases mentioned above, amyloid proteins, like Aβ, display normal physiological functions, for instance in neuronal survival (25), depending on microscopic environmental conditions. Therefore, the homeostasis of amyloid proteins should be tightly regulated (26). Amyloid proteins interact with a variety of cellular constituents, which affect their aggregation behaviors and normal functions. In this thesis, I investigate the multivariate effect of different cellular constituents or micro-environmental conditions on the properties of amyloid proteins. These covariate effects make the interpretation of experimental data closer to the reality in study field of amyloid proteins.

1.2 Effects of micro-environmental factors on amyloid proteins

ApoE protein and Heat-shock proteins (Hsps) participate in the regulation of lipids (27, 28) and the refolding, degradation, or aggregation of misfoled proteins, respectively, while the pH values, ionic strength, and the homeostasis of metal ions in AD and other neurodegenerative diseases are altered (11, 29). Thus, the properties of amyloid proteins involved in various kinds of misfolding diseases can be modulated by a variety of micro-environmental factors like proteins, pH, ionic strength (salt), metal ions, and lipid membranes and so on (11, 29).

1.2.1 Proteins: ApoE protein, amyloid proteins, and chaperone protein Hsp90

Apolipoprotein E (ApoE) proteins are synthesized and secreted mainly by liver cells, macrophages, astrocytes, and microglia in peripheral and central nervous systems (30-32). The three common polymorphic isoforms of ApoE are ApoE4, ApoE3, and ApoE2, which are expressed by three alleles (ϵ4, ϵ3, and ϵ2), respectively (33). ApoE plays pivotal roles in the transportation and metabolism of lipids (27, 28) as well as in other physiological functions (34-44), by regulating the binding of lipoproteins to ApoE receptors including low density lipoprotein receptors (LDLR), heparin sulfate proteoglycans (HSPGs), and LDL-receptor related proteins (LRP) (45). The LDLR-binding site and the lipid-binding site of ApoE locate at its N- and C-terminal domains, respectively.

These three ApoE isoforms differ from each other at residues 112 and 158 (ApoE2: 112Cys/158Cys, ApoE3: 112Cys/158Arg, ApoE4: 112Arg/158Arg) (45). This Cys/Arg exchange in sequences of three isoforms influences the interaction between the N- and C-terminal domains of ApoE, resulting in profound differences in the structures and functions (45, 46). As a result, ApoE4, ApoE3, and ApoE2 are involved in disorders including some amyloid-related diseases such as AD (47), Transmissible spongiform encephalopathies (TSEs) (48), and T2D (49). Not only ApoE can influence the properties of amyloid proteins including transactive response DNA-binding protein 43 (TDP-43), Aβ, tau, α-Syn, prion, Islet amyloid polypeptide (IAPP), superoxide dismutase 1 (SOD1) and others, amyloid proteins can affect ApoE as well. In addition, one type of amyloid protein can also interact with other types of amyloids. Thus, a specific amyloid protein can be synergistically affected by ApoE and other amyloid proteins. For details about the cross interactions between ApoE and amyloid proteins and the intercommunications among amyloid proteins, as well as their involvements in amyloid-related diseases, please refer to **Chapter 2** .

Chaperone proteins play essential roles in various cellular processes (50-59) including the folding and conformation maintenance of nascent proteins under physiological conditions, protecting mature proteins against cellular stresses, and disaggregating amyloid protein aggregates. Heat shock protein 90 (Hsp90) is a common chaperone protein (60) that usually locates intracellularly (61, 62), but it can also be secreted outside cells (63). The ATP-binding site and the client protein-binding site of Hsp90 locate within the N-terminal and middle domains, respectively, while the C-terminal domain is for the dimerization (60). Hsp90 proteins usually function synergistically with a variety of partner proteins and Adenosine triphosphate (ATP) (53, 64). It has been reported that Hsp90 inhibits the aggregation of Aβ peptide (65), however, the mechanism remains to be illuminated. In this thesis, I investigated the covariate effect of Hsp90 protein and ATP on the fibrillation of Aβ_{40} peptides, which provides us with a possible mechanism of how Hsp90 protein and its variants modulate Aβ fibrillation, for details, please refer to **Chapter 3** .

1.2.2 pH, Ionic strength, and Metal ions

The dyshomeostases of pH, ionic strength, and metal ions were observed in neurodegenerative diseases like AD and PD. In AD brains, the pH ranges from 6.3 to 6.8 (66), while the pH in the healthy subjects varies from 7.1 to 7.3 (67). The low pH in AD may be associated with the inflammatory processes. In addition, changes in pH values can influence the aggregation behavior of Aβ peptides. For instance, decreasing pH values from 7 reduces the fibrillation rate of Aβ_{42}, while pH 7-9 does not significantly affect

this fibrillation rate (68). Meanwhile, pH 6 strongly stabilizes the fibrillary assembly of Aβ (69). This suggests that pH values influence both the aggregation process and the stability of end-point aggregates of Aβ peptides. The ionic strength in AD changes as well. An increased ionic strength of sodium or chloride ions in AD has been reported (70). Like pH, changes in ionic strength can also influence the fibrillation of Aβ peptides. Increased ionic strength can not only promote Aβ_{40} fibrillation, but also modulate the morphology and structure of Aβ_{40} aggregates, very likely via the electrostatic interactions [16], leading to more heterogeneous fibrils. Metal ions possess various physiological functions under normal conditions, however, the disturbance of metal homeostasis is involved in the development of many neurodegenerative diseases like AD and PD. Varied levels of metals like copper and zinc were observed in these diseases, but without consensus on whether the levels of metals are elevated or decreased (71-80). Zn^{2+} ions bind to the H13/H14 residues within the N-terminus of Aβ peptides (81, 82). At neutral pH, Zn^{2+} ions have been reported to protect Aβ from the damage of reactive oxygen species (ROS) by competing with Cu^{2+} for the H13/H14 residues (83-85). However, at low pH values, Cu^{2+} retains its specific binding sites involving all the three histidines (H6/H13/H14) of Aβ peptide and Zn^{2+} seems lack its specificity for H13/H14 binding (83-85). In AD, Zn^{2+} ions enriched in amyloid plaques, reaching a concentration of 1 mM (86). Under near-physiological conditions (pH 7.2-7.4), substoichiometric amounts of Zn^{2+} ions can both retard (87) and promote (88) Aβ_{40} aggregation by binding to Aβ peptides. The difference in the experimental conditions may contribute to this inconsistency. Notably, copper levels in PD brain, expecially in the substantia nigra (SN) are decreased (75-78). Cu^{2+} ions can interact with both lipid membranes and amyloid proteins, thus play important roles in neurodegnerative diseases (89, 90). Cu^{2+} ions can induce α-Syn aggregation (91-94) and catalyze protein oxidation, leading to subsequent denaturation (95).

1.2.3 Lipids

As mentioned above, ApoE proteins participate in the transport and metabolism of lipids, and both amyloid proteins and metal ions can interact with lipid membranes. Thus, lipids play crucial roles in neurodegenerative diseases. Lipid membranes and Aβ peptides influence each other. On the one hand, lipid membranes promote the production and oligomerization of Aβ peptides, on the other hand, lipid membranes cluster aberrantly in the presence of Aβ oligomers (96, 97). Intracellular chaperones can modulate intracellular Aβ metabolism and toxicity in vivo (98). Heat shock proteins like Hsp90, can be released from intracellular space, in response to the variations in the raft-lipid composition or cell membranes (99, 100). Upon binding to lipid vesicles,

the 95-residue N-terminus of α-Syn converts from random coil to α-helix (101), acting as the membrane anchor, while the central domain sensors the properties of lipids and determines the affinity of α-Syn membrane binding, the disordered C-terminal region, however, associates with lipid membranes weakly (102). Interactions between α-Syn and lipid membranes affect the properties of both α-Syn and membranes (101, 103-106).

1.3 Aim and scope of the thesis

It has been intensively investigated how one binding factor or protein interacts with amyloid protein. As discussed above, Aβ and other amyloid proteins can be structurally and functionally influenced by multiple micro-environmental factors simultaneously *in vivo* including proteins, pH, ionic strength, metal ions, and lipid membranes. In this thesis, a number of biophysical methods have been implemented for studying the multivariate effects of AD or PD related brain constitutes on amyloid interaction and aggregation. In **chapter 2**, I summerized which amyloid proteins interact with ApoE protein and how multiple factors influence their interactions. As a Hsp90 conformational trigger, ATP was selected to understand how ATP influences the inhibitory effect of Hsp90 on Aβ. By using crystallization robotics, a 96-condition buffer matrix was created with varied pH, salt, and Zn^{2+} ions. In combination with the global fitting analysis, it allowed me to further understand the multivariate effects of these important brain constitutes on aggregation at microscopic level. In the end, I implemented small angle X-ray scattering and NMR to study how PD associated metal ions and lipids take covariate effects on α-Syn at atomic and mesoscopic levels. Briefly, my PhD work reveals that mutiple binding factors play a vital role in the secondary structure, assembly and functions of amyloid proteins, as these factors may synergistically modulate amyloid proteins *in vivo*. The multivariate effects of these brain consititutes on amyloid proteins have been investigated in detail by using a varity of biophysical and biochemical techniques at different atomic, molecule and mesocopic scales. Thereby, investigating the multivariate effects of these brain constituents on amyloids systematically will provide comprehensive knowledge for the understanding of the molecular pathogenesis in neurodegenerative diseases.

This thesis work can be split into several parts as described below. (1) I review how and where ApoE protein intercommunicates with various amyloid proteins in **Chapter 2**. (2) I investigated how Hsp90 and ATP modulate the fibrillation of Aβ_{40} peptides in **Chapter 3**. (3) I studied the covariant effect of pH, Zn^{2+} ions, and ionic strength on the fibrillation kinetics of Aβ_{40} peptides and the morphology of Aβ_{40} aggregates in **Chapter 4**. (4) I explored the covariant effects of copper ions and lipid membranes

on α-Syn protein in **Chapter 5**. These chapters have either been published, are under review, or are being submitted for publication in the near future.

1.4 References

1. F. U. Hartl, Protein Misfolding Diseases. Annu Rev Biochem 86, 21-26 (2017).
2. F. Chiti, C. M. Dobson, Protein Misfolding, Amyloid Formation, and Human Disease: A Summary of Progress Over the Last Decade. Annu Rev Biochem 86, 27-68 (2017).
3. S. C. Shin, J. Robinson-Papp, Amyloid neuropathies. Mt Sinai J Med 79, 733-748 (2012).
4. J. Haan, R. A. Roos, Amyloid in central nervous system disease. Clinical neurology and neurosurgery 92, 305-310 (1990).
5. S. Przedborski, M. Vila, V. Jackson-Lewis, Neurodegeneration: what is it and where are we? J Clin Invest 111, 3-10 (2003).
6. T. Wyss-Coray, Ageing, neurodegeneration and brain rejuvenation. Nature 539, 180-186 (2016).
7. A. Dogan, Amyloidosis: Insights from Proteomics. Annual Review of Pathology: Mechanisms of Disease 12, 277-304 (2017).
8. M. Fandrich, On the structural definition of amyloid fibrils and other polypeptide aggregates. Cellular and molecular life sciences : CMLS 64, 2066-2078 (2007).
9. M. R. Nilsson, Techniques to study amyloid fibril formation in vitro. Methods 34, 151-160 (2004).
10. P. R. Bharadwaj, A. K. Dubey, C. L. Masters, R. N. Martins, I. G. Macreadie, Abeta aggregation and possible implications in Alzheimer's disease pathogenesis. Journal of cellular and molecular medicine 13, 412-421 (2009).
11. M. C. Owen et al., Effects of in vivo conditions on amyloid aggregation. Chemical Society reviews 48, 3946-3996 (2019).
12. D. C. Bode, M. D. Baker, J. H. Viles, Ion Channel Formation by Amyloid-β42 Oligomers but Not Amyloid-β40 in Cellular Membranes. J Biol Chem 292, 1404-1413 (2017).
13. A. Surguchev, A. Surguchov, Effect of α-synuclein on membrane permeability and synaptic transmission: a clue to neurodegeneration? J Neurochem 132, 619-621 (2015).
14. M. L. Choi, S. Gandhi, Crucial role of protein oligomerization in the pathogenesis of Alzheimer's and Parkinson's diseases. The FEBS journal 285, 3631-3644 (2018).
15. J. D. Sipe et al., Nomenclature 2014: Amyloid fibril proteins and clinical classification of the amyloidosis. Amyloid 21, 221-224 (2014).
16. B. P. C. Hazenberg, Amyloidosis: A Clinical Overview. Rheumatic Disease Clinics of North America 39, 323-345 (2013).

17. A. Burns, S. Iliffe, Alzheimer's disease. BMJ 338, b158 (2009).
18. B. N. Dugger, D. W. Dickson, Pathology of Neurodegenerative Diseases. Cold Spring Harb Perspect Biol 9, (2017).
19. D. J. Selkoe, Alzheimer's disease: genes, proteins, and therapy. Physiol Rev 81, 741-766 (2001).
20. T. C. Gamblin et al., Caspase cleavage of tau: linking amyloid and neurofibrillary tangles in Alzheimer's disease. Proc Natl Acad Sci U S A 100, 10032-10037 (2003).
21. F. M. LaFerla, K. N. Green, S. Oddo, Intracellular amyloid-beta in Alzheimer's disease. Nature reviews. Neuroscience 8, 499-509 (2007).
22. C. Ripoli et al., Intracellular accumulation of amyloid-β (Aβ) protein plays a major role in Aβ-induced alterations of glutamatergic synaptic transmission and plasticity. J Neurosci 34, 12893-12903 (2014).
23. M. Li, L. Chen, D. H. S. Lee, L.-C. Yu, Y. Zhang, The role of intracellular amyloid β in Alzheimer's disease. Progress in Neurobiology 83, 131-139 (2007).
24. J. Burre, The Synaptic Function of alpha-Synuclein. J Parkinsons Dis 5, 699-713 (2015).
25. H. A. Pearson, C. Peers, Physiological roles for amyloid beta peptides. J Physiol 575, 5-10 (2006).
26. G. F. Chen et al., Amyloid beta: structure, biology and structure-based therapeutic development. Acta pharmacologica Sinica 38, 1205-1235 (2017).
27. B. P. Nathan et al., Differential effects of apolipoproteins E3 and E4 on neuronal growth in vitro. Science 264, 850-852 (1994).
28. R. E. Pitas, Z. S. Ji, K. H. Weisgraber, R. W. Mahley, Role of apolipoprotein E in modulating neurite outgrowth: potential effect of intracellular apolipoprotein E. Biochemical Society transactions 26, 257-262 (1998).
29. Y. Goto, M. Adachi, H. Muta, M. So, Salt-induced formations of partially folded intermediates and amyloid fibrils suggests a common underlying mechanism. Biophys Rev 10, 493-502 (2018).
30. C. G. Fernandez, M. E. Hamby, M. L. McReynolds, W. J. Ray, The Role of APOE4 in Disrupting the Homeostatic Functions of Astrocytes and Microglia in Aging and Alzheimer's Disease. Front Aging Neurosci 11, 14 (2019).
31. G. S. Getz, C. A. Reardon, Apoprotein E as a lipid transport and signaling protein in the blood, liver, and artery wall. J Lipid Res 50 Suppl, S156-161 (2009).
32. Y. Huang, K. H. Weisgraber, L. Mucke, R. W. Mahley, Apolipoprotein E: diversity of cellular origins, structural and biophysical properties, and effects in Alzheimer's disease. J Mol Neurosci 23, 189-204 (2004).
33. J. Davignon, R. E. Gregg, C. F. Sing, Apolipoprotein E polymorphism and atherosclerosis. Arteriosclerosis 8, 1-21 (1988).
34. R. D. Bell et al., Apolipoprotein E controls cerebrovascular integrity via cyclophilin

A. Nature 485, 512-516 (2012).
35. K. Koizumi et al., Apoepsilon4 disrupts neurovascular regulation and undermines white matter integrity and cognitive function. Nature communications 9, 3816 (2018).
36. O. Levi, A. L. Jongen-Relo, J. Feldon, A. D. Roses, D. M. Michaelson, ApoE4 impairs hippocampal plasticity isoform-specifically and blocks the environmental stimulation of synaptogenesis and memory. Neurobiology of disease 13, 273-282 (2003).
37. Y. Tensaouti, E. P. Stephanz, T. S. Yu, S. G. Kernie, ApoE Regulates the Development of Adult Newborn Hippocampal Neurons. eNeuro 5, (2018).
38. M. Wozniak et al., Apolipoprotein E-ϵ4 protects against severe liver disease caused by hepatitis C. Hepatology (Baltimore, Md.) 36, 456-463 (2002).
39. P. E. Cramer et al., ApoE-directed therapeutics rapidly clear beta-amyloid and reverse deficits in AD mouse models. Science (New York, N.Y.) 335, 1503-1506 (2012).
40. J. M. Castellano et al., Human apoE isoforms differentially regulate brain amyloid-beta peptide clearance. Sci Transl Med 3, 89ra57 (2011).
41. P. B. Verghese et al., ApoE influences amyloid-beta (Abeta) clearance despite minimal apoE/Abeta association in physiological conditions. Proc Natl Acad Sci U S A 110, E1807-1816 (2013).
42. P. Eline Slagboom, N. van den Berg, J. Deelen, Phenome and genome based studies into human ageing and longevity: An overview. Biochimica et Biophysica Acta (BBA) - Molecular Basis of Disease 1864, 2742-2751 (2018).
43. J. Deelen et al., Genome-wide association meta-analysis of human longevity identifies a novel locus conferring survival beyond 90 years of age. Hum Mol Genet 23, 4420-4432 (2014).
44. J. Deelen et al., Genome-wide association study identifies a single major locus contributing to survival into old age; the APOE locus revisited. Aging Cell 10, 686-698 (2011).
45. M. C. Phillips, Apolipoprotein E isoforms and lipoprotein metabolism. IUBMB life 66, 616-623 (2014).
46. C. Frieden, H. Wang, C. M. W. Ho, A mechanism for lipid binding to apoE and the role of intrinsically disordered regions coupled to domain-domain interactions. Proc Natl Acad Sci U S A 114, 6292-6297 (2017).
47. H. C. Hunsberger, P. D. Pinky, W. Smith, V. Suppiramaniam, M. N. Reed, The role of APOE4 in Alzheimer's disease: strategies for future therapeutic interventions. Health Psychol Behav Med 3, NS20180203-NS20180203 (2019).
48. P. Amouyel, O. Vidal, J. M. Launay, J. L. Laplanche, The apolipoprotein E alleles as major susceptibility factors for Creutzfeldt-Jakob disease. The French Research Group on Epidemiology of Human Spongiform Encephalopathies. Lancet (London, England) 344, 1315-1318 (1994).
49. J. Guan et al., Histopathological correlations of islet amyloidosis with apolipoprotein

E polymorphisms in type 2 diabetic Chinese patients. Pancreas 42, 1129-1137 (2013).
50. K. A. Borkovich, F. W. Farrelly, D. B. Finkelstein, J. Taulien, S. Lindquist, hsp82 is an essential protein that is required in higher concentrations for growth of cells at higher temperatures. Molecular and cellular biology 9, 3919-3930 (1989).
51. P. Csermely, T. Schnaider, C. Soti, Z. Prohaszka, G. Nardai, The 90-kDa molecular chaperone family: structure, function, and clinical applications. A comprehensive review. Pharmacology & therapeutics 79, 129-168 (1998).
52. K. Richter, M. Haslbeck, J. Buchner, The heat shock response: life on the verge of death. Molecular cell 40, 253-266 (2010).
53. F. H. Schopf, M. M. Biebl, J. Buchner, The HSP90 chaperone machinery. Nature reviews. Molecular cell biology 18, 345-360 (2017).
54. R. Zhao et al., Navigating the chaperone network: an integrative map of physical and genetic interactions mediated by the hsp90 chaperone. Cell 120, 715-727 (2005).
55. G. E. Karagoz et al., Hsp90-Tau complex reveals molecular basis for specificity in chaperone action. Cell 156, 963-974 (2014).
56. A. J. McClellan et al., Diverse cellular functions of the Hsp90 molecular chaperone uncovered using systems approaches. Cell 131, 121-135 (2007).
57. D. Picard, Heat-shock protein 90, a chaperone for folding and regulation. Cellular and molecular life sciences : CMLS 59, 1640-1648 (2002).
58. W. B. Pratt, D. O. Toft, Steroid receptor interactions with heat shock protein and immunophilin chaperones. Endocrine reviews 18, 306-360 (1997).
59. K. Liberek, A. Lewandowska, S. Zietkiewicz, Chaperones in control of protein disaggregation. EMBO J 27, 328-335 (2008).
60. M. M. Ali et al., Crystal structure of an Hsp90-nucleotide-p23/Sba1 closed chaperone complex. Nature 440, 1013-1017 (2006).
61. W. K. Huh et al., Global analysis of protein localization in budding yeast. Nature 425, 686-691 (2003).
62. C. Didelot et al., Interaction of heat-shock protein 90 beta isoform (HSP90 beta) with cellular inhibitor of apoptosis 1 (c-IAP1) is required for cell differentiation. Cell death and differentiation 15, 859-866 (2008).
63. S. Suzuki, A. B. Kulkarni, Extracellular heat shock protein HSP90beta secreted by MG63 osteosarcoma cells inhibits activation of latent TGF-beta1. Biochemical and biophysical research communications 398, 525-531 (2010).
64. G. E. Karagöz, S. G. Rüdiger, Hsp90 interaction with clients. Trends in biochemical sciences 40, 117-125 (2015).
65. C. G. Evans, S. Wisen, J. E. Gestwicki, Heat shock proteins 70 and 90 inhibit early stages of amyloid beta-(1-42) aggregation in vitro. J Biol Chem 281, 33182-33191 (2006).

66. C. M. Yates, J. Butterworth, M. C. Tennant, A. Gordon, Enzyme activities in relation to pH and lactate in postmortem brain in Alzheimer-type and other dementias. J Neurochem 55, 1624-1630 (1990).
67. M. Chesler, Regulation and modulation of pH in the brain. Physiol Rev 83, 1183-1221 (2003).
68. A. Tiiman, J. Krishtal, P. Palumaa, V. Tõugu, In vitro fibrillization of Alzheimer's amyloid-β peptide (1-42). AIP Advances 5, 092401 (2015).
69. K. Brannstrom, T. Islam, L. Sandblad, A. Olofsson, The role of histidines in amyloid beta fibril assembly. FEBS Lett 591, 1167-1175 (2017).
70. V. M. Vitvitsky, S. K. Garg, R. F. Keep, R. L. Albin, R. Banerjee, Na+ and K+ ion imbalances in Alzheimer's disease. Biochim Biophys Acta 1822, 1671-1681 (2012).
71. I. Hozumi et al., Patterns of levels of biological metals in CSF differ among neurodegenerative diseases. J Neurol Sci 303, 95-99 (2011).
72. S. Ayton, D. I. Finkelstein, R. A. Cherny, A. I. Bush, P. A. Adlard, in Encyclopedia of Metalloproteins, R. H. Kretsinger, V. N. Uversky, E. A. Permyakov, Eds. (Springer New York, New York, NY, 2013), pp. 2433-2441.
73. R. Squitti et al., Meta-analysis of serum non-ceruloplasmin copper in Alzheimer's disease. J Alzheimers Dis 38, 809-822 (2014).
74. E. Y. Ilyechova et al., A low blood copper concentration is a co-morbidity burden factor in Parkinson's disease development. Neurosci Res 135, 54-62 (2018).
75. D. T. Dexter et al., Increased nigral iron content and alterations in other metal ions occurring in brain in Parkinson's disease. J Neurochem 52, 1830-1836 (1989).
76. K. M. Davies et al., Copper pathology in vulnerable brain regions in Parkinson's disease. Neurobiol Aging 35, 858-866 (2014).
77. S. Genoud et al., Subcellular compartmentalisation of copper, iron, manganese, and zinc in the Parkinson's disease brain. Metallomics 9, 1447-1455 (2017).
78. M. Scholefield et al., Widespread Decreases in Cerebral Copper Are Common to Parkinson's Disease Dementia and Alzheimer's Disease Dementia. Front Aging Neurosci 13, 641222 (2021).
79. P. A. Adlard, A. I. Bush, Metals and Alzheimer's disease. J Alzheimers Dis 10, 145-163 (2006).
80. M. A. Lovell, J. D. Robertson, W. J. Teesdale, J. L. Campbell, W. R. Markesbery, Copper, iron and zinc in Alzheimer's disease senile plaques. J Neurol Sci 158, 47-52 (1998).
81. S. A. Kozin, S. Zirah, S. Rebuffat, G. H. Hoa, P. Debey, Zinc binding to Alzheimer's Abeta(1-16) peptide results in stable soluble complex. Biochem Biophys Res Commun 285, 959-964 (2001).
82. N. T. Watt, I. J. Whitehouse, N. M. Hooper, The role of zinc in Alzheimer's disease. Int J Alzheimers Dis 2011, 971021 (2010).

83. C. A. Damante et al., Zn^{2+} 's ability to alter the distribution of Cu^{2+} among the available binding sites of Abeta(1-16)-polyethylenglycol-ylated peptide: implications in Alzheimer's disease. Inorg Chem 50, 5342-5350 (2011).
84. L. Ghalebani, A. Wahlstrom, J. Danielsson, S. K. Warmlander, A. Graslund, pH-dependence of the specific binding of Cu(II) and Zn(II) ions to the amyloid-beta peptide. Biochem Biophys Res Commun 421, 554-560 (2012).
85. S. Warmlander et al., Biophysical studies of the amyloid beta-peptide: interactions with metal ions and small molecules. Chembiochem 14, 1692-1704 (2013).
86. M. A. Lovell, J. D. Robertson, W. J. Teesdale, J. L. Campbell, W. R. Markesbery, Copper, iron and zinc in Alzheimer's disease senile plaques. Journal of the Neurological Sciences 158, 47-52 (1998).
87. A. Abelein, A. Graslund, J. Danielsson, Zinc as chaperone-mimicking agent for retardation of amyloid beta peptide fibril formation. Proc Natl Acad Sci U S A 112, 5407-5412 (2015).
88. A. I. Bush et al., Rapid induction of Alzheimer A beta amyloid formation by zinc. Science 265, 1464-1467 (1994).
89. E. Carboni, P. Lingor, Insights on the interaction of alpha-synuclein and metals in the pathophysiology of Parkinson's disease. Metallomics 7, 395-404 (2015).
90. G. Gromadzka, B. Tarnacka, A. Flaga, A. Adamczyk, Copper Dyshomeostasis in Neurodegenerative Diseases-Therapeutic Implications. Int J Mol Sci 21, (2020).
91. A. Caragounis et al., Zinc induces depletion and aggregation of endogenous TDP-43. Free radical biology & medicine 48, 1152-1161 (2010).
92. H. Xu, D. I. Finkelstein, P. A. Adlard, Interactions of metals and Apolipoprotein E in Alzheimer's disease. Frontiers in aging neuroscience 6, 121 (2014).
93. I. Singh et al., Low levels of copper disrupt brain amyloid-beta homeostasis by altering its production and clearance. Proceedings of the National Academy of Sciences of the United States of America 110, 14771-14776 (2013).
94. D. L. Sparks, B. G. Schreurs, Trace amounts of copper in water induce beta-amyloid plaques and learning deficits in a rabbit model of Alzheimer's disease. Proceedings of the National Academy of Sciences of the United States of America 100, 11065-11069 (2003).
95. A. I. Bush, Metals and neuroscience. Current opinion in chemical biology 4, 184-191 (2000).
96. J. V. Rushworth, N. M. Hooper, Lipid Rafts: Linking Alzheimer's Amyloid-β Production, Aggregation, and Toxicity at Neuronal Membranes. International journal of Alzheimer's disease 2011, 603052 (2010).
97. F. Tofoleanu, N.-V. Buchete, Alzheimer Aβ peptide interactions with lipid membranes: fibrils, oligomers and polymorphic amyloid channels. Prion 6, 339-345 (2012).
98. V. Fonte et al., Interaction of intracellular beta amyloid peptide with chaperone

proteins. Proc Natl Acad Sci U S A 99, 9439-9444 (2002).
99. S. K. Calderwood, S. S. Mambula, P. J. Gray, J. R. Theriault, Extracellular heat shock proteins in cell signaling. FEBS Letters 581, 3689-3694 (2007).
100. I. Horváth, G. Multhoff, A. Sonnleitner, L. Vígh, Membrane-associated stress proteins: more than simply chaperones. Biochimica et biophysica acta 1778, 1653-1664 (2008).
101. M. Kiechle, V. Grozdanov, K. M. Danzer, The Role of Lipids in the Initiation of alpha-Synuclein Misfolding. Front Cell Dev Biol 8, 562241 (2020).
102. G. Fusco et al., Direct observation of the three regions in alpha-synuclein that determine its membrane-bound behaviour. Nature communications 5, 3827 (2014).
103. C. Masaracchia et al., Membrane binding, internalization, and sorting of alpha-synuclein in the cell. Acta Neuropathol Commun 6, 79 (2018).
104. M. Pantusa et al., Alpha-synuclein and familial variants affect the chain order and the thermotropic phase behavior of anionic lipid vesicles. Biochim Biophys Acta 1864, 1206-1214 (2016).
105. C. Galvagnion, The Role of Lipids Interacting with alpha-Synuclein in the Pathogenesis of Parkinson's Disease. Journal of Parkinson's disease 7, 433-450 (2017).
106. C. Galvagnion et al., Lipid vesicles trigger alpha-synuclein aggregation by stimulating primary nucleation. Nature chemical biology 11, 229-234 (2015).

Chapter 2

Cross Interactions between Apolipoprotein E and Amyloid Proteins in Neurodegenerative and other Diseases

Hongzhi Wang[1], Rolf Antonie Loch[1], Alex Perálvarez Marín[2], Philipp Berger[1], Henrietta Nielsen[4], Angeliki Chroni[3], Jinghui Luo[1]*

1. Department of Biology and Chemistry, Paul Scherrer Institute, 5232 Villigen, Switzerland

2. Biophysics Unit, Department of Biochemistry and Molecular Biology, School of Medicine, Universitat Autònoma de Barcelona, 08193 Cerdanyola del Vallés, Catalonia, Spain

3. Institute of Biosciences and Applications, National Center for Scientific Research 'Demokritos', 15341 Athens, Greece

4. Department of Biochemistry and Biophysics, Stockholm University, Svante Arrhenius Väg 16B, 10691, Stockholm, Sweden

Corresponding author: Jinghui.luo@psi.ch;

Submitted to Molecular Neurodegeneration

2.1 Abstract

Three common Apolipoprotein E isoforms, ApoE2, ApoE3, and ApoE4, are key regulators of lipid homeostasis. They differ by one or two residues at positions 112 and 158, and possess distinct structural conformations and functions, leading to isoform-specific roles in neurodegenerative diseases. Over 20 different amyloid proteins share similar characteristics of structure and toxicity, suggesting a common interactome in neurodegenerative diseases and other amyloidoses. The physical molecular and genetic interactions of ApoE with amyloid proteins are extensive in neurodegenerative diseases, but have not yet been well connected and clarified. Here we summarize essential features of the interactome of ApoE with different amyloid proteins. Perhaps more importantly, this review outlines what we can learn from the interactome of ApoE and amyloids, that is the need to see both ApoE and amyloid proteins as a basis to understand the neurodegenerative diseases.

Keywords: ApoE; amyloid proteins; interaction; endogenous molecules; cytotoxicity; therapeutics

2.2 Background

Amyloidosis is often pathologicallymanifested by the abnormal deposition of amyloid proteins in cells, tissue or organs, of which the shapes and normal function would be affected (1). Amyloid proteins are a class of protein with the ability to convert stepwise from normally soluble monomers into more toxic oligomers and then into insoluble, less toxic beta-sheet fibrils (2, 3), which relate to disease development. Amyloid oligomers are presumed to elicit pore formation in cellular membranes and then cause cellular dysfunctions (4, 5). Besides, the oligomers can trigger various other toxic pathways, like mitochondrial dysfunction, synaptic dysregulation and oxidative stress (6). On the other hand, the disease-related amyloid protein like Aβ (7) can, sometimes, display protective functions, depending on the microscopic environmental conditions and their location, duration and intensity. This means that amyloid proteins can be both protective and damaging, and therefore amyloid homeostasis requires tight regulation (8) which involves production, post-translational maintenance, aggregation, degradation and clearance (9). There are around 30 different types of amyloidosis, which can be classified into localized and systemic forms (10, 11), including various peripheral (12) and central (13) variations of these disorders.

Apolipoprotein E (ApoE) protein is a component of chylomicron remnants and very low density lipoprotein (VLDL) in plasma (14) and a major risk factor for some amyloid-related diseases, including Alzheimer's disease (AD) (15), Transmissible spongiform encephalopathies (TSEs) (16), and type 2 diabetes (T2D) (17). ApoE is a main component of lipoproteins in plasma and the predominant apolipoprotein in the central nervous system (CNS) (14, 18). Peripheral and central nervous system ApoE are synthesized and secreted mainly by liver cells and macrophages, and by astrocytes and microglia, respectively (19-21). It plays a crucial role in the transportation and metabolism of lipids (22, 23), cerebrovascular integrity and cerebral blood flow (24, 25), synaptogenesis (26), hippocampal neurogenesis (27), innate immunity (28), and amyloid clearance (29-31), and longevity (32-34). ApoE mediates the binding of lipoproteins to ApoE receptors (35). The ApoE receptors include heparin sulfate proteoglycans (HSPGs), low density lipoprotein receptors (LDLR), and LDL-receptor related proteins (LRP), with the latter two belonging to the LDLR family (35). ApoE is polymorphic with three common isoforms (ApoE4, ApoE3, and ApoE2) expressed by three alleles (ϵ4, ϵ3, and ϵ2) (36). Allels ϵ4, ϵ3, and ϵ2 represent in the human population about 14%, 78%, and 8%, respectively (36), and show a geographical variation (37). ApoEϵ4 is considered to be the ancestral allele, and the evolution of this allele to other alleles is diet-adaptive and infection susceptibility-related in varied environmental and lifestyle conditions (38-40).

Within ApoE, an LDLR-binding site locates at the N-terminal domain, connected by the hinge to the C-terminal domain with a lipid-binding site. The three common ApoE isoforms differ from each other at only two residues: 112 and 158 (ApoE2: 112Cys/158Cys, ApoE3: 112Cys/158Arg, ApoE4: 112Arg/158Arg) (35). The single Cys/Arg interchange at sites 112 and 158 influences two domains interaction in ApoE, presumably achieved by hydrogen-bonds and salt-bridges (35). This results in profound differences in structure and function (35), and consequently affects the disease risks in carriers.

ApoE3 is linked to 'normal' plasma lipid levels because of its high efficiency in promoting the clearance of triglyceride (TG)-rich lipoproteins (41). However, ApoE2 is disabled in the clearance of TG-rich lipoprotein remnant particles due to its impaired ability to bind to the LDL receptor (41). In a study including subjects with either APOEϵ3/ϵ3 or APOEϵ4/ϵ4 genotypes, plasma triglycerides were found to be associated with an ApoE isoform-dependent distribution of monomers, homodimers and heterodimers, which is different between AD patients and controls (42). In the same study, ApoE dimers were only observed in the APOEϵ3-carriers and was associated with total plasma ApoE levels (42). The 112Arg substitution in ApoE4 modulates the inter-domain interaction, which can increase the affinity of ApoE4 with lipids and ApoE receptors (43, 44). ApoE4 is less stable and more susceptible to proteolysis. This proteolysis can lead to the degradation

of ApoE4 into small neurotoxic segments, which may eventually interfere with the normal functions of ApoE4 (45-47). A body of evidence has demonstrated that compared with ApoE3 and ApoE2, ApoE4 and its proteolytic, neurotoxic C-terminal truncated fragments are more associated with dysfunctions. A study conducted with transgenic mice expressing ApoE3 or ApoE4 in neurons or astrocytes showed that the C-termianl-truncated fragments of neuro-specific ApoE4 are related to increased tau phosphorylation (45), and another study performed with Neuro-2a cells expressing ApoE4 with C- or N-termianl truncations or mutations indicated that the receptor-binding region (amino acides 135-150) and the lipid-binding region (amino acids 241-272) of ApoE4 act together to induce mitochondrial dysfunction and neurotoxicity (48). In ApoE4-knock in mice, ApoE4 causes age- and Tau-dependent impairment of hilar interneurons, resulting in learning and memory deficits (49). In SK-N-SH cells, a specific fragment of lipid-free ApoE4, ApoE4[Δ(166-299)], promote cellular uptake and accumulation of Aβ42 (50) and ApoE4[Δ(186-299)] fragment influences inflammatory molecule levels (51), while carboxyl-terminal-truncated ApoE4 forms affect BACE1 levels and Aβ production (52). Compared to ApoE2 and ApoE3, ApoE4 more efficiently induces APP transcription and amyloid-beta (Aβ) production (53), facilitates Aβfibrillation (54)interferes with cleaning up Aβ [53], and utilizes lipid binding (55, 56). Therefore, ApoE4 is considered 'worse' or less protective than ApoE2 and ApoE3 for patients at the risk of neurodegenerative diseases, like Alzheimer's Disease due to their ApoE genotype. A complexity, sometimes even contradiction, exists in the functions of ApoE, since contrary to the popular assumption that ApoE4 protein is always detrimental as compared to ApoE3 protein, there are nevertheless also positive effects related to the ϵ4 allele (57, 58). There may be benefits arising from its direct antimicrobial activity, the indirect link to inflammation, the differential binding to receptors or amyloid proteins (59, 60). Both ApoE2 and ApoE4 are linked to various kinds of disorders and neurodegenerative diseases, for instance, the involvement of ApoE2 in primary tauopathies such as progressive supranuclear palsy (PSP) and corticobasal degeneration (CBD) (61) and ApoE4 ine AD, PD and T2D (14, 18, 35).

Amyloid and ApoE proteins possess intrinsically disordered regions. These disordered regions control structural motions and interactions of these proteins with lipid membranes. Besides, amyloid and ApoE proteins interact to each other and constitute two main risk factors for amyloidoses. These connections between amyloid and ApoE proteins are predominantly associated with amyloid deposition, with ApoE protein being able to directly modulate the structure and nucleation of amyloid proteins. The function and toxicity of ApoE and amyloid proteins like Aβ and Tau can be also influenced by their interactions in amyloidoses (62-64). Though there are many amyloid based

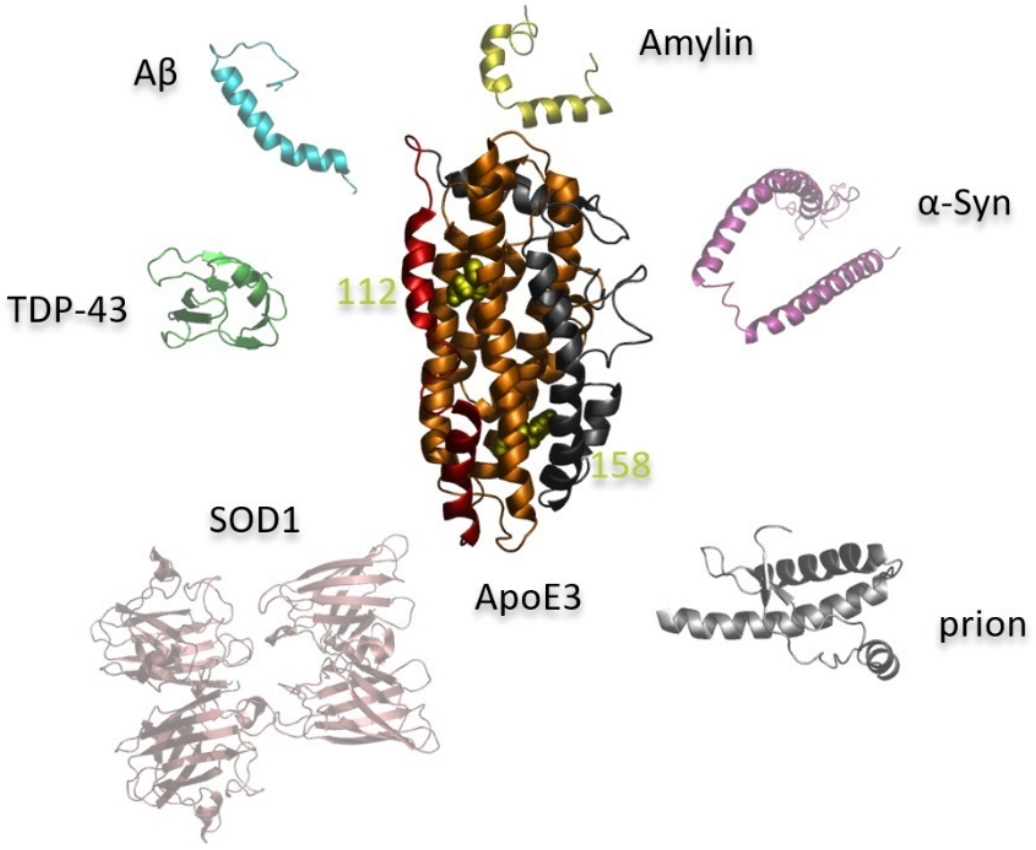

FIGURE 1: Schematic illustration of structures of ApoE (pdb ID: 2L7b) and Amyloid proteins (pdb ID: 1BA4 (Aβ), 1QLX (prion protein), 3ECU (superoxide dismutase 1(SOD1)), 1XQ8 (α-syn protein), 2L86 (Islet amyloid polypeptide precursor (IAPP)), 5X4F (TAR DNA binding protein 43 (TDP-43))). As shown in spheres, residues 112 and 158 distinguish the ApoE isoforms. ApoE2 has Cys112 and Cys158 residues, ApoE3 has Cys112 and Arg158 residues, and ApoE4 has Arg112 and Arg158 residues. The N-termial domain (orange) and C-terminal domain (gray) of apoE are connected by a hinge domain (red ribbon). Amyloid forming proteins have been reported to interact with ApoE proteins. Reciprocally, ApoE isoforms influence amyloid associated diseases. The ApoE isoforms and amyloid proteins involved will be discussed in details in section 2.3.

approaches (65) that could respectively treat AD, no effective therapy has been established.

Both ApoE and amyloid proteins play important roles in amyloidoses. However, the physical molecular and/or genetic cross-interactions between ApoE and various amyloids have not been clearly elucidated. Therefore, it might be of great benefit to enhance the understanding of the cross-interactions between ApoE and different kinds of amyloid proteins, which is the main focus of this review paper. Here, we will discuss how ApoE interferes with the generation, aggregation, and clearance of amyloid proteins, and how amyloids affect the intracellular fate of ApoE as well as where they meet.

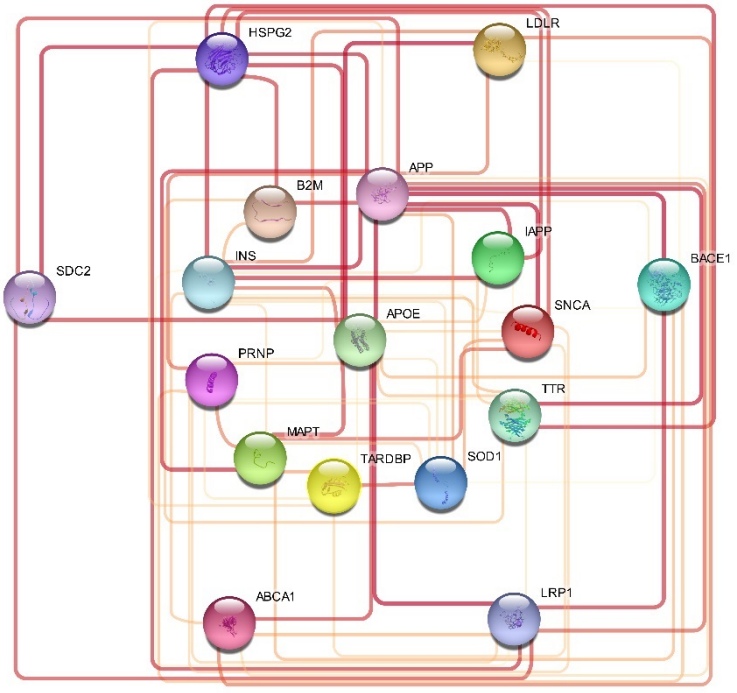

FIGURE 2: Interaction network of ApoE and amyloid proteins. This interaction network is obtained with Cytoscape software via String protein query by setting genes including APP, IAPP, SNCA, TTR, SOD1, TARDBP, MAPT, PRNP, INS, B2M, APOE, HSPG, LDLR, LRP1, ABCA1, and BACE1 as the query list. The query settings are: Species: Human; Confidence cutoff: 0.4; Maximum additional interactors: 0. The intial network was filtered by a node degree range from 2 to 20. The result shows not only the interactions between ApoE and amyloid proteins, but also the interplays between amyloid proteins. The colors (from the lightest to darkest) of edges correspond to the confidence scores (from 0.4 to 1) of interactions. For details on how they interact each other, please refer to Section 2.3.

2.3 Cross-interactions of ApoE with amyloid proteins

The schematic illustration of the structures of ApoE and some mentioned amyloid proteins is shown in **Fig.1**. In this section we discuss specifically the physical molecular and/or genetic interactions of ApoE with various amyloid proteins that have been mostly studied, including Aβ, tau, alpha-synuclein (α-Syn), prion, Islet amyloid polypeptide (IAPP), superoxide dismutase 1 (SOD1), transactive response DNA-binding protein 43 (TDP-43) and a few others. The network of these interactions is shown in **Fig.2**.

2.3.1 Interactions between ApoE and Alzheimer's disease-associated amyloid-beta peptide

Aβ_{42} and Aβ_{40} are the most abundant components of the amyloid plaques manifested in the brains of patients with AD, the most common form of dementia (66, 67), and

cerebral amyloid angiopathy (CAA) where Aβ42 and Aβ40 accumulate and deposit on the wall of cerebral vessels. It has been shown that more than 80% of autopsy-confirmed AD cases have some degree of CAA (68, 69). It is generally accepted that the formation of Aβ oligomers and aggregates (plaques) is an integrated part of AD pathophysiology (8, 70, 71). These plaques mainly appear as relatively neutral 'diffuse' plaques and disrupting 'neuritic' plaques that mostly have a fibrillary or dense-cored morphology (72, 73). Furthermore, multiple studies (74, 75) have shown that total amyloid-plaque load does not correlate well with cognitive impairment, which might be due to the difference in initial inflammatory responses between different case groups, especially the response induced by activated glial cells (76, 77).

The inheritance of ApoEϵ4 is related to late-onset familial and sporadic AD (78, 79), and ApoEϵ4 increases the risk of developing CAA and AD, while ApoEϵ2 lowers the risk of frontotemporal dementia (FTD) in a very small cohort (80). ApoEϵ2 appears as protective factor against AD and Lewy bodies (DLB) (81, 82). Recent study indicated that, among six genotypes of three alleles, ApoE2/2 is related to a low odds ratios of Alzheimer's dementia in comparison to other genotypes, particularly with an remarkably lower odds ratio than ApoE4/4 (83). Additionally, an ApoE3 Christchurch homozygote was reported to resist autosomal major Alzheimer's disease (84). With ApoEϵ4 as a main genetic risk factor for AD, the cross-interaction between ApoE and Aβ is expected to have a major contribution to the progression of CAA and AD.

ApoE is one of many proteins that can interact with Aβ, and the interaction of ApoE with Aβ can affect various stages of Aβ homeostasis as discussed below. However, the binding strength/affinity of ApoE/Aβ complexes varies depending on many factors (85-88) such as the isoforms, lipidation state, oxidation or concentration of ApoE and the length, concentration, morphology or source (native or synthetic) of Aβ, as well as the local environmental conditions like receptor concentrations. For instance, ApoE2, E3 or E4 preferably binds to higher β-sheet structure of Aβ peptides with a binding affinity of 20 nM (89), and lipid-free ApoE binds stronger to immobilized Aβ than lipidated ApoE does (in a nanomolar range, for detailed Kd data, please refer to Table S1 in Ref 98) (90). Dissimilarities in these stringent conditions, especially the extent of ApoE lipidation, can, to a large extent, explain the seemingly substantially contradictory results from in vitro and in vivo studies. This is because that different lipid-binding states can lead to considerable conformational differences of ApoE and that the presence of lipids can alter the binding properties of ApoE with other proteins, like Aβ (86). We will discuss how these factors affect the metabolism, aggregation, degradation or clearance of Aβ peptides.

The production of Aβ involves a series of sequential endoproteolytic cleavage by β- and γ-secretases (shown in Fig.3) of the transmembrane protein, amyloid precursor protein (APP), through an anti-trophic amyloidogenic pathway (8, 91-94). The influence of ApoE on Aβ production remains controversial and seems to be strongly dependent on the experimental conditions (69). Despite the fact that several studies (95) reported no apparent ApoE isoform-dependent effect on APP, one in vitro study conducted with rat neuroblastoma B103 cells transfected with human wild-type APP695 (B103-APP) (96) proposed that lipid-poor ApoE4 enhances higher Aβ production from APP compared with lipid-poor ApoE3, which was mediated through the LRP pathway. In another in vitro study using ES-cell-derived human neurons (53), ApoE triggers a non-canonical MAP kinase cascade by differentially (ApoE4 >ApoE3 >ApoE2) binding to ApoE receptors, leading to the enhancement of APP transcription and Aβ synthesis in the same isoform-dependent manner. In addition, a recent study suggested that reconstituted ApoE isoforms increases BACE1 levels and promotes Aβ production and oligomerization in human neuroblastoma SK-NSH cells with distinct efficiency (ApoE4 $\geq$ ApoE3 >ApoE2) (52). The cleavage of APP by γ-secretase and then the production of the APP intra-cellular domain (AICD) in the CNS can attenuate the expression and function of LRP1 (97, 98). Reduce in LRP1 level leads to an increased ApoE that could further increase APP transcription as mentioned above, although reduced LRP1 also reduces the amyloidogenic processing of APP. Meanwhile, reduce in LRP1level can also decrease cholesterol level within the CNS, and result in the loss of neuronal membrane cholesterol that was also found to enhance the Aβ production, suggesting a feed-forward loop. Actually, in AD patients, the LRP1 levels are significantly reduced (99) and sometimes brain cholesterol likewise (100), particularly in amyloid plaques deposited areas, which is consistent with the aforementioned observations. This amyloidogenic pathway can also be initiated by the withdrawal of trophic support, inflammation or some medical drugs like statins (93, 101) that lower cholesterol. The combined results can explain to a certain degree the relationship between APP, ApoE, and AD (97).

As for the effect of ApoE on Aβ aggregation (102), it has been reported that substoichiometric concentrations of ApoE dramatically inhibits Aβ fibril growth via binding to and stabilizing oligomers, and higher concentrations of ApoE can also bind to and stabilize Aβ fibrils (102). In addition, ApoE4 is the most efficient in influencing the fibrillation of Aβ40 while the ApoE3 and ApoE2 function less efficiently (102, 103). Besides, ApoE3 binds preferentially to Aβ42 oligomers, leading to the inhibition of the Aβ42-induced neurotoxicity, which has been shown to be ApoE-isoform dependent (104-106). This isoform-dependent effect of ApoE might arise from the differential binding affinities of the ApoE isoforms to different aggregation intermediates (86) or from the altered lipidation states of ApoE in the brain, which can be regulated by ATP binding cassette

transporter A1 (ABCA1) (86). Thus, the destructive role of ApoE4 in AD could be partly due to stabilization of the soluble cytotoxic oligomeric intermediates, as well as the insoluble fibrils.

In addition to the effect of ApoE, especially ApoE4, on the kinetics of Aβ oligomerization or/and fibrillization process and subsequently on AD pathogenesis (107), the role of Aβ on ApoE4 oligomerization, aggregation as well as neurotoxicity has recently been investigated. When co-incubated in human neuroblastoma SK-N-SH cells, Aβ42 increases the formation of SDS-stable ApoE4 oligomers and the cytotoxicity of ApoE4 (108). These data highlight that ApoE4 could be pathogenic due to its capacity of oligomer assembling that are augmented by Aβ42 and lead to increased neurotoxicity.

ApoE can also affect the degradation and clearance processes of Aβ, which can be influenced by the lipidation state of ApoE as well (86, 109). The promoting effect of ApoE on the cellular degradation of Aβ has been reported by in vitro studies (110, 111), and the impaired degradation may subsequently deteriorate further clearance, or the other way around. There are several mechanisms underlying the clearance of Aβ from the brain, among which the receptor-mediated clearance via microglia/astrocytes or through the blood-brain barrier (BBB), and the clearance through the interstitial fluid (ISF) drainage play the dominant roles (112). The effect of ApoE on Aβ clearance can be affected by the direct binding of ApoE to Aβ or by the indirect competition, since evidences indicate that different Aβ levels can be transported across the BBB in an ApoE-isoform and -lipidation state dependent manner (113-115), as well as by the size and composition of Aβ aggregates and cell species. It was shown in vitro that astrocytes preferably take up oligomeric Aβ over fibrillar Aβ (116), while microglia more efficiently take up fibrilar Aβ compared with astrocytes (117). Furthermore, ApoE and ApoJ alter the uptake in microglia and astrocytes, and appear to behave differently in rodents than in human cells (117). ApoE receptor-mediated clearance of Aβ generally occurs in microglia and astrocytes,where soluble Aβ can bind directly to LRP1 of astrocytes in competition with ApoE isoforms (31, 112). The clearance of Aβ from ISF into the blood can befacilitated by p-glycoprotein (Pgp) and LPR1 expressed by the vascular endothelial cells (118). However, ApoE4, compared with ApoE2 and ApoE3, shows a relatively low affinity for LRP1 and is therefore less efficient in promoting Aβ excretion through the BBB (118). This is consistent with the observation that ApoE2, ApoE3, Aβ /ApoE2 and Aβ/ApoE3 complexes were cleared at the BBB via both LRP1 and VLDLR (very low density lipoprotein receptors) at a faster rate than Aβ/ApoE4 complexes that was cleared mainly via VLDLR (113). In addition, lipidation greatly slows down the clearance of all the ApoE isoforms and ApoE/Aβ complexes at the BBB (113). ApoE4-containing lipoproteins are less lipidated than ApoE3 (85), which might

lead to the less stable ApoE4/Aβ complexes, resulting in reduced ApoE4/Aβ levels, decreased clearance, and increased accumulation of Aβ, especially in oligomeric form. An additional degree of complication in the interaction of ApoE/Aβ and LRP1 is that the significantly reduced LRP1 levels in the vascular endothelial cells and pericytes of AD patients is related to a noticeable decrease in the ApoE-dependent removal of soluble Aβ (118). This is consistent with the above-mentioned observation that the formation of Aβ is accompanied by the APP processing product, the APP intracellular domain that suppresses the expression of LRP1. Alternatively, it has been proposed that the presence of ApoE4 reduces, while ApoE3 enhances, the efficiency of perivascular clearance of Aβ (119). This is because that the attachment of ApoE4/Aβ complexes to the arterial basement membranes is weaker than that ApoE3/Aβ complexes (119). In addition, the attachment of ApoE/Aβ complexes to the arterial basement membranes again strongly depends on the type of Aβ and the ApoE lipidation status (85, 120), and may result from the strong destabilization of the salt bridge network of ApoE4 by Aβ. Thus, compared with ApoE2 and ApoE3, ApoE4 correlates with higher Aβ levels in cerebrospinal fluid (CSF) and cerebral vasculature, acting as a biomarker in the preclinical phase of AD (102, 114, 121, 122).

Despite the fact that the ApoE/Aβ interaction has been investigated in vitro (119, 123), the direct physical interaction between ApoE and soluble Aβ under physiological conditions has been shown to be minimal. Rather the uptake and subsequent degradation of Aβ in astrocytes are blocked by ApoE isoforms that compete for the same cellular receptors, transporters, and/or cellular/membrane surfaces, especially the LRP1-dependent cellular uptake pathway in astrocytes (31). Thus, the role of ApoE in the clearance of Aβ from CNS is highly complex and remains yet to be resolved. However, this controversy has not prevented the use of ApoE-derived peptides, ApoE/Aβ antibodies, and ApoE antisense oligonucletodies (ASO) as therapeutic agents for AD treatment (124-131).

2.3.2 Interactions between ApoE and Alzheimer's disease-associated tau

Tau is mainly a neuronal protein existing in axons, and can be modified by phosphorylation, the state of which will in turn influence the distribution of tau, since, tau tends to be phosphorylated in the cytosol while dephosphorylated in the distal region of the axon (133). Furthermore, the phosphorylation state differs according to development stages and healthy states. The extent of phosphorylation is higher in fetal neurons and decreases during development period, while increases hugely in pathological situations (tauopathies), which may be related to the normal and abnormal functions of tau (134). Under physiology conditions, tau binds to microtubules, as well as lipid membranes, to

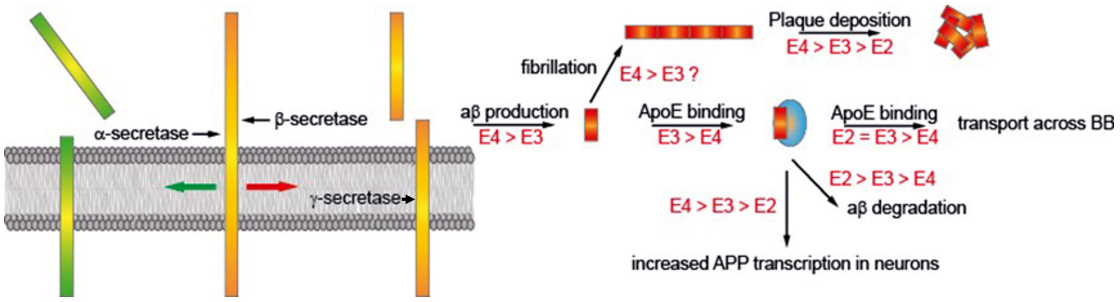

FIGURE 3: Roles of ApoE isoforms in the processing of APP and Aβ regulation (132): APP is initially cleaved by α-secretase in the extracellular part near the plasma membrane to generate a soluble protein and a membrane standing part. Metalloprotease of the ADAM family (e.g. ADAM10) possess α-secretase activity. This pathway is also known as beneficial pathway. APP can also be cleaved by β-secretase and γ-secretase leading to Aβ and soluble intra- and extracellular proteins (amyloidogenic pathway). β-secretase is an aspartic acid protease (also known as BACE1). γ-secretase is an integral membrane protein composed of PSEN1 (presenilin-1), nicastrin, APH-1 (anterior pharynx-defective 1), and PEN-2 (presenilin enhancer 2). The influence of ApoE isoforms in further processing of Aβ is shown on the right side (see text for details).

maintain the normal shape and function of neurons, however, under pathological conditions, tau phosphorylation increases, leading to the reduced affinity for microtubules and then cytoskeleton destabilization, particularly in neurons. The detached, hyperphosphorylated tau then undergoes self-aggregation, forming oligomers and various higher ordered aggregates, which are involved in AD and some other tauopathies (133, 135). In fact, AD patients usually have high levels of CSF tau (136) and more hyperphosphorylated brain tau (137) Besides, mild cognitive impairment (MCI) patients who are ApoE4 carriers also have high levels of CSF tau and bear elevated risk for AD (138). However, CSF ApoE levels do not show a consistent association with AD and MCI among different studies, although CSF ApoE levels might be more closely correlated with tau, phosphorylated tau, and Aβ42 in AD and MCI patients than plasma ApoE levels (139-141). In addition, it has been reported that ApoE4 significantly aggravated tau-mediated neurodegeneration in a tauopathy mouse model (142). Recent cellular studies showed that the treatment of P301S tau-expressing neurons with recombinant ApoE results in some neuronal damage and death compared to the non-ApoE treated cells, with ApoE4 inducing the most prominent effect (142). In an earlier study, a C-terminal truncated ApoE form, the ApoE4 [Δ(272–299)] in neurons, was found to induce the intracellular NFT-like inclusions via interacting with neuronal phosphorylated tau as well as phosphorylated neurofilaments (143), leading to mitochondrial dysfunction and a 35% greater cell death than full-length ApoE4 (144). These studies indicate the role of ApoE in influencing tau pathogenesis, in which ApoE-induced neuroinflammation may be involved.

As a major genetic risk factor for AD, ApoE exerts isoform-specific effect on the hyperphosphorylation of tau and the neuronal cytoskeleton. ApoE3 binds in vitro stably to the microtubule-binding repeat region of tau, thus stabilizing it and inhibiting the formation of paired helical filaments (PHF) (145). This interaction can be inhibited by the phosphorylation of tau (146), suggesting that ApoE3 may protect tau by perturbing the hyperphosphorylation in vivo (145, 147-149). In contrast to the protective role of ApoE3, ApoE4 shows a reduced binding to Tau, and may have a loss of protective function by stimulating tau phosphorylation (150-152) in a neuron-specific way (45, 153), resulting in increased and unbound Tau in CSF (45, 150), which is consistent with the observation in AD and MCI patients as mentioned above.

ApoE regulates tau phosphorylation partly due to the modulation of the activities of tau phosphatases and kinases. It has been reported that ApoE dephosphorylates tau by enhancing the activity of protein phosphatases 2A/2B (PP2A/2B) (154). This effect is more pronounced in ApoE3 or ApoE2, since ApoE4 enhances tau phosphorylation by promoting the activation of zinc-induced extracellular signal-regulated kinase (Erk) in neurons (152), while there is also a reduction in PP2A activity by ApoE4 compared with ApoE3 via epigenetic mechanisms (155). Another study suggested that ApoE controls tau phosphorylation by the assembly of the ApoE receptor/disabled-1/glycogen synthase kinase-3β (RAD) complex, which in turn suppresses the kinase activity (156). Furthermore, ApoE-deficient mice have hyperphosphorylated tau in the brain compared to wild-type controls, and show repair impairments after closed head injury related to transient hyperphosphorylation (157). Interestingly, some researchers even argued that only at the high concentration (2 μM), ApoE reduced the levels of tau kinases and then the levels of tau phosphorylation in primary neurons (158). This concentration dependency of ApoE on tau illustrates that there can be significant differences in ApoE-tau interactions under in vivo and in vitro conditions which have to be taken into account.

Except from the effect of ApoE on tau, tau also influences the intracellular fate of ApoE in an ApoE isoform-specific manner, when transiently express tau and LDLR in mammalian cells, ApoE can be taken up from the CSF, but only ApoE3, not ApoE4, reaches the cytoplasm (64). Another study showed that especially non-lipidated ApoE2 could form a complex with tau in-vitro (61). In addition, increased ApoE4 lipidation by the intraperitoneal injection of an ABCA1 agonist, CS-6253, decreased tau hyperphosphorylation and reduced cognitive dificits in ApoE4-TR mice (159). This highlights the isoform- and lipidation-dependent cross talk between ApoE and tau.

In summary, the phosphorylation state of tau plays crucial roles under both physiological and pathological conditions. ApoE influences the phosphorylation state of tau in an

isoform-specific way, with ApoE3 binding stably to tau while ApoE4 binding less efficiently. This results in the inhibitory effect of ApoE3 and promoting effect of ApoE4 on tau phosphorylation, influencing the cytoskeleton stability and the formation of NFTs in AD.

2.3.3 Interactions between ApoE and Parkinson's disease-related α-Syn

α-Syn is a neuronal protein in the brain, meanwhile, it can also be generated in the intestine and transported through the vagus nerve to the brain. Located primarily in the pre-synapses, α-Syn functions in the neurotransmitter release by interacting with lipid rafts, and this interaction may be enhanced by the high curvature of synaptic vesicles and the property of α-Syn to promote and sense membrane curvature (160). Except from the role on the maintenance of synaptic vesicles, α-Syn may also function as a lipid acceptor, since it shares biophysical similarities with other lipid-carrying proteins (161-164). α-Syn is an intrincally disordered protein (165, 166) that is prone to aggregate into intracellular inclusions (167). Mutations within the α-Syn gene (SNCA) has been linked to Parkinson's disease (PD) (168), one kind of α-synucleinopathies (169) characterized by Lewy bodies (LB) (170). Besides, high α-Syn levels have also been observed in 50%of AD patients (171).

Even though ApoE4 exacerbated α-Syn pathology in recent studies (172, 173), the role of ApoE on PD pathogenesis seems contradictory. A study among 3465 cases and controls revealed no significant association between ApoE alleles and PD (174), and another study even reported that ApoE ϵ4 carriers among non-Hispanic Caucasians may have lower PD risk (175). Besides, the level of ApoE in CSF increase in the early PD patients, and α-Syn was observed to colocalize with ApoE on lipoprotein particles (176). An agreement has not yet been reached on whether a combined genotype for ApoE4 and α-Syn (SNCA) polymorphism (NACP-Rep) plays an important role in the susceptibility to PD (177, 178). However, ApoE ϵ4 frequency is higher in both PD patients with dementia (PDD) and pure dementia with Lewy bodies (DLB) than that in healthy controls (179, 180), and among PD patients, ApoE4 frequency is higher in familial PD than that in sporadic PD (181). ApoE4 is also associated with earlier age of onset of PD . It is therefore most likely that ApoE ϵ4 carriers are more possible to develop PD and might have an earlier age of the disease onset, meanwhile, PD patients carrying ApoE ϵ4 might have a greater risk to develop dementia, in comparison to non-ApoE4-carriers. Besides, the ApoE ϵ2 allele frequency in PD patients is also higher than that in controls (182), and thus ApoE ϵ2 allele can also be a risk factor for developing PD (183, 184), because of its disturbance of the ApoE homeostasis and then the subsequent dysfunction of the protein.

As mentioned above, α-Syn acts as a lipid binding acceptor, thus, the effect of ApoE on PD might be achieved by the cross talks between α-Syn, ApoE, lipoproteins, and lipid, which mutually influence both lipid (especially cholesterol) metabolism and α-Syn properties such as the aggregation propensity and uptake (185-187). These cross talks heavily depend on several other factors like the lipidation state of ApoE as well. It has also been reported that α-Syn potently stimulates cholesterol efflux (188) and a higher level of plasma cholesterol is related to a lower risk of PD (189-191). In both incidental LB disease (iLBD) and symptomatic stages of PD, the up-regulation of ApoE and LRP1 in the melanized neurons of the substantia nigra (SN) is associated with alterations in lipoprotein homeostasis, presumably as an early event in the process of PD development (192). An in vitro study showed that ApoE influences the aggregation of α-Syn in a concentration dependent way (193): at the concentration of 15 nM, the three ApoE isoforms promote the aggregation of α-Syn with ApoE4 showing the strongest efficacy, while at the higher concentrations (>15 nM), the isoforms suppress the aggregation of α-Syn. This study suggests that the concentration and isoforms of ApoE significantly influence the kinetics of α-Syn and thus ApoE might be both protective and toxic. Furthermore, ApoE reduces α-Syn uptake through cell surface HSPGs in an isoform-dependent way, and this process can be further modulated by ApoE post-translational modification and/or lipidation (194, 195). A molecular link (196) between α-Syn, ApoE and Aβ has also been revealed in a study with transgenic mice expressing either wild type or mutant α-Syn, where the increased ApoE is injurious, leading to α-Syn-induced neurodegeneration, as well as the elevated accumulation of insoluble mouse Aβ. This study indicates a common pathogenic mechanism of ApoE in various neurodegenerative diseases, including AD and PD. Through the cross interaction between ApoE, α-syn, and lipids (especially cholesterol), ApoE therefore influences the uptake and aggregation of α-Syn as well as the lipid metabolism, which might lead to the neurodegeneration of PD, suggesting that the cross talk between ApoE, α-syn, and lipids plays crucial roles in PD pathology.

2.3.4 Interactions between ApoE and TSE-related prion

The aggregation of the pathological isoform of the prion protein (PrP) in the CNS is the main hallmark of a group of neurodegenerative disorders termed Transmissible spongiform encephalopathies (TSEs), including Creutzfeldt–Jakob disease (CJD) (197). Aβ42 was observed in most of the sporadic Creutzfeldt-Jakob disease (sCJD) cases, while ApoE further increases in these sCJD cases (198) and ApoE co-occurs and co-deposits with PrP in TSE infected brains (199, 200). Furthermore, ApoE was co-purified with PrP identified by proteomic analysis (197, 201-203). Biophysical and biochemical studies

revealed that the recombinant PrP protein interacts with both recombinant ApoE and native ApoE from hamster liver tissue in vitro (204) and that the ApoE-PrP interaction has been mapped to the N-terminus of both proteins, namely, the residues 1-194 of ApoE and the residues 23-90 of PrP (204). Aβ42 and ApoE were identified in the majority of the sCJD, (198) and ϵ4 allele is a risk factor for CJD, while ϵ2 delays the occurrence of death (16), but the different distributions of ApoEϵ4 and ϵ2 genotypes among CJD subtypes has not been observed (205). However, a meta-analysis showed no significant evidence between ApoE2 and CJD, although the ApoE 3/4 and ApoE 4/4 genotypes are risk factors for CJD, and ApoE 3/3 genotype is prone to protect against CJD (206, 207). The synergistic age-dependent interaction in AD and sCJD has been observed between ApoE and prion protein gene (PRNP) (208). A recent study (205) suggested that AD/primary age-related tauopathy (AD/PART) and CJD pathology may occur in the same brain. Still, ApoE correlates only to Aβ pathology and does not influence the age of onset and subtypes of CJD, indicating that the synergistic mechanisms of AD and CJD remain to be better understood. The findings of the aforementioned studies suggest that ApoE4 mainly plays a predominant role in TSEs, but with few conflicting results (16, 79, 207).

2.3.5 Interactions between ApoE and T2D-associated IAPP

IAPP is cleaved from the pro-islet amyloid polypeptide (proIAPP) and co-secreted with insulin from the pancreatic β-cells. IAPP, on the one hand, plays various roles physiologically (209-212), on the other hand, it can transform from soluble, functional states into highly organized amyloid deposits, which contribute to the death of pancreatic β-cells and thus act as one of the most important hallmarks of type 2 diabetes (T2D) (213, 214).

In addition to the aforementioned cross interactions between Aβ, tau, α-Syn, or prion and ApoE, the association of ApoE with IAPP also exists. In particular, the colocalization of ApoE and IAPP suggests that ApoE plays an important role in the development of multiple amyloid deposits (215). However, it remains contradictory whether the role is protective, toxic or a loss of the protection.

ApoE was found not to be crucial for the IAPP amyloid fibrillaton in both the ApoE knockout (KO) mouse and a transgenic mouse model of T2D (209, 216), unlike the case in AD. A clinical study with T2D patients from China indicated that ApoE ϵ4 enhances islet amyloidosis (17), while another study conducted among Caucasian patients argued that the distributions of ApoE ϵ2, ϵ3 and ϵ4 are similar in both T2D and non-diabetic groups and thus ApoE genotype does not relate to the severity of the disease (217).

It is still not clear if two distinct results are caused by the geographical difference. Nonetheless, it has been shown in human samples and AD mouse models that ApoE4 attenuates the IAPP assisted release of Aβ40, from the AD brain into blood (218), suggesting the risk factor of IAPP and ApoE4 interaction in AD. However, one has to be careful when interpreting the data obtained from mouse models on how they applicable to humans, because not all mammals naturally form IAPP aggregates (at least mice or rats do not) (209).

The effect of ApoE on T2D may be achieved by modulating IAPP aggregation in a concentration dependent manner, and together with IAPP, ApoE and the incompletely processed proIAPP promotes the fibrillation of IAPP and coexists with the amyloid (209). The fibrillation of IAPP can be inhibited at a low concentration of ApoE4 but promoted at a high concentration of ApoE4, implying that ApoE4 may prevent IAPP aggregation by efficiently binding and sequestering IAPP under physiological conditions, however, the enhanced binding affinity between ApoE4 and IAPP in T2D results in the critical accumulation of IAPP and subsequent islet amyloid formation (219). This can be found in the case of the interaction between ApoE and Aβ that ApoE efficiently binds and sequesters Aβ in normal brains, subsequently preventing Aβ aggregation, while the impaired ApoE/Aβ binding in AD leads to the critical accumulation of Aβ, thus facilitating plaque formation (220). This similarity between the two interactions can result from the similar biophysical and physiological properties as well as cytotoxic mechanisms shared by IAPP and Aβ (221, 222). Like the interaction between ApoE and Aβ, the interaction between ApoE and IAPP partially depends on the state of ApoE (concentration and lipidation) (89). These studies suggest again that the cross interactions of ApoE and amyloid proteins presumably rely on specific conditions. Besides, cholesterol homeostasis is strongly related to ApoE, and recent studies suggest that gangliosides and cholesterol affect hIAPP-membrane interaction and the uptake and clearance of hIAPP (223-225), which might imply the role of ApoE in IAPP clearance.

2.3.6 Potential interactions between ApoE and ALS-related SOD1

SOD1 is an important antioxidant enzyme thatcaninternalize the superoxide (O^{2-}) (226) into relatively nontoxic molecules. There are three known forms of SOD in human. Mutations in a gene encoding copper, zinc superoxide dismutase 1 (Cu, Zn-SOD1) are associated with amyotrophic lateral sclerosis (ALS) (227, 228). ALS is a common motor neuron disease, and mutations in SOD1 gene present in 2%–6% of all ALS patients (227, 228). In addition, ApoE is also involved in ALS, however, the consensus about the role of ApoE in ALS has not been reached among various related studies.

In a familial ALS-linked transgenic mice, ApoE expression is strongly upregulated by SOD1 (G93A-SOD1) mutation in the spinal cord of end-stage disease mice. This up-regulation is closely linked to the time and spatial distribution of both the axonal and neuronal degeneration, as well as the glial activation and the activation of genes in the mitochondrial destruction (229, 230). This is consistent with other studies in which ApoEϵ4 allele is associated with earlier onset (231, 232) and reduced life span (233, 234). This means that ApoE4 is more toxic or less protective in ALS. In agreement with it, ApoEϵ2 has been reported to delay the onset for 3 years compared to that of non-ApoEϵ2 carriers (235). However, a meta-analysis concluded that there is a lack of association between ApoE and ALS (236). A recent study argued that ApoEϵ2 allele can significantly promote the risk of FTD in ALS patients from Italy (237). The inconsistence of the effect of ApoE in ALS presumably caused by the different sample sizes, experimental conditions, and/or geographic areas.

2.3.7 Interactions between ApoE and TDP-43

TDP-43 is an 414–amino acid RNA-binding protein involved in several cellular processes (238-241). In addition, during cellular stress, TDP-43 enters into the cytoplasma as a component of insoluble aggregates with a ubiquitinated, hyper-phosphorylated and cleaved form of TDP-43 with a higher molecular mass at ˜45 kDa (242). The latter form is the major disease protein in some sporadic and familial ALS, most cases of frontotemporal dementia (FTLD-TDP) (242, 243). Besides, the cleaved form of TDP-43 has recently been observed in AD and some PD patients (244-246). Moreover, it was shown to be associated with memory loss and progressive hippocampal atrophy (247-250). Recently, a strong association was reported between ApoE4 and TDP-43 (247, 248, 251, 252). In particular, the ApoE4 isoform appears to affect synergetically with TDP-43 the cognitive impairment of AD patients. This effect of ApoE4 and TDP-43 is independent of Aβ, especially during the early phases of neurodegeneration, while normal cognition was strongly associated with the absence of TDP-43, even though subjects with and without TDP-43 had similar degrees of AD pathology (240, 250). TDP-43 was also found to be co-localized with tau, and both amyloids are present in a number of diseases (253).

Furthermore, abnormal levels of TDP-43 were observed in the majority of patients with AD, ALS, and FTLD, and there is a substantial increase (200%) in TDP-43 levels in cortical autopsies of late stage AD patients (254). It was suggested that overexpression of TDP-43 might be harmful and induce neurodegeneration, possibly with or without formation of insoluble protein aggregates, while the mutant TDP-43 (A315T, G348C and A382T) may cause disease via both loss-of-positive-function and gain-of-toxicity (240,

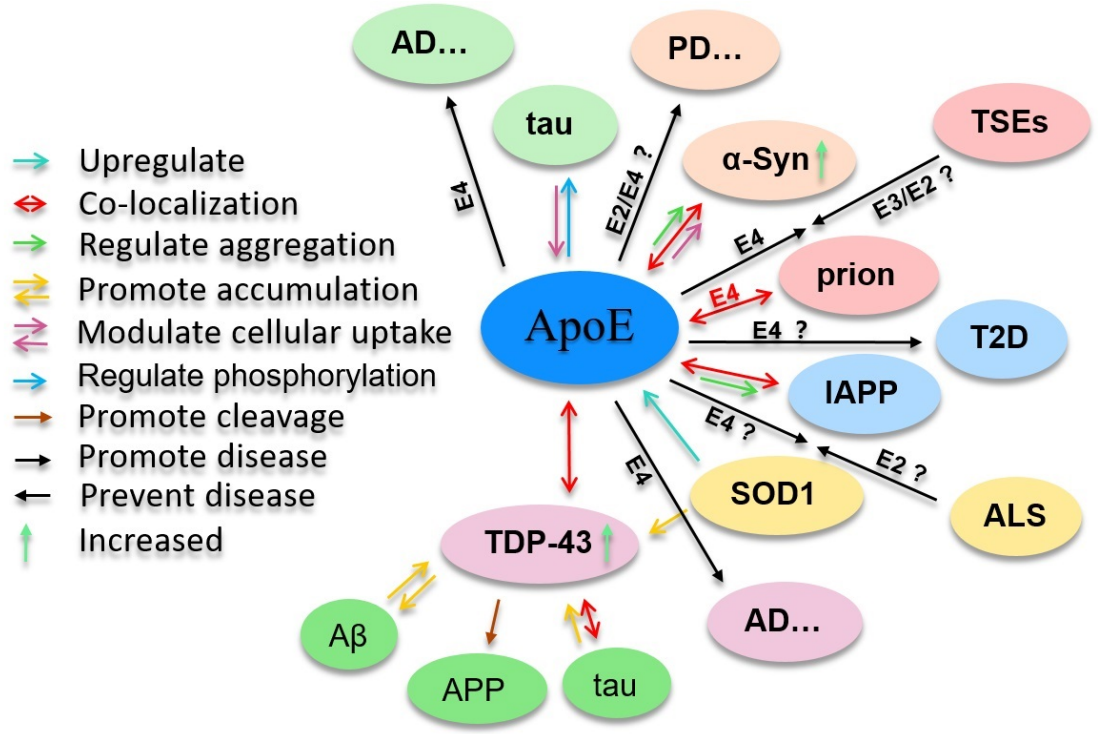

FIGURE 4: Interactions between ApoE and tau, α -Syn, prion, IAPP, SOD1, or TDP-43. For details, please refer to **sections 2.2 to 2.7**. The question marker means that even though most reachers agree but an agreement has not been reached in the whole field. One specific amyloid protein and the disease it involves in are shown in the same color.

255). The loss of functional TDP-43 may disrupt key nuclear functions, resulting in the loss of cellular homeostasis, transcriptional deregulation, disintegration of nuclear bodies, or aberrant messenger RNA splicing (239, 242). An overexpression of TDP-43 resulted in an increase of the amyloidogenic APP cleavage pathway via increased activity of the β-secretase (240) and consequently an increased intraneuronal Aβ accumulation, where expression of Aβ42 was associated with TDP-43 phosphorylation and accumulation in the cytosol (254). TDP-43 oligomers can cross-seed amyloid oligomers with Aβ (256).

There exists another link between TDP-43 and Aβ, and indirectly with ApoE4. The depletion, aggregation, as well as the disease-associated mutation of TDP-43 can disturb intracellular sorting and subsequent activity-dependent secretion of the neurotrophin brain-derived neurotrophic factor (BDNF) (257). ApoE4 subjects were found to have significantly lower serum BDNF levels (258), and the interruption of BDNF signaling in hippocampal neurons was found to rapidly activate the amyloidogenic pathway for Aβ production, cause neuronal apoptotic death (92). Moreover, the BDNF reduction contributes to lower cognitive performance in both AD apathetic patients and female ApoE4 carriers (259) and non-demented subjects (260).

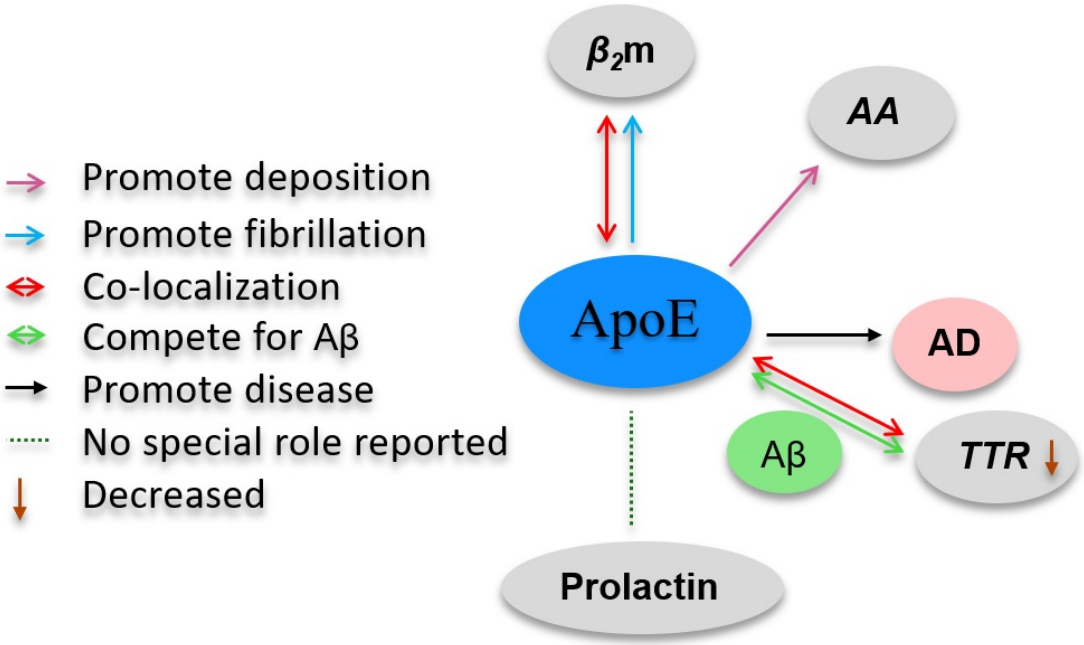

FIGURE 5: Interactions between ApoE and other amyloid proteins.

2.3.8 Interactions between ApoE and other amyloid proteins

In addition to the interactions with the aforementioned amyloid proteins, ApoE also interacts with other amyloids such as transthyretin (TTR), β2-microglobulin (β2m), Prolactin, and Amyloid A (AA), as described in **Fig.5**.

The co-localization of ApoE and TTR has been reported in the systemic organs except the liver and spleen of an aged male vervet monkey, especially the extracellular stroma among muscle fibers and external tunica of arterioles (261). Both ApoE and TTR are Aβ sequestering proteins. CSF TTR levels in AD decreased and even further in AD with an ApoEϵ4 allele. Reduce in CSF TTR levels leads to the decreased levels of CSF Aβ42 and increased levels of the senile plaque (SP) abundance in AD brain (262, 263). Due to the facts that ApoE induces the accumulation of Aβ and that TTR facilitates the transport of Aβ from the brain and prevents fibril formation (264, 265), ApoE and TTR may act competitively in the aggregation of Aβ and its deposition in the SP of AD brain. Regarding β2m, the co-precipitation of ApoE with β2m in amyloid depositions has also been reported (266). Furthermore, ApoE can enhance β2m fibrillogenesis process by stabilizing preformed seeds (267, 268), and then stabilize β2m fibrils (269) by inhibiting its depolymerization (270). In the AA amyloid tissue of an amyloid-induced mouse model, ApoE levels increase (271). Another study employing ApoE-deficient mice with or without injecting adenoviruses expressing the human ApoE3 gene showed that ApoE (ApoE3) promotes the deposition of AA (272).

2.4 Loci of cross interactions

Phase-Separated Droplets — Through phase separation, an emerging paradigm underlies intracellular processes, like amyloid protein aggregation in neurodegenerative diseases (273). Phase separation enhances the concentration of amyloid proteins and promote their self-assembly, typically in membrane-less organelles. Full-length tau proteins (tau441-GFP) were observed to form droplets in cultured neurons, with more rapid droplet formation in the presence of heparin and RNA, or under higher temperature or phosphorylation (274). The C-terminal domain of TDP-43 undergoes phase separation into droplets, with slower dynamics or faster aggregation in all disease mutants (275). A series of other amyloid proteins have been found to form droplet summarized in this review paper (276). Similar phase-separation droplets, lipid droplets (LDs), surrounded by a layer of lipids and proteins, act as inert cellular reservoirs and are associated with ApoE and neurodegenerative diseases (277). Phase-separated droplets or organelles apparently offer ideal mesoscopic locations for cross-interactions of ApoE with amyloid proteins, although how the interactions in the droplets take place remains to be investigated.

Lipid membranes — Playing a key role in lipid metabolism, ApoE binds and redistributes lipids, especially from astrocytes in the CNS to other types of cells, including neurons (44, 278). Likewise, most amyloid proteins experience conformational changes upon binding lipid membranes and self-propagate (279) through a lipid membrane-enriched environment such as membrane boundaries, cellular compartments and tissues (280). Lipid induced conformational changes of amyloid proteins, on the other hand, modulate amyloid protein aggregation and toxicity. The co-occurrence, accumulation and interaction of amyloid proteins and ApoE in/on lipid membranes or the membrane boundaries seem highly plausible at the microscopic level.

Cholesterol and lipidation — The disturbance of lipid related molecules and biological processes are deeply involved in neurodegenerative diseases, especially AD (281-283), we therefore take a step further to discuss the roles of cholesterol and lipid raft, the most common modulators for both amyloid and ApoE proteins. Cholesterol is an important constituent of the plasma membrane, as a molecular spacer, it can stabilize lipid rafts by occupying the space between raft proteins and other raft lipids (284, 285). There is an interplay between raft proteins and raft lipids. On one hand, the regulation of cholesterol homeostasis can lead to the dissociation, dysregulation, and/or inactivation of raft proteins. On the other hand, raft proteins including amyloids can influence cholesterol homeostasis. The cholesterol/amyloids interplay is enhanced in the most cholesterol-rich brain (286), and includes the interaction of cholesterol with tau (287-289), prion (290,

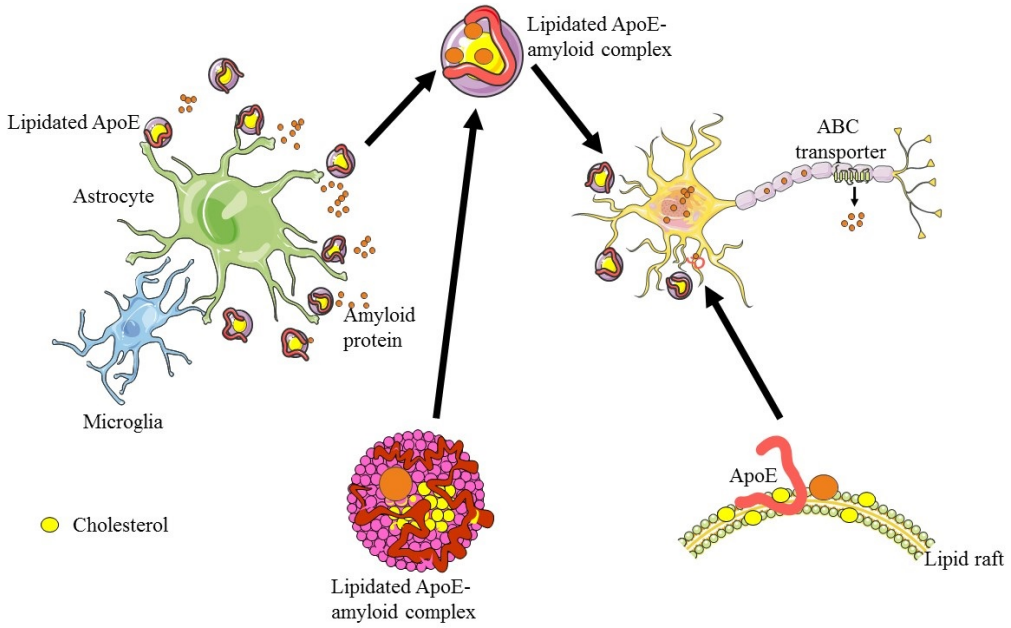

FIGURE 6: Secretion of lipidated ApoE by microglia and astrocytes and complex formation with extracellular and intracellular amyloid proteins.

291), Aβ and APP (55, 286, 292-295) and other amyloids. Interestingly, the amyloidogenic processing of APP takes place in lipid rafts while the non-amyloidogenic processing predominantly happens in the non-raft regions (286).

ApoE, together with other apolipoproteins, lipoprotein receptors, and lipid transporters, are important for the maintenance of cholesterol homeostasis in the brain (296). Generally, ApoE is lipidated, and lipid association can enhance the affinity of ApoE for the LDL receptors via the lipid binding-induced conformational changes (297). Lipidated ApoE is mostly produced by microglia and astrocytes show in **Fig.6**. It can bind to soluble Aβ in an isoform-dependent manner (ApoE2 >ApoE3 >ApoE4), facilitating Aβ degradation via receptor-mediated endocytosis in various brain cells or clearance via the BBB (286). In contrast to this differential binding affinity of lipidated ApoE for soluble Aβ, ApoE4 is less lipidated than E3 and E2. Furthermore, ApoE4 cannot efficiently protect neuronal cells by assisting liquid droplet formation in glia in response to elevated reactive oxygen species (ROS) (19, 298, 299). Together these factors indicate the intensive involvement of ApoE4 in AD and other amyloidosis. However, the effect of cholesterol on the Aβ processing pathway may be both harmful and favorable, probably due to the promotion effect of high cholesterol levels within lipid rafts on Aβ generation (harmful) as well as degradation or clearance (favorable) (286), suggesting the importance of maintaining lipid homeostasis.

As mentioned before, α-Syn potently stimulates cholesterol efflux in a dose- and time-dependent manner via ABCA1 transporter (188), which also regulates the lipidation

state of ApoE [85]. Tau pathology promotes the level of cellular unesterified cholesterol in neurons that is independent of apolipoprotein E deficiency. Synergically, a loss of cholesterol homeostasis may simulate tau pathology (287). Obviously, interactions between cholesterol, ApoE and amyloid proteins like Aβ (300) and tau (301) and α-Syn occur in various neurodegenerative disorders, and lipid rafts may provide an important site for this kind of interaction. However, if lipid raft is a specific mechanism on how manipulation of cholesterol levels modifies APP/Aβ and if cholesterol is a causal or non-causal factor for AD or both still remains uncertain (100), since cholesterol may be both deleterious when its homeostasis is perturbed and favorable when this homeostasis is perturbed. A study has reported that the transfer of cholesterol from the cytofacial leaflet to the exofacial leaflet, not the change in total cholesterol concentration, functions to promote APP and Aβ expressions (302). Besides, this transfer could disrupt membrane structure including lipid rafts and different kinds of cell functions including disruption in cholesterol homeostasis (302). This is consistent with the fact that both increasing age and the inheritance of the ApoE4 allele can lead to the doubling of cholesterol levels in the exofacial leaflet (302). On the other hand, cholesterol changes the lateral organization of lipid membranes with condensation effect and therefore induces the interaction of amyloid protein and ApoE protein in lipid draft or lipidated complex. These suggest that lipid related modulators, such as cholesterol, involve in the interactions between ApoE and amyloid proteins, perhaps occurred in lipid raft and lipidated complex.

A theoretical model may be applied to explain the interactions of ApoE and amyloid proteins in the presence of lipid. With a coupling assumption, amyloid aggregates are stabilized through intramoleculer and intermolecular interactions (303). Intramolecular interaction occurs among amyloid or ApoE protein, due to its disordered and flexible conformations. These conformational states can be contributed and interchanged by ordered alpha-helix/beta-sheet and disordered turn/coil structures (304). The conformational interchanges may allow to minimize the total free energy, but coupling to intermolecular assembly. Once amyloid protein interacts with ApoE, the conformational interchanges and intermolecular assembly spontaneously emerge to reach a lower total free energy than ApoE or amyloid protein alone. While, lipid-enriched environment converts the intramolecular conformations of ApoE and amyloid proteins with more ordered alpha-helix/beta-sheet structures and lower energy (305, 306). This may explain why amyloid protein interaction with ApoE happen and is prone to the lipid related loci mentioned above.

2.5 Conclusions

Collectively, all the studies described above suggest the important role of the interactions of ApoE with amyloid proteins in the pathogenesis of several neurodegenerative diseases. Therefore, the modulation of ApoE structure, expression, lipidation and function could be utilized for developing novel therapeutic approaches for degenerative diseases. More specifically, ApoE-based therapies are currently being investigated, mainly in the treatment for AD, with major focus on: a) the use of small molecule structural correctors that are able to convert the ApoE4 structure and function into those of ApoE3 (307-310), b) the overexpression of protective ApoE2, by adeno-associated virus delivery in brain (311-313) and the downregulation of ApoE4, by ApoE4 antisense oligonucletodies (129), c) the inhibition of the binding between ApoE and Aβ, by using antibodies against Aβ targeting the ApoE binding site or antibodies against ApoE targeting the Aβ binding site (124, 125, 130, 314-317), d) increase of ApoE lipidation via ABCA1 (318).

The discrepancies and concerns of in vitro studies, animal experiments, and clinical trials described in the previous sections, can be caused by the different experimental systems in which several or many variable factors, like ApoE, amyloids and many other molecules are involved. Furthermore, many studies ignore or fail to report specific parameters, such as the lipidation or glycation state of ApoE, which makes it more difficult to compare results and draw consistent conclusions. Combining all the studies we were not able to conclude what is the isoform-dependent optimal range of ApoE concentration and lipidation state. We discussed that the isoform-dependent lipidation state of ApoE affects the binding to cholesterol, which in turn differently affects the production, stabilization, degradation, clearance, binding and transport of different amyloids in various aggregation states (monomers, oligomers or fibrils). As the strongest genetic risk factor for AD, ApoE4 affects normal brain function before gross AD pathological changes in mice and humans as well (319). ApoE4 seems less stable and (its fragments) more toxic or less protective in comparison with ApoE2 or ApoE3. It is most likely that all ApoE isoforms are highly functional within homeostasis. The detrimental effects of ApoE can be subscribe to either the loss of protective function or gain of toxic effect. And this change in functions of ApoE will occur when changes in the concentration, morphology and/or modification levels of ApoE are too dramatic. Besides, it is probable that compared to ApoE3 and ApoE2, ApoE4 is more susceptible and shows a stronger negative response to an induced loss of homeostasis. This enhanced susceptibility of ApoE4 can be induced mainly by the difference in structures of ApoE isoforms.

There is an increasing awareness that neurodegenerative disorders including AD and PD are multifactorial diseases (320, 321) and an increasing interest in multimodal therapy (322). We therefore suggest that some of the aforementioned ApoE-based therapies

might be more successful when combined with other therapies and/or other known risk factors (e.g., lifestyles) that are most likely being ignored in monotherapies.

ApoE-based therapies for amyloidosis show great therapeutic potentials in this field, especially after the failure of therapies by targeting only amyloids. However, developing an ApoE-based therapy targeting only the pathology-related function is challenging. On the on hand, ApoE has various functions, on the other hand, ApoE is closely interweaved with amyloid proteins involved in various amyloidosis. Even though confronted with challenges, there are important points that can be taken into account when developing ApoE-based therapies. Firstly, try to understand as much as possible the exact normal functions and the roles in amyloidosis of ApoE, and to restore the balance of ApoE. Secondly, learn more about the cross-interactions between ApoE and amyloids and the stress conditions that ApoE are involved in, which is the main purpose of this review. Thirdly, recognize the discrepancies in the conditions of the *in vitro* and *in vivo* studies, as well as the differences between animal models and clinical trials, when interpreting the investigation results. Otherwise, the intended therapeutic effects may not be achieved and unintended negative consequences might occur. Besides, the change in the epigenetic modification of ApoE gene (323), the epigenetic effects of ApoE on a variety of genes (324, 325), and the connection between ApoE and the microbiome–gut–brain axis (326, 327) are strongly associated with neurodegenerative diseases, further investigation in these fields will absolutely benefit the therapies for amyloidosis.

2.6 Abbreviations

ApoE: Apolipoprotein E protein; AD: Alzheimer's disease; PD: Parkinson's disease; TSEs: Transmissible spongiform encephalopathies; T2D: type 2 diabetes; ALS: Amyotrophic lateral sclerosis; CNS: Central nervous system; HSPGs: heparin sulfate proteoglycans; LDLR: Low density lipoprotein receptors; LRP: LDL-receptor related proteins; TG: triglyceride; NFT: neurofibrillary tangles; Aβ: amyloid-beta; IAPP: Islet amyloid polypeptide precursor; SOD1: superoxide dismutase 1; α-Syn: alpha-synuclein; TDP-43: DNA-binding protein 43; CAA: cerebral amyloid angiopathy; FTD: frontotemporal dementia; DLB: dementia with Lewy bodies; APP: amyloid precursor protein; AICD: APP intra-cellular domain; ABCA1: ATP binding cassette transporter A1; BBB: blood-brain barrier; ISF: interstitial fluid; Pgp: p-glycoprotein; VLDLR: very low density lipoprotein receptors; ASO: antisense oligonucletodies; BACE1: β-secretase; PSEN1: presenilin-1; APH-1: anterior pharynx-defective 1; PEN-2: presenilin enhancer 2; MCI: mild cognitive impairment; PHF: paired helical filaments; PP2A/2B: protein phosphatases 2A/2B; Erk: extracellular signal-regulated kinase; RAD: receptor/disabled-1/glycogen

synthase kinase-3β; LB: Lewy bodies; PDD: PD patients with dementia; SNCA: α-Syn gene; iLBD: incidental LB disease; SN: substantia nigra; PrP: prion protein; TSEs: Transmissible spongiform encephalopathies; CJD: Cr eutzfeldt–Jakob disease; PRNP: prion protein gene; AD/PART: AD/primary age-related tauopathy; proIAPP: pro-islet amyloid polypeptide; FTLD-TDP: frontotemporal dementia; BDNF: brain-derived neurotrophic factor; TTR: transthyretin; β2m: β2-microglobulin; AA: Amyloid A; SP: senile plaque; sIBM: sporadic inclusion-body myositis; LDs: lipid droplets; ROS: reactive oxygen species;

2.7 References

1. A. Dogan, Amyloidosis: Insights from Proteomics. Annual Review of Pathology: Mechanisms of Disease 12, 277-304 (2017).
2. M. Fandrich, On the structural definition of amyloid fibrils and other polypeptide aggregates. Cellular and molecular life sciences : CMLS 64, 2066-2078 (2007).
3. M. R. Nilsson, Techniques to study amyloid fibril formation in vitro. Methods 34, 151-160 (2004).
4. D. C. Bode, M. D. Baker, J. H. Viles, Ion Channel Formation by Amyloid-β42 Oligomers but Not Amyloid-β40 in Cellular Membranes. J Biol Chem 292, 1404-1413 (2017).
5. A. Surguchev, A. Surguchov, Effect of α-synuclein on membrane permeability and synaptic transmission: a clue to neurodegeneration? J Neurochem 132, 619-621 (2015).
6. M. L. Choi, S. Gandhi, Crucial role of protein oligomerization in the pathogenesis of Alzheimer's and Parkinson's diseases. The FEBS journal 285, 3631-3644 (2018).
7. H. A. Pearson, C. Peers, Physiological roles for amyloid beta peptides. J Physiol 575, 5-10 (2006).
8. G. F. Chen et al., Amyloid beta: structure, biology and structure-based therapeutic development. Acta pharmacologica Sinica 38, 1205-1235 (2017).
9. D. M. Fowler, A. V. Koulov, W. E. Balch, J. W. Kelly, Functional amyloid–from bacteria to humans. Trends in biochemical sciences 32, 217-224 (2007).
10. J. D. Sipe et al., Nomenclature 2014: Amyloid fibril proteins and clinical classification of the amyloidosis. Amyloid 21, 221-224 (2014).
11. B. P. C. Hazenberg, Amyloidosis: A Clinical Overview. Rheumatic Disease Clinics of North America 39, 323-345 (2013).
12. S. C. Shin, J. Robinson-Papp, Amyloid neuropathies. Mt Sinai J Med 79, 733-748 (2012).
13. J. Haan, R. A. Roos, Amyloid in central nervous system disease. Clinical neurology and neurosurgery 92, 305-310 (1990).

14. R. W. Mahley, S. C. Rall, Jr., Apolipoprotein E: far more than a lipid transport protein. Annual review of genomics and human genetics 1, 507-537 (2000).
15. H. C. Hunsberger, P. D. Pinky, W. Smith, V. Suppiramaniam, M. N. Reed, The role of APOE4 in Alzheimer's disease: strategies for future therapeutic interventions. Health Psychol Behav Med 3, NS20180203-NS20180203 (2019).
16. P. Amouyel, O. Vidal, J. M. Launay, J. L. Laplanche, The apolipoprotein E alleles as major susceptibility factors for Creutzfeldt-Jakob disease. The French Research Group on Epidemiology of Human Spongiform Encephalopathies. Lancet 344, 1315-1318 (1994).
17. J. Guan et al., Histopathological correlations of islet amyloidosis with apolipoprotein E polymorphisms in type 2 diabetic Chinese patients. Pancreas 42, 1129-1137 (2013).
18. M. Takeda et al., Apolipoprotein E and central nervous system disorders: reviews of clinical findings. Psychiatry and clinical neurosciences 64, 592-607 (2010).
19. C. G. Fernandez, M. E. Hamby, M. L. McReynolds, W. J. Ray, The Role of APOE4 in Disrupting the Homeostatic Functions of Astrocytes and Microglia in Aging and Alzheimer's Disease. Frontiers in aging neuroscience 11, 14 (2019).
20. G. S. Getz, C. A. Reardon, Apoprotein E as a lipid transport and signaling protein in the blood, liver, and artery wall. J Lipid Res 50 Suppl, S156-161 (2009).
21. Y. Huang, K. H. Weisgraber, L. Mucke, R. W. Mahley, Apolipoprotein E: diversity of cellular origins, structural and biophysical properties, and effects in Alzheimer's disease. J Mol Neurosci 23, 189-204 (2004).
22. B. P. Nathan et al., Differential effects of apolipoproteins E3 and E4 on neuronal growth in vitro. Science 264, 850-852 (1994).
23. R. E. Pitas, Z. S. Ji, K. H. Weisgraber, R. W. Mahley, Role of apolipoprotein E in modulating neurite outgrowth: potential effect of intracellular apolipoprotein E. Biochemical Society transactions 26, 257-262 (1998).
24. R. D. Bell et al., Apolipoprotein E controls cerebrovascular integrity via cyclophilin A. Nature 485, 512-516 (2012).
25. K. Koizumi et al., Apoepsilon4 disrupts neurovascular regulation and undermines white matter integrity and cognitive function. Nature communications 9, 3816 (2018).
26. O. Levi, A. L. Jongen-Relo, J. Feldon, A. D. Roses, D. M. Michaelson, ApoE4 impairs hippocampal plasticity isoform-specifically and blocks the environmental stimulation of synaptogenesis and memory. Neurobiology of disease 13, 273-282 (2003).
27. Y. Tensaouti, E. P. Stephanz, T. S. Yu, S. G. Kernie, ApoE Regulates the Development of Adult Newborn Hippocampal Neurons. eNeuro 5, (2018).
28. M. Wozniak et al., Apolipoprotein E-ϵ4 protects against severe liver disease caused by hepatitis C. Hepatology (Baltimore, Md.) 36, 456-463 (2002).
29. P. E. Cramer et al., ApoE-directed therapeutics rapidly clear beta-amyloid and reverse deficits in AD mouse models. Science (New York, N.Y.) 335, 1503-1506 (2012).

30. J. M. Castellano et al., Human apoE isoforms differentially regulate brain amyloid-beta peptide clearance. Sci Transl Med 3, 89ra57 (2011).
31. P. B. Verghese et al., ApoE influences amyloid-beta (Abeta) clearance despite minimal apoE/Abeta association in physiological conditions. Proceedings of the National Academy of Sciences of the United States of America 110, E1807-1816 (2013).
32. P. Eline Slagboom, N. van den Berg, J. Deelen, Phenome and genome based studies into human ageing and longevity: An overview. Biochimica et Biophysica Acta (BBA) - Molecular Basis of Disease 1864, 2742-2751 (2018).
33. J. Deelen et al., Genome-wide association meta-analysis of human longevity identifies a novel locus conferring survival beyond 90 years of age. Hum Mol Genet 23, 4420-4432 (2014).
34. J. Deelen et al., Genome-wide association study identifies a single major locus contributing to survival into old age; the APOE locus revisited. Aging Cell 10, 686-698 (2011).
35. M. C. Phillips, Apolipoprotein E isoforms and lipoprotein metabolism. IUBMB life 66, 616-623 (2014).
36. J. Davignon, R. E. Gregg, C. F. Sing, Apolipoprotein E polymorphism and atherosclerosis. Arteriosclerosis 8, 1-21 (1988).
37. R. M. CORBO, R. SCACCHI, Apolipoprotein E (APOE) allele distribution in the world. Is APOE*4 a 'thrifty' allele? Annals of Human Genetics 63, 301-310 (1999).
38. R. W. Mahley, K. H. Weisgraber, Y. Huang, Apolipoprotein E: structure determines function, from atherosclerosis to Alzheimer's disease to AIDS. Journal of lipid research 50 Suppl, S183-188 (2009).
39. Holly C. Hunsberger, Priyanka D. Pinky, W. Smith, V. Suppiramaniam, Miranda N. Reed, The role of APOE4 in Alzheimer's disease: strategies for future therapeutic interventions. Neuronal Signaling 3, (2019).
40. C. E. Finch, T. E. Morgan, Systemic inflammation, infection, ApoE alleles, and Alzheimer disease: a position paper. Current Alzheimer research 4, 185-189 (2007).
41. K. H. Weisgraber, T. L. Innerarity, R. W. Mahley, Abnormal lipoprotein receptor-binding activity of the human E apoprotein due to cysteine-arginine interchange at a single site. J Biol Chem 257, 2518-2521 (1982).
42. K. Patra et al., Plasma Apolipoprotein E Monomer and Dimer Profile and Relevance to Alzheimer's Disease. Journal of Alzheimer's disease : JAD 71, 1217-1231 (2019).
43. P. S. Chetty, L. Mayne, S. Lund-Katz, S. W. Englander, M. C. Phillips, Helical structure, stability, and dynamics in human apolipoprotein E3 and E4 by hydrogen exchange and mass spectrometry. Proceedings of the National Academy of Sciences 114, 968 (2017).
44. C. Frieden, H. Wang, C. M. W. Ho, A mechanism for lipid binding to apoE and the role of intrinsically disordered regions coupled to domain-domain interactions. Proc

Natl Acad Sci U S A 114, 6292-6297 (2017).
45. W. J. Brecht et al., Neuron-specific apolipoprotein e4 proteolysis is associated with increased tau phosphorylation in brains of transgenic mice. J Neurosci 24, 2527-2534 (2004).
46. Y. Huang et al., Apolipoprotein E fragments present in Alzheimer's disease brains induce neurofibrillary tangle-like intracellular inclusions in neurons. Proc Natl Acad Sci U S A 98, 8838-8843 (2001).
47. S. S. Munoz, B. Garner, L. Ooi, Understanding the Role of ApoE Fragments in Alzheimer's Disease. Neurochemical research 44, 1297-1305 (2019).
48. S. Chang et al., Lipid- and receptor-binding regions of apolipoprotein E4 fragments act in concert to cause mitochondrial dysfunction and neurotoxicity. Proc Natl Acad Sci U S A 102, 18694-18699 (2005).
49. Y. Andrews-Zwilling et al., Apolipoprotein E4 causes age- and Tau-dependent impairment of GABAergic interneurons, leading to learning and memory deficits in mice. The Journal of neuroscience : the official journal of the Society for Neuroscience 30, 13707-13717 (2010).
50. I. Dafnis et al., An apolipoprotein E4 fragment can promote intracellular accumulation of amyloid peptide beta 42. J Neurochem 115, 873-884 (2010).
51. I. Dafnis, A. K. Tzinia, E. C. Tsilibary, V. I. Zannis, A. Chroni, An apolipoprotein E4 fragment affects matrix metalloproteinase 9, tissue inhibitor of metalloproteinase 1 and cytokine levels in brain cell lines. Neuroscience 210, 21-32 (2012).
52. I. Dafnis et al., ApoE isoforms and carboxyl-terminal-truncated apoE4 forms affect neuronal BACE1 levels and Abeta production independently of their cholesterol efflux capacity. The Biochemical journal 475, 1839-1859 (2018).
53. Y. A. Huang, B. Zhou, M. Wernig, T. C. Sudhof, ApoE2, ApoE3, and ApoE4 Differentially Stimulate APP Transcription and Abeta Secretion. Cell 168, 427-441 e421 (2017).
54. E. M. Castano et al., Fibrillogenesis in Alzheimer's disease of amyloid beta peptides and apolipoprotein E. The Biochemical journal 306 (Pt 2), 599-604 (1995).
55. A. Rapp, B. Gmeiner, M. Huttinger, Implication of apoE isoforms in cholesterol metabolism by primary rat hippocampal neurons and astrocytes. Biochimie 88, 473-483 (2006).
56. M. Michikawa, Q. W. Fan, I. Isobe, K. Yanagisawa, Apolipoprotein E exhibits isoform-specific promotion of lipid efflux from astrocytes and neurons in culture. Journal of neurochemistry 74, 1008-1016 (2000).
57. L. M. Tai et al., APOE-modulated Abeta-induced neuroinflammation in Alzheimer's disease: current landscape, novel data, and future perspective. J Neurochem 133, 465-488 (2015).

58. B. C. Trumble et al., Apolipoprotein E4 is associated with improved cognitive function in Amazonian forager-horticulturalists with a high parasite burden. FASEB J 31, 1508-1515 (2017).

59. L. M. Tai et al., APOE-modulated Aβ-induced neuroinflammation in Alzheimer's disease: current landscape, novel data, and future perspective. J Neurochem 133, 465-488 (2015).

60. T. Mueller et al., Apolipoprotein E allele frequencies in chronic and self-limited hepatitis C suggest a protective effect of APOE4 in the course of hepatitis C virus infection. Liver international : official journal of the International Association for the Study of the Liver 36, 1267-1274 (2016).

61. N. Zhao et al., APOE ϵ2 is associated with increased tau pathology in primary tauopathy. Nature communications 9, 4388 (2018).

62. D. M. Holtzman, Role of apoE/Aβ interactions in the pathogenesis of Alzheimer's disease and cerebral amyloid angiopathy. Journal of Molecular Neuroscience 17, 147-155 (2001).

63. T. Wisniewski, E. Drummond, APOE-amyloid interaction: Therapeutic targets. Neurobiology of disease 138, 104784 (2020).

64. S. Lovestone, B. H. Anderton, C. Hartley, T. G. Jensen, A. L. Jorgensen, The intracellular fate of apolipoprotein E is tau dependent and apoe allele-specific. Neuroreport 7, 1005-1008 (1996).

65. F. Panza, M. Lozupone, G. Logroscino, B. P. Imbimbo, A critical appraisal of amyloid-β-targeting therapies for Alzheimer disease. Nature reviews. Neurology 15, 73-88 (2019).

66. M. P. Murphy, H. LeVine, 3rd, Alzheimer's disease and the amyloid-beta peptide. Journal of Alzheimer's disease : JAD 19, 311-323 (2010).

67. S. D. Mulder, R. Veerhuis, M. A. Blankenstein, H. M. Nielsen, The effect of amyloid associated proteins on the expression of genes involved in amyloid-β clearance by adult human astrocytes. Experimental Neurology 233, 373-379 (2012).

68. R. J. Ellis et al., Cerebral amyloid angiopathy in the brains of patients with Alzheimer's disease: the CERAD experience, Part XV. Neurology 46, 1592-1596 (1996).

69. T. V. Huynh, A. A. Davis, J. D. Ulrich, D. M. Holtzman, Apolipoprotein E and Alzheimer's disease: the influence of apolipoprotein E on amyloid-beta and other amyloidogenic proteins. Journal of lipid research 58, 824-836 (2017).

70. C. Haass, D. J. Selkoe, Soluble protein oligomers in neurodegeneration: lessons from the Alzheimer's amyloid beta-peptide. Nat.Rev.Mol.Cell Biol. 8, 101-112 (2007).

71. K. N. Dahlgren et al., Oligomeric and fibrillar species of amyloid-beta peptides differentially affect neuronal viability. J.Biol.Chem. 277, 32046-32053 (2002).

72. T. C. Dickson, J. C. Vickers, The morphological phenotype of beta-amyloid plaques and associated neuritic changes in Alzheimer's disease. Neuroscience 105, 99-107 (2001).

73. J. Liu et al., Amyloid structure exhibits polymorphism on multiple length scales in human brain tissue. Scientific reports 6, 33079 (2016).
74. P. V. Arriagada, J. H. Growdon, E. T. Hedley-Whyte, B. T. Hyman, Neurofibrillary tangles but not senile plaques parallel duration and severity of Alzheimer's disease. Neurology 42, 631-639 (1992).
75. J. L. Price, J. C. Morris, Tangles and plaques in nondemented aging and "preclinical" Alzheimer's disease. Annals of neurology 45, 358-368 (1999).
76. B. DaRocha-Souto et al., Brain oligomeric beta-amyloid but not total amyloid plaque burden correlates with neuronal loss and astrocyte inflammatory response in amyloid precursor protein/tau transgenic mice. Journal of neuropathology and experimental neurology 70, 360-376 (2011).
77. A. Serrano-Pozo et al., Reactive glia not only associates with plaques but also parallels tangles in Alzheimer's disease. The American journal of pathology 179, 1373-1384 (2011).
78. W. J. Strittmatter et al., Apolipoprotein E: high-avidity binding to beta-amyloid and increased frequency of type 4 allele in late-onset familial Alzheimer disease. Proceedings of the National Academy of Sciences of the United States of America 90, 1977-1981 (1993).
79. A. M. Saunders et al., Apolipoprotein E epsilon 4 allele distributions in late-onset Alzheimer's disease and in other amyloid-forming diseases. Lancet 342, 710-711 (1993).
80. L. Bernardi et al., The effects of APOE and tau gene variability on risk of frontotemporal dementia. Neurobiology of aging 27, 702-709 (2006).
81. G. Berge, S. B. Sando, A. Rongve, D. Aarsland, L. R. White, Apolipoprotein E $\epsilon 2$ genotype delays onset of dementia with Lewy bodies in a Norwegian cohort. Journal of neurology, neurosurgery, and psychiatry 85, 1227-1231 (2014).
82. Z. Li, F. Shue, N. Zhao, M. Shinohara, G. Bu, APOE2: protective mechanism and therapeutic implications for Alzheimer's disease. Mol Neurodegener 15, 63 (2020).
83. E. M. Reiman et al., Exceptionally low likelihood of Alzheimer's dementia in APOE2 homozygotes from a 5,000-person neuropathological study. Nature communications 11, 667 (2020).
84. J. F. Arboleda-Velasquez et al., Resistance to autosomal dominant Alzheimer's disease in an APOE3 Christchurch homozygote: a case report. Nature medicine 25, 1680-1683 (2019).
85. L. M. Tai et al., Soluble apoE/Abeta complex: mechanism and therapeutic target for APOE4-induced AD risk. Molecular neurodegeneration 9, 2 (2014).
86. J. Kim, J. M. Basak, D. M. Holtzman, The role of apolipoprotein E in Alzheimer's disease. Neuron 63, 287-303 (2009).
87. T. Kanekiyo, H. Xu, G. Bu, ApoE and Aβ in Alzheimer's disease: accidental encounters or partners? Neuron 81, 740-754 (2014).

88. S. Ghosh, T. B. Sil, S. Dolai, K. Garai, High-affinity multivalent interactions between apolipoprotein E and the oligomers of amyloid-β. The FEBS journal 286, 4737-4753 (2019).

89. A. A. Golabek, C. Soto, T. Vogel, T. Wisniewski, The interaction between apolipoprotein E and Alzheimer's amyloid beta-peptide is dependent on beta-peptide conformation. The Journal of biological chemistry 271, 10602-10606 (1996).

90. P. B. Verghese et al., ApoE influences amyloid-β (Aβ) clearance despite minimal apoE/Aβ association in physiological conditions. Proceedings of the National Academy of Sciences of the United States of America 110, E1807-E1816 (2013).

91. D. E. Bredesen, Inhalational Alzheimer's disease: an unrecognized - and treatable - epidemic. Aging 8, 304-313 (2016).

92. C. Matrone, M. T. Ciotti, D. Mercanti, R. Marolda, P. Calissano, NGF and BDNF signaling control amyloidogenic route and Abeta production in hippocampal neurons. Proc Natl Acad Sci U S A 105, 13139-13144 (2008).

93. K. S. Poksay et al., Screening for Small Molecule Inhibitors of Statin-Induced APP C-terminal Toxic Fragment Production. Frontiers in pharmacology 8, 46 (2017).

94. V. Theendakara et al., Neuroprotective Sirtuin ratio reversed by ApoE4. Proceedings of the National Academy of Sciences of the United States of America 110, 18303-18308 (2013).

95. T.-P. V. Huynh, A. A. Davis, J. D. Ulrich, D. M. Holtzman, Apolipoprotein E and Alzheimer's disease: the influence of apolipoprotein E on amyloid-β and other amyloidogenic proteins. Journal of lipid research 58, 824-836 (2017).

96. S. Ye et al., Apolipoprotein (apo) E4 enhances amyloid beta peptide production in cultured neuronal cells: apoE structure as a potential therapeutic target. Proceedings of the National Academy of Sciences of the United States of America 102, 18700-18705 (2005).

97. Q. Liu et al., Amyloid precursor protein regulates brain apolipoprotein E and cholesterol metabolism through lipoprotein receptor LRP1. Neuron 56, 66-78 (2007).

98. T. Pohlkamp, C. R. Wasser, J. Herz, Functional Roles of the Interaction of APP and Lipoprotein Receptors. Frontiers in molecular neuroscience 10, 54 (2017).

99. D. E. Kang et al., Modulation of amyloid beta-protein clearance and Alzheimer's disease susceptibility by the LDL receptor-related protein pathway. J Clin Invest 106, 1159-1166 (2000).

100. W. G. Wood, L. Li, W. E. Muller, G. P. Eckert, Cholesterol as a causative factor in Alzheimer's disease: a debatable hypothesis. Journal of neurochemistry 129, 559-572 (2014).

101. O. Descamps, Q. Zhang, V. John, D. E. Bredesen, Induction of the C-terminal proteolytic cleavage of AbetaPP by statins. Journal of Alzheimer's disease : JAD 25, 51-57 (2011).

102. K. Garai, P. B. Verghese, B. Baban, D. M. Holtzman, C. Frieden, The binding of apolipoprotein E to oligomers and fibrils of amyloid-beta alters the kinetics of amyloid aggregation. Biochemistry 53, 6323-6331 (2014).
103. E. Cerf, A. Gustot, E. Goormaghtigh, J. M. Ruysschaert, V. Raussens, High ability of apolipoprotein E4 to stabilize amyloid-beta peptide oligomers, the pathological entities responsible for Alzheimer's disease. FASEB J. 25, 1585-1595 (2011).
104. B. L. Trommer et al., ApoE isoform-specific effects on LTP: blockade by oligomeric amyloid-beta1-42. Neurobiology of disease 18, 75-82 (2005).
105. J. E. Pankiewicz et al., Blocking the apoE/Abeta interaction ameliorates Abeta-related pathology in APOE epsilon2 and epsilon4 targeted replacement Alzheimer model mice. Acta neuropathologica communications 2, 75 (2014).
106. A. M. Manelli, W. B. Stine, L. J. Van Eldik, M. J. LaDu, ApoE and Abeta1-42 interactions: effects of isoform and conformation on structure and function. J.Mol.Neurosci. 23, 235-246 (2004).
107. T. V. Huynh, A. A. Davis, J. D. Ulrich, D. M. Holtzman, Apolipoprotein E and Alzheimer's disease: the influence of apolipoprotein E on amyloid-beta and other amyloidogenic proteins. J.Lipid Res. 58, 824-836 (2017).
108. I. Dafnis, L. Argyri, A. Chroni, Amyloid-peptide beta 42 Enhances the Oligomerization and Neurotoxicity of apoE4: The C-terminal Residues Leu279, Lys282 and Gln284 Modulate the Structural and Functional Properties of apoE4. Neuroscience. 394, 144-155 (2018).
109. X. Zhang, Z. Fu, L. Meng, M. He, Z. Zhang, The Early Events That Initiate beta-Amyloid Aggregation in Alzheimer's Disease. Frontiers in aging neuroscience 10, 359 (2018).
110. C. Y. D. Lee, W. Tse, J. D. Smith, G. E. Landreth, Apolipoprotein E Promotes β-Amyloid Trafficking and Degradation by Modulating Microglial Cholesterol Levels. Journal of Biological Chemistry 287, 2032-2044 (2012).
111. Q. Jiang et al., ApoE promotes the proteolytic degradation of Abeta. Neuron 58, 681-693 (2008).
112. C. M. Wolfe, N. F. Fitz, K. N. Nam, I. Lefterov, R. Koldamova, The Role of APOE and TREM2 in Alzheimer's Disease-Current Understanding and Perspectives. International journal of molecular sciences 20, (2018).
113. R. Deane et al., apoE isoform-specific disruption of amyloid beta peptide clearance from mouse brain. The Journal of clinical investigation 118, 4002-4013 (2008).
114. P. T. Nelson et al., APOE-epsilon2 and APOE-epsilon4 correlate with increased amyloid accumulation in cerebral vasculature. Journal of neuropathology and experimental neurology 72, 708-715 (2013).
115. D. R. Riddell et al., Impact of apolipoprotein E (ApoE) polymorphism on brain

ApoE levels. The Journal of neuroscience : the official journal of the Society for Neuroscience 28, 11445-11453 (2008).

116. H. M. Nielsen et al., Astrocytic Aβ1-42 uptake is determined by Aβ-aggregation state and the presence of amyloid-associated proteins. Glia 58, 1235-1246 (2010).

117. S. D. Mulder, H. M. Nielsen, M. A. Blankenstein, P. Eikelenboom, R. Veerhuis, Apolipoproteins E and J interfere with amyloid-beta uptake by primary human astrocytes and microglia in vitro. Glia 62, 493-503 (2014).

118. A. Louveau, S. Da Mesquita, J. Kipnis, Lymphatics in Neurological Disorders: A Neuro-Lympho-Vascular Component of Multiple Sclerosis and Alzheimer's Disease? Neuron 91, 957-973 (2016).

119. J. Zekonyte, K. Sakai, J. A. Nicoll, R. O. Weller, R. O. Carare, Quantification of molecular interactions between ApoE, amyloid-beta (Abeta) and laminin: Relevance to accumulation of Abeta in Alzheimer's disease. Biochimica et biophysica acta 1862, 1047-1053 (2016).

120. S. Tamamizu-Kato et al., Interaction with amyloid beta peptide compromises the lipid binding function of apolipoprotein E. Biochemistry 47, 5225-5234 (2008).

121. J. C. Lambert et al., Is there a relation between APOE expression and brain amyloid load in Alzheimer's disease? Journal of neurology, neurosurgery, and psychiatry 76, 928-933 (2005).

122. P. Vemuri et al., Effect of apolipoprotein E on biomarkers of amyloid load and neuronal pathology in Alzheimer disease. Annals of neurology 67, 308-316 (2010).

123. E. Kara et al., A flow cytometry-based in vitro assay reveals that formation of apolipoprotein E (ApoE)-amyloid beta complexes depends on ApoE isoform and cell type. The Journal of biological chemistry 293, 13247-13256 (2018).

124. J. Kim et al., Anti-apoE immunotherapy inhibits amyloid accumulation in a transgenic mouse model of Abeta amyloidosis. The Journal of experimental medicine 209, 2149-2156 (2012).

125. F. Liao et al., Anti-ApoE antibody given after plaque onset decreases Abeta accumulation and improves brain function in a mouse model of Abeta amyloidosis. The Journal of neuroscience : the official journal of the Society for Neuroscience 34, 7281-7292 (2014).

126. F. Re et al., Functionalization with ApoE-derived peptides enhances the interaction with brain capillary endothelial cells of nanoliposomes binding amyloid-beta peptide. Journal of biotechnology 156, 341-346 (2011).

127. M. J. Sadowski et al., Blocking the apolipoprotein E/amyloid-beta interaction as a potential therapeutic approach for Alzheimer's disease. Proc Natl Acad Sci U S A 103, 18787-18792 (2006).

128. M. M. Evers, L. J. Toonen, W. M. van Roon-Mom, Antisense oligonucleotides in therapy for neurodegenerative disorders. Advanced drug delivery reviews 87, 90-103

(2015).v 129. T. V. Huynh et al., Age-Dependent Effects of apoE Reduction Using Antisense Oligonucleotides in a Model of beta-amyloidosis. Neuron 96, 1013-1023 e1014 (2017).
130. F. Liao et al., Targeting of nonlipidated, aggregated apoE with antibodies inhibits amyloid accumulation. The Journal of clinical investigation 128, 2144-2155 (2018).
131. M. Sadowski et al., A synthetic peptide blocking the apolipoprotein E/beta-amyloid binding mitigates beta-amyloid toxicity and fibril formation in vitro and reduces beta-amyloid plaques in transgenic mice. The American journal of pathology 165, 937-948 (2004).
132. E. Dorey, N. Chang, Q. Y. Liu, Z. Yang, W. Zhang, Apolipoprotein E, amyloid-beta, and neuroinflammation in Alzheimer's disease. Neurosci Bull 30, 317-330 (2014).
133. J. Avila, J. J. Lucas, M. Perez, F. Hernandez, Role of tau protein in both physiological and pathological conditions. Physiological reviews 84, 361-384 (2004).
134. G. Lee, C. J. Leugers, Tau and tauopathies. Prog Mol Biol Transl Sci 107, 263-293 (2012).
135. T. Guo, W. Noble, D. P. Hanger, Roles of tau protein in health and disease. Acta neuropathologica 133, 665-704 (2017).
136. K. Blennow et al., Tau protein in cerebrospinal fluid: a biochemical marker for axonal degeneration in Alzheimer disease? Mol Chem Neuropathol 26, 231-245 (1995).
137. K. Iqbal, F. Liu, C. X. Gong, I. Grundke-Iqbal, Tau in Alzheimer disease and related tauopathies. Curr Alzheimer Res 7, 656-664 (2010).
138. S. K. Herukka et al., CSF Abeta42, Tau and phosphorylated Tau, APOE epsilon4 allele and MCI type in progressive MCI. Neurobiology of aging 28, 507-514 (2007).
139. E. Martínez-Morillo et al., Total apolipoprotein E levels and specific isoform composition in cerebrospinal fluid and plasma from Alzheimer's disease patients and controls. Acta Neuropathologica 127, 633-643 (2014).
140. A. T. Baker-Nigh et al., Human Central Nervous System (CNS) ApoE Isoforms Are Increased by Age, Differentially Altered by Amyloidosis, and Relative Amounts Reversed in the CNS Compared with Plasma. Journal of Biological Chemistry 291, 27204-27218 (2016).
141. M. Shafaati, A. Solomon, M. Kivipelto, I. Bjorkhem, V. Leoni, Levels of ApoE in cerebrospinal fluid are correlated with Tau and 24S-hydroxycholesterol in patients with cognitive disorders. Neuroscience letters 425, 78-82 (2007).
142. Y. Shi et al., ApoE4 markedly exacerbates tau-mediated neurodegeneration in a mouse model of tauopathy. Nature 549, 523-527 (2017).
143. Y. Huang et al., Apolipoprotein E fragments present in Alzheimer's disease brains induce neurofibrillary tangle-like intracellular inclusions in neurons. Proc.Natl.Acad.Sci.U.S.A 98, 8838-8843 (2001).
144. S. Chang et al., Lipid- and receptor-binding regions of apolipoprotein E4 fragments

act in concert to cause mitochondrial dysfunction and neurotoxicity. Proc.Natl.Acad.Sci.U.S.A 102, 18694-18699 (2005).

145. W. J. Strittmatter et al., Hypothesis: microtubule instability and paired helical filament formation in the Alzheimer disease brain are related to apolipoprotein E genotype. Experimental neurology 125, 163-171; discussion 172-164 (1994).

146. D. Y. Huang et al., ApoE3 binding to tau tandem repeat I is abolished by tau serine262 phosphorylation. Neuroscience letters 192, 209-212 (1995).

147. D. Y. Huang et al., Isoform-specific interactions of apolipoprotein E with the microtubule-associated protein MAP2c: implications for Alzheimer's disease. Neuroscience letters 182, 55-58 (1994).

148. W. J. Strittmatter et al., Isoform-specific interactions of apolipoprotein E with microtubule-associated protein tau: implications for Alzheimer disease. Proceedings of the National Academy of Sciences of the United States of America 91, 11183-11186 (1994).

149. I. Genis, I. Gordon, E. Sehayek, D. M. Michaelson, Phosphorylation of tau in apolipoprotein E-deficient mice. Neuroscience letters 199, 5-8 (1995).

150. F. M. Harris et al., Carboxyl-terminal-truncated apolipoprotein E4 causes Alzheimer's disease-like neurodegeneration and behavioral deficits in transgenic mice. Proc Natl Acad Sci U S A 100, 10966-10971 (2003).

151. I. Tesseur et al., Expression of human apolipoprotein E4 in neurons causes hyperphosphorylation of protein tau in the brains of transgenic mice. The American journal of pathology 156, 951-964 (2000).

152. F. M. Harris, W. J. Brecht, Q. Xu, R. W. Mahley, Y. Huang, Increased tau phosphorylation in apolipoprotein E4 transgenic mice is associated with activation of extracellular signal-regulated kinase: modulation by zinc. The Journal of biological chemistry 279, 44795-44801 (2004).

153. I. Dewachter et al., Modeling Alzheimer's disease in transgenic mice: effect of age and of presenilin1 on amyloid biochemistry and pathology in APP/London mice. Experimental gerontology 35, 831-841 (2000).

154. X. Wang, P. Luebbe, E. Gruenstein, F. Zemlan, Apolipoprotein E (ApoE) peptide regulates tau phosphorylation via two different signaling pathways. Journal of neuroscience research 51, 658-665 (1998).

155. V. Theendakara, D. E. Bredesen, R. V. Rao, Downregulation of protein phosphatase 2A by apolipoprotein E: Implications for Alzheimer's disease. Molecular and Cellular Neuroscience 83, 83-91 (2017).

156. N. Ohkubo et al., Apolipoprotein E and Reelin ligands modulate tau phosphorylation through an apolipoprotein E receptor/disabled-1/glycogen synthase kinase-3beta cascade. FASEB journal : official publication of the Federation of American Societies for Experimental Biology 17, 295-297 (2003).

157. L. Genis, Y. Chen, E. Shohami, D. M. Michaelson, Tau hyperphosphorylation in apolipoprotein E-deficient and control mice after closed head injury. Journal of neuroscience research 60, 559-564 (2000).
158. H. S. Hoe, J. Freeman, G. W. Rebeck, Apolipoprotein E decreases tau kinases and phospho-tau levels in primary neurons. Molecular neurodegeneration 1, 18 (2006).
159. A. Boehm-Cagan et al., ABCA1 Agonist Reverses the ApoE4-Driven Cognitive and Brain Pathologies. J Alzheimers Dis 54, 1219-1233 (2016).
160. D. Sulzer, R. H. Edwards, The Physiological Role of alpha-Synuclein and Its Relationship to Parkinson's Disease. Journal of neurochemistry, (2019).
161. J. Fantini, D. Carlus, N. Yahi, The fusogenic tilted peptide (67-78) of alpha-synuclein is a cholesterol binding domain. Biochimica et biophysica acta 1808, 2343-2351 (2011).
162. D. L. Fortin et al., Lipid rafts mediate the synaptic localization of alpha-synuclein. The Journal of neuroscience : the official journal of the Society for Neuroscience 24, 6715-6723 (2004).
163. D. F. Clayton, J. M. George, The synucleins: a family of proteins involved in synaptic function, plasticity, neurodegeneration and disease. Trends in neurosciences 21, 249-254 (1998).
164. J. Varkey et al., alpha-Synuclein oligomers with broken helical conformation form lipoprotein nanoparticles. The Journal of biological chemistry 288, 17620-17630 (2013).
165. A. Surguchov, Intracellular Dynamics of Synucleins: "Here, There and Everywhere". International review of cell and molecular biology 320, 103-169 (2015).
166. V. N. Uversky, H. J. Lee, J. Li, A. L. Fink, S. J. Lee, Stabilization of partially folded conformation during alpha-synuclein oligomerization in both purified and cytosolic preparations. The Journal of biological chemistry 276, 43495-43498 (2001).
167. M. G. Spillantini et al., Alpha-synuclein in Lewy bodies. Nature 388, 839-840 (1997).
168. P. Pals et al., alpha-Synuclein promoter confers susceptibility to Parkinson's disease. Ann Neurol 56, 591-595 (2004).
169. J. T. Hsiao, G. M. Halliday, W. S. Kim, α-Synuclein Regulates Neuronal Cholesterol Efflux. Molecules (Basel, Switzerland) 22, (2017).
170. F. N. Emamzadeh, Role of Apolipoproteins and alpha-Synuclein in Parkinson's Disease. Journal of molecular neuroscience : MN 62, 344-355 (2017).
171. D. Twohig, H. M. Nielsen, alpha-synuclein in the pathophysiology of Alzheimer's disease. Molecular neurodegeneration 14, 23 (2019).
172. A. A. Davis et al., APOE genotype regulates pathology and disease progression in synucleinopathy. Sci Transl Med 12, (2020).
173. N. Zhao et al., APOE4 exacerbates alpha-synuclein pathology and related toxicity independent of amyloid. Sci Transl Med 12, (2020).

174. M. Federoff, B. Jimenez-Rolando, M. A. Nalls, A. B. Singleton, A large study reveals no association between APOE and Parkinson's disease. Neurobiology of disease 46, 389-392 (2012).
175. J. Gao et al., Apolipoprotein E genotypes and the risk of Parkinson disease. Neurobiology of aging 32, 2106 e2101-2106 (2011).
176. W. Paslawski et al., alpha-synuclein-lipoprotein interactions and elevated ApoE level in cerebrospinal fluid from Parkinson's disease patients. Proceedings of the National Academy of Sciences of the United States of America 116, 15226-15235 (2019).
177. R. Kruger et al., Increased susceptibility to sporadic Parkinson's disease by a certain combined alpha-synuclein/apolipoprotein E genotype. Annals of neurology 45, 611-617 (1999).
178. N. Khan et al., Parkinson's disease is not associated with the combined alpha-synuclein/apolipoprotein E susceptibility genotype. Annals of neurology 49, 665-668 (2001).
179. A. Parsian, B. Racette, L. J. Goldsmith, J. S. Perlmutter, Parkinson's disease and apolipoprotein E: possible association with dementia but not age at onset. Genomics 79, 458-461 (2002).
180. D. Tsuang et al., APOE epsilon4 increases risk for dementia in pure synucleinopathies. JAMA neurology 70, 223-228 (2013).
181. L. Blazquez et al., Apolipoprotein E epsilon4 allele in familial and sporadic Parkinson's disease. Neuroscience letters 406, 235-239 (2006).
182. T. Pulkes et al., Association between apolipoprotein E genotypes and Parkinson's disease. Journal of clinical neuroscience : official journal of the Neurosurgical Society of Australasia 18, 1333-1335 (2011).
183. X. Huang, P. C. Chen, C. Poole, APOE-[epsilon]2 allele associated with higher prevalence of sporadic Parkinson disease. Neurology 62, 2198-2202 (2004).
184. C. H. Williams-Gray et al., Apolipoprotein E genotype as a risk factor for susceptibility to and dementia in Parkinson's disease. Journal of neurology 256, 493-498 (2009).
185. F. N. Emamzadeh, D. Allsop, alpha-Synuclein Interacts with Lipoproteins in Plasma. Journal of molecular neuroscience : MN 63, 165-172 (2017).
186. V. Ruiperez, F. Darios, B. Davletov, Alpha-synuclein, lipids and Parkinson's disease. Progress in lipid research 49, 420-428 (2010).
187. G. Barcelo-Coblijn, M. Y. Golovko, I. Weinhofer, J. Berger, E. J. Murphy, Brain neutral lipids mass is increased in alpha-synuclein gene-ablated mice. Journal of neurochemistry 101, 132-141 (2007).
188. J. T. Hsiao, G. M. Halliday, W. S. Kim, alpha-Synuclein Regulates Neuronal Cholesterol Efflux. Molecules 22, (2017).
189. L. M. de Lau, P. J. Koudstaal, A. Hofman, M. M. Breteler, Serum cholesterol levels and the risk of Parkinson's disease. American journal of epidemiology 164, 998-1002

(2006).
190. X. Huang, R. D. Abbott, H. Petrovitch, R. B. Mailman, G. W. Ross, Low LDL cholesterol and increased risk of Parkinson's disease: prospective results from Honolulu-Asia Aging Study. Movement disorders : official journal of the Movement Disorder Society 23, 1013-1018 (2008).
191. K. C. Simon, H. Chen, M. Schwarzschild, A. Ascherio, Hypertension, hypercholesterolemia, diabetes, and risk of Parkinson disease. Neurology 69, 1688-1695 (2007).
192. M. M. Wilhelmus et al., Apolipoprotein E and LRP1 Increase Early in Parkinson's Disease Pathogenesis. The American journal of pathology 179, 2152-2156 (2011).
193. F. N. Emamzadeh, H. Aojula, P. C. McHugh, D. Allsop, Effects of different isoforms of apoE on aggregation of the alpha-synuclein protein implicated in Parkinson's disease. Neuroscience letters 618, 146-151 (2016).
194. H. Nielsen, Y. Fu, G. Bu, APOLIPOPROTEIN E: AN UNEXPLORED MODULATOR OF CELLULAR ALPHA-SYNUCLEIN UPTAKE. (2014), vol. 10.
195. H. Nielsen et al., Apolipoprotein e affects neuronal alpha-synuclein uptake in an isoform-dependent manner. (2015), vol. 11, pp. P231.
196. G. Gallardo, O. M. Schlüter, T. C. Südhof, A molecular pathway of neurodegeneration linking alpha-synuclein to ApoE and Abeta peptides. Nature neuroscience 11, 301-308 (2008).
197. A. Giorgi et al., Proteomic profiling of PrP27-30-enriched preparations extracted from the brain of hamsters with experimental scrapie. Proteomics 9, 3802-3814 (2009).
198. R. A. Moore et al., Relative Abundance of apoE and Abeta1-42 Associated with Abnormal Prion Protein Differs between Creutzfeldt-Jakob Disease Subtypes. Journal of proteome research 15, 4518-4531 (2016).
199. R. Kordek, J. A. Hainfellner, P. P. Liberski, H. Budka, Deposition of the prion protein (PrP) during the evolution of experimental Creutzfeldt-Jakob disease. Acta neuropathologica 98, 597-602 (1999).
200. S. Nakamura et al., Immunohistochemical detection of apolipoprotein E within prion-associated lesions in squirrel monkey brains. Acta neuropathologica 100, 365-370 (2000).
201. R. A. Moore, A. G. Timmes, P. A. Wilmarth, D. Safronetz, S. A. Priola, Identification and removal of proteins that co-purify with infectious prion protein improves the analysis of its secondary structure. Proteomics 11, 3853-3865 (2011).
202. R. A. Moore, A. Timmes, P. A. Wilmarth, S. A. Priola, Comparative profiling of highly enriched 22L and Chandler mouse scrapie prion protein preparations. Proteomics 10, 2858-2869 (2010).
203. J. F. Graham et al., Na+/K+-ATPase is present in scrapie-associated fibrils, modulates PrP misfolding in vitro and links PrP function and dysfunction. PloS one 6, e26813 (2011).

204. C. Gao et al., Recombinant neural protein PrP can bind with both recombinant and native apolipoprotein E in vitro. Acta biochimica et biophysica Sinica 38, 593-601 (2006).
205. M. Rossi et al., The characterization of AD/PART co-pathology in CJD suggests independent pathogenic mechanisms and no cross-seeding between misfolded Abeta and prion proteins. Acta neuropathologica communications 7, 53 (2019).
206. Y. Wei et al., APOE gene polymorphisms and susceptibility to Creutzfeldt-Jakob disease. Journal of clinical neuroscience : official journal of the Neurosurgical Society of Australasia 21, 390-394 (2014).
207. B. Van Everbroeck et al., Influence of the prion protein and the apolipoprotein E genotype on the Creutzfeldt-Jakob Disease phenotype. Neuroscience letters 313, 69-72 (2001).
208. O. Calero et al., Genetic cross-interaction between APOE and PRNP in sporadic Alzheimer's and Creutzfeldt-Jakob diseases. PloS one 6, e22090 (2011).
209. R. Akter et al., Islet Amyloid Polypeptide: Structure, Function, and Pathophysiology. Journal of diabetes research 2016, 2798269 (2016).
210. P. Cao, A. Abedini, D. P. Raleigh, Aggregation of islet amyloid polypeptide: from physical chemistry to cell biology. Current opinion in structural biology 23, 82-89 (2013).
211. N. B. Last, A. D. Miranker, Common mechanism unites membrane poration by amyloid and antimicrobial peptides. Proceedings of the National Academy of Sciences of the United States of America 110, 6382-6387 (2013).
212. L. Wang et al., Antimicrobial activity of human islet amyloid polypeptides: an insight into amyloid peptides' connection with antimicrobial peptides. Biological chemistry 393, 641-646 (2012).
213. G. J. Cooper et al., Purification and characterization of a peptide from amyloid-rich pancreases of type 2 diabetic patients. Proceedings of the National Academy of Sciences of the United States of America 84, 8628-8632 (1987).
214. P. Westermark et al., Amyloid fibrils in human insulinoma and islets of Langerhans of the diabetic cat are derived from a neuropeptide-like protein also present in normal islet cells. Proceedings of the National Academy of Sciences of the United States of America 84, 3881-3885 (1987).
215. S. B. Charge, M. M. Esiri, C. A. Bethune, B. C. Hansen, A. Clark, Apolipoprotein E is associated with islet amyloid and other amyloidoses: implications for Alzheimer's disease. The Journal of pathology 179, 443-447 (1996).
216. J. Vidal et al., The effect of apolipoprotein E deficiency on islet amyloid deposition in human islet amyloid polypeptide transgenic mice. Diabetologia 46, 71-79 (2003).
217. D. S. Powell et al., Apolipoprotein E genotype, islet amyloid deposition and severity of Type 2 diabetes. Diabetes research and clinical practice 60, 105-110 (2003).
218. W. Q. Qiu et al., Association between amylin and amyloid-beta peptides in plasma

in the context of apolipoprotein E4 allele. PloS one 9, e88063 (2014).
219. P. Lei et al., Prevention and promotion effects of apolipoprotein E4 on amylin aggregation. Biochemical and biophysical research communications 368, 414-418 (2008).
220. C. Russo et al., Opposite roles of apolipoprotein E in normal brains and in Alzheimer's disease. Proceedings of the National Academy of Sciences of the United States of America 95, 15598-15602 (1998).
221. Y. Zhang, W. Song, Islet amyloid polypeptide: Another key molecule in Alzheimer's pathogenesis? Progress in neurobiology 153, 100-120 (2017).
222. G. R. Tundo et al., Multiple functions of insulin-degrading enzyme: a metabolic crosslight? Critical reviews in biochemistry and molecular biology 52, 554-582 (2017).
223. P. Cao et al., Islet amyloid: from fundamental biophysics to mechanisms of cytotoxicity. FEBS letters 587, 1106-1118 (2013).
224. S. Trikha, A. M. Jeremic, Clustering and internalization of toxic amylin oligomers in pancreatic cells require plasma membrane cholesterol. The Journal of biological chemistry 286, 36086-36097 (2011).
225. M. Wakabayashi, K. Matsuzaki, Ganglioside-induced amyloid formation by human islet amyloid polypeptide in lipid rafts. FEBS letters 583, 2854-2858 (2009).
226. M. Hayyan, M. A. Hashim, I. M. AlNashef, Superoxide Ion: Generation and Chemical Implications. Chemical reviews 116, 3029-3085 (2016).
227. R. H. Brown, A. Al-Chalabi, Amyotrophic Lateral Sclerosis. The New England journal of medicine 377, 162-172 (2017).
228. P. M. Andersen, Amyotrophic lateral sclerosis associated with mutations in the CuZn superoxide dismutase gene. Current neurology and neuroscience reports 6, 37-46 (2006).
229. E. D. Haasdijk, A. Vlug, M. T. Mulder, D. Jaarsma, Increased apolipoprotein E expression correlates with the onset of neuronal degeneration in the spinal cord of G93A-SOD1 mice. Neuroscience letters 335, 29-33 (2002).
230. M. K. Olsen et al., Disease mechanisms revealed by transcription profiling in SOD1-G93A transgenic mouse spinal cord. Annals of neurology 50, 730-740 (2001).
231. B. Moulard, A. Sefiani, A. Laamri, A. Malafosse, W. Camu, Apolipoprotein E genotyping in sporadic amyotrophic lateral sclerosis: evidence for a major influence on the clinical presentation and prognosis. Journal of the neurological sciences 139 Suppl, 34-37 (1996).
232. H. Zetterberg, J. Jacobsson, L. Rosengren, K. Blennow, P. M. Andersen, Association of APOE with age at onset of sporadic amyotrophic lateral sclerosis. Journal of the neurological sciences 273, 67-69 (2008).
233. V. E. Drory, M. Birnbaum, A. D. Korczyn, J. Chapman, Association of APOE epsilon4 allele with survival in amyotrophic lateral sclerosis. Journal of the neurological sciences 190, 17-20 (2001).

234. L. Lacomblez et al., APOE: a potential marker of disease progression in ALS. Neurology 58, 1112-1114 (2002).

235. Y. J. Li et al., Apolipoprotein E is associated with age at onset of amyotrophic lateral sclerosis. Neurogenetics 5, 209-213 (2004).

236. F. Govone et al., Lack of association between APOE gene polymorphisms and amyotrophic lateral sclerosis: a comprehensive meta-analysis. Amyotrophic lateral sclerosis & frontotemporal degeneration 15, 551-556 (2014).

237. A. Chio et al., The Role of APOE in the Occurrence of Frontotemporal Dementia in Amyotrophic Lateral Sclerosis. JAMA neurology 73, 425-430 (2016).

238. H. Y. Wang, I. F. Wang, J. Bose, C. K. Shen, Structural diversity and functional implications of the eukaryotic TDP gene family. Genomics 83, 130-139 (2004).

239. L. Heyburn, C. E. Moussa, TDP-43 in the spectrum of MND-FTLD pathologies. Molecular and cellular neurosciences 83, 46-54 (2017).

240. K. L. Youmans, B. Wolozin, TDP-43: a new player on the AD field? Experimental neurology 237, 90-95 (2012).

241. E. Buratti, F. E. Baralle, Multiple roles of TDP-43 in gene expression, splicing regulation, and human disease. Frontiers in bioscience : a journal and virtual library 13, 867-878 (2008).

242. M. Neumann, L. K. Kwong, D. M. Sampathu, J. Q. Trojanowski, V. M. Lee, TDP-43 proteinopathy in frontotemporal lobar degeneration and amyotrophic lateral sclerosis: protein misfolding diseases without amyloidosis. Archives of neurology 64, 1388-1394 (2007).

243. I. R. Mackenzie et al., A harmonized classification system for FTLD-TDP pathology. Acta neuropathologica 122, 111-113 (2011).

244. A. Kadokura, T. Yamazaki, C. A. Lemere, M. Takatama, K. Okamoto, Regional distribution of TDP-43 inclusions in Alzheimer disease (AD) brains: their relation to AD common pathology. Neuropathology : official journal of the Japanese Society of Neuropathology 29, 566-573 (2009).

245. K. Uryu et al., Concomitant TAR-DNA-binding protein 43 pathology is present in Alzheimer disease and corticobasal degeneration but not in other tauopathies. Journal of neuropathology and experimental neurology 67, 555-564 (2008).

246. C. Lagier-Tourenne, M. Polymenidou, D. W. Cleveland, TDP-43 and FUS/TLS: emerging roles in RNA processing and neurodegeneration. Human molecular genetics 19, R46-64 (2010).

247. M. Safieh, A. D. Korczyn, D. M. Michaelson, ApoE4: an emerging therapeutic target for Alzheimer's disease. BMC medicine 17, 64 (2019).

248. A. M. Wennberg et al., Association of Apolipoprotein E epsilon4 With Transactive Response DNA-Binding Protein 43. JAMA neurology 75, 1347-1354 (2018).

249. K. A. Josephs et al., Rates of hippocampal atrophy and presence of post-mortem

TDP-43 in patients with Alzheimer's disease: a longitudinal retrospective study. The Lancet. Neurology 16, 917-924 (2017).
250. K. A. Josephs et al., TDP-43 is a key player in the clinical features associated with Alzheimer's disease. Acta neuropathologica 127, 811-824 (2014).
251. K. A. Josephs, Fitting TDP-43 into the APOE epsilon4 and neurodegeneration story. The Lancet. Neurology 17, 735-737 (2018).
252. H. S. Yang et al., Evaluation of TDP-43 proteinopathy and hippocampal sclerosis in relation to APOE epsilon4 haplotype status: a community-based cohort study. The Lancet. Neurology 17, 773-781 (2018).
253. Y. Chornenkyy, D. W. Fardo, P. T. Nelson, Tau and TDP-43 proteinopathies: kindred pathologic cascades and genetic pleiotropy. Laboratory investigation; a journal of technical methods and pathology 99, 993-1007 (2019).
254. A. M. Herman, P. J. Khandelwal, B. B. Stanczyk, G. W. Rebeck, C. E. Moussa, beta-amyloid triggers ALS-associated TDP-43 pathology in AD models. Brain research 1386, 191-199 (2011).
255. E. B. Lee, V. M. Lee, J. Q. Trojanowski, Gains or losses: molecular mechanisms of TDP43-mediated neurodegeneration. Nat Rev Neurosci 13, 38-50 (2011).
256. Y. S. Fang et al., Full-length TDP-43 forms toxic amyloid oligomers that are present in frontotemporal lobar dementia-TDP patients. Nature communications 5, 4824 (2014).
257. J. Y. Tann, L. W. Wong, S. Sajikumar, C. F. Ibanez, Abnormal TDP-43 function impairs activity-dependent BDNF secretion, synaptic plasticity, and cognitive behavior through altered Sortilin splicing. The EMBO journal 38, (2019).
258. Y. H. Liu et al., Associations Between ApoEepsilon4 Carrier Status and Serum BDNF Levels–New Insights into the Molecular Mechanism of ApoEepsilon4 Actions in Alzheimer's Disease. Molecular neurobiology 51, 1271-1277 (2015).
259. A. Alvarez, M. Aleixandre, C. Linares, E. Masliah, H. Moessler, Apathy and APOE4 are associated with reduced BDNF levels in Alzheimer's disease. Journal of Alzheimer's disease : JAD 42, 1347-1355 (2014).
260. O. V. Forlenza et al., Decreased Neurotrophic Support is Associated with Cognitive Decline in Non-Demented Subjects. Journal of Alzheimer's disease : JAD 46, 423-429 (2015).
261. S. Nakamura et al., Transthyretin amyloidosis and two other aging-related amyloidoses in an aged vervet monkey. Veterinary pathology 45, 67-72 (2008).
262. A. Merched et al., Apolipoprotein E, transthyretin and actin in the CSF of Alzheimer's patients: relation with the senile plaques and cytoskeleton biochemistry. FEBS letters 425, 225-228 (1998).
263. S. Craft et al., P-027: CSF transthyretin levels are associated with APOE genotype and CSF Aβ42 in AD. (2007), vol. 3, pp. S104–S105.
264. B. Mazur-Kolecka, J. Frackowiak, H. M. Wisniewski, Apolipoproteins E3 and E4

induce, and transthyretin prevents accumulation of the Alzheimer's beta-amyloid peptide in cultured vascular smooth muscle cells. Brain research 698, 217-222 (1995).
265. A. L. Schwarzman et al., Transthyretin sequesters amyloid beta protein and prevents amyloid formation. Proceedings of the National Academy of Sciences of the United States of America 91, 8368-8372 (1994).
266. M. Jadoul, C. Garbar, C. Strihou, Pathological Aspects of β2-Microglobulin Amyloidosis. (2001), vol. 14, pp. 86-89.
267. S. L. Myers et al., A systematic study of the effect of physiological factors on beta2-microglobulin amyloid formation at neutral pH. Biochemistry 45, 2311-2321 (2006).
268. F. Gejyo, I. Narita, Current clinical and pathogenetic understanding of beta2-m amyloidosis in long-term haemodialysis patients. Nephrology 8 Suppl, S45-49 (2003).
269. S. Yamamoto, J. J. Kazama, I. Narita, H. Naiki, F. Gejyo, Recent progress in understanding dialysis-related amyloidosis. Bone 45 Suppl 1, S39-42 (2009).
270. I. Yamaguchi, K. Hasegawa, N. Takahashi, F. Gejyo, H. Naiki, Apolipoprotein E inhibits the depolymerization of beta 2-microglobulin-related amyloid fibrils at a neutral pH. Biochemistry 40, 8499-8507 (2001).
271. M. S. Kindy, A. R. King, G. Perry, M. C. de Beer, F. C. de Beer, Association of apolipoprotein E with murine amyloid A protein amyloid. Laboratory investigation; a journal of technical methods and pathology 73, 469-475 (1995).
272. M. S. Kindy, D. J. Rader, Reduction in amyloid A amyloid formation in apolipoprotein-E-deficient mice. The American journal of pathology 152, 1387-1395 (1998).
273. J. Shorter, Phase separation of RNA-binding proteins in physiology and disease: An introduction to the JBC Reviews thematic series. The Journal of biological chemistry 294, 7113-7114 (2019).
274. S. Wegmann et al., Tau protein liquid-liquid phase separation can initiate tau aggregation. The EMBO journal 37, (2018).
275. A. E. Conicella, G. H. Zerze, J. Mittal, N. L. Fawzi, ALS Mutations Disrupt Phase Separation Mediated by alpha-Helical Structure in the TDP-43 Low-Complexity C-Terminal Domain. Structure 24, 1537-1549 (2016).
276. S. Elbaum-Garfinkle, Matter over mind: Liquid phase separation and neurodegeneration. The Journal of biological chemistry 294, 7160-7168 (2019).
277. B. C. Farmer, J. Kluemper, L. A. Johnson, Apolipoprotein E4 Alters Astrocyte Fatty Acid Metabolism and Lipid Droplet Formation. Cells 8, (2019).
278. Y. Yamazaki, N. Zhao, T. R. Caulfield, C. C. Liu, G. Bu, Apolipoprotein E and Alzheimer disease: pathobiology and targeting strategies. Nat Rev Neurol 15, 501-518 (2019).
279. M. Jucker, L. C. Walker, Self-propagation of pathogenic protein aggregates in neurodegenerative diseases. Nature 501, 45-51 (2013).

280. J. Luo, S. K. Warmlander, A. Graslund, J. P. Abrahams, Cross-interactions between the Alzheimer Disease Amyloid-beta Peptide and Other Amyloid Proteins: A Further Aspect of the Amyloid Cascade Hypothesis. The Journal of biological chemistry 291, 16485-16493 (2016).
281. A. Schneider, W. Schulz-Schaeffer, T. Hartmann, J. B. Schulz, M. Simons, Cholesterol depletion reduces aggregation of amyloid-beta peptide in hippocampal neurons. Neurobiol Dis 23, 573-577 (2006).
282. K. Matsuzaki, K. Kato, K. Yanagisawa, Abeta polymerization through interaction with membrane gangliosides. Biochim Biophys Acta 1801, 868-877 (2010).
283. M. Corraliza-Gomez, D. Sanchez, M. D. Ganfornina, Lipid-Binding Proteins in Brain Health and Disease. Front Neurol 10, 1152 (2019).
284. J. L. Browning, Motions and interactions of phospholipid head groups at the membrane surface. 2. Simple alkyl head groups. Biochemistry 20, 7123-7133 (1981).
285. Z. Jiang, R. E. Redfern, Y. Isler, A. H. Ross, A. Gericke, Cholesterol stabilizes fluid phosphoinositide domains. Chemistry and physics of lipids 182, 52-61 (2014).
286. B. X. Wong, Y. H. Hung, A. I. Bush, J. A. Duce, Metals and cholesterol: two sides of the same coin in Alzheimer's disease pathology. Frontiers in aging neuroscience 6, 91 (2014).
287. F. Glöckner, T. G. Ohm, Tau pathology induces intraneuronal cholesterol accumulation. Journal of neuropathology and experimental neurology 73, 846-854 (2014).
288. A. Rahman et al., High cholesterol diet induces tau hyperphosphorylation in apolipoprotein E deficient mice. FEBS letters 579, 6411-6416 (2005).
289. R. van der Kant et al., Cholesterol Metabolism Is a Druggable Axis that Independently Regulates Tau and Amyloid-beta in iPSC-Derived Alzheimer's Disease Neurons. Cell stem cell 24, 363-375 e369 (2019).
290. H. L. Cui et al., Prion infection impairs cholesterol metabolism in neuronal cells. The Journal of biological chemistry 289, 789-802 (2014).
291. S. Hannaoui, S. Y. Shim, Y. C. Cheng, E. Corda, S. Gilch, Cholesterol balance in prion diseases and Alzheimer's disease. Viruses 6, 4505-4535 (2014).
292. A. J. Beel, M. Sakakura, P. J. Barrett, C. R. Sanders, Direct binding of cholesterol to the amyloid precursor protein: An important interaction in lipid-Alzheimer's disease relationships? Biochimica et biophysica acta 1801, 975-982 (2010).
293. M. Simons et al., Cholesterol depletion inhibits the generation of beta-amyloid in hippocampal neurons. Proceedings of the National Academy of Sciences of the United States of America 95, 6460-6464 (1998).
294. N. A. Avdulov et al., Lipid binding to amyloid beta-peptide aggregates: preferential binding of cholesterol as compared with phosphatidylcholine and fatty acids. Journal of neurochemistry 69, 1746-1752 (1997).

295. R. M. Lane, M. R. Farlow, Lipid homeostasis and apolipoprotein E in the development and progression of Alzheimer's disease. Journal of lipid research 46, 949-968 (2005).

296. Y. H. Hung, A. I. Bush, S. La Fontaine, Links between copper and cholesterol in Alzheimer's disease. Frontiers in physiology 4, 111 (2013).

297. P. S. Hauser, V. Narayanaswami, R. O. Ryan, Apolipoprotein E: from lipid transport to neurobiology. Prog Lipid Res 50, 62-74 (2011).

298. L. Liu et al., Glial Lipid Droplets and ROS Induced by Mitochondrial Defects Promote Neurodegeneration. Cell 160, 177-190 (2015).

299. L. Liu, K. R. MacKenzie, N. Putluri, M. Maletić-Savatić, H. J. Bellen, The Glia-Neuron Lactate Shuttle and Elevated ROS Promote Lipid Synthesis in Neurons and Lipid Droplet Accumulation in Glia via APOE/D. Cell Metabolism 26, 719-737.e716 (2017).

300. R. Lahdo, L. De La Fourniere-Bessueille, Insertion of the amyloid precursor protein into lipid monolayers: effects of cholesterol and apolipoprotein E. The Biochemical journal 382, 987-994 (2004).

301. T. Kawarabayashi et al., Dimeric amyloid beta protein rapidly accumulates in lipid rafts followed by apolipoprotein E and phosphorylated tau accumulation in the Tg2576 mouse model of Alzheimer's disease. The Journal of neuroscience : the official journal of the Society for Neuroscience 24, 3801-3809 (2004).

302. W. Gibson Wood, G. P. Eckert, U. Igbavboa, W. E. Muller, Amyloid beta-protein interactions with membranes and cholesterol: causes or casualties of Alzheimer's disease. Biochimica et biophysica acta 1610, 281-290 (2003).

303. C. La Rosa et al., Symmetry-breaking transitions in the early steps of protein self-assembly. European Biophysics Journal 49, 175-191 (2020).

304. F. Scollo, C. La Rosa, Amyloidogenic Intrinsically Disordered Proteins: New Insights into Their Self-Assembly and Their Interaction with Membranes. Life (Basel, Switzerland) 10, (2020).

305. C. Frieden, H. Wang, C. M. W. Ho, A mechanism for lipid binding to apoE and the role of intrinsically disordered regions coupled to domain–domain interactions. Proceedings of the National Academy of Sciences 114, 6292 (2017).

306. J. Walter, G. van Echten-Deckert, Cross-talk of membrane lipids and Alzheimer-related proteins. Molecular Neurodegeneration 8, 34 (2013).

307. C. Wang et al., Gain of toxic apolipoprotein E4 effects in human iPSC-derived neurons is ameliorated by a small-molecule structure corrector. Nature medicine 24, 647-657 (2018).

308. H.-K. Chen et al., Small Molecule Structure Correctors Abolish Detrimental Effects of Apolipoprotein E4 in Cultured Neurons. (2011), vol. 287, pp. 5253-5266.

309. R. W. Mahley, Y. Huang, Small-molecule structure correctors target abnormal protein structure and function: structure corrector rescue of apolipoprotein E4-associated neuropathology. Journal of medicinal chemistry 55, 8997-9008 (2012).
310. M. Goyal et al., Novel Natural Structure Corrector of ApoE4 for Checking Alzheimer's Disease: Benefits from High Throughput Screening and Molecular Dynamics Simulations. (2013), vol. 2013, pp. 620793.
311. J. B. Rosenberg et al., AAVrh.10-Mediated APOE2 Central Nervous System Gene Therapy for APOE4-Associated Alzheimer's Disease. Human gene therapy. Clinical development 29, 24-47 (2018).
312. J. Hu et al., Opposing effects of viral mediated brain expression of apolipoprotein E2 (apoE2) and apoE4 on apoE lipidation and Abeta metabolism in apoE4-targeted replacement mice. Molecular neurodegeneration 10, 6 (2015).
313. L. Zhao et al., Intracerebral adeno-associated virus gene delivery of apolipoprotein E2 markedly reduces brain amyloid pathology in Alzheimer's disease mouse models. Neurobiology of aging 44, 159-172 (2016).
314. S. Liu et al., Targeting Apolipoprotein E/Amyloid beta Binding by Peptoid CPO_Abeta17-21 P Ameliorates Alzheimer's Disease Related Pathology and Cognitive Decline. Scientific reports 7, 8009 (2017).
315. J. Legleiter et al., Effect of different anti-Abeta antibodies on Abeta fibrillogenesis as assessed by atomic force microscopy. Journal of molecular biology 335, 997-1006 (2004).
316. B. Solomon, R. Koppel, D. Frankel, E. Hanan-Aharon, Disaggregation of Alzheimer beta-amyloid by site-directed mAb. Proceedings of the National Academy of Sciences of the United States of America 94, 4109-4112 (1997).
317. D. Frenkel, O. Katz, B. Solomon, Immunization against Alzheimer's beta -amyloid plaques via EFRH phage administration. Proceedings of the National Academy of Sciences of the United States of America 97, 11455-11459 (2000).
318. G. L. Suidan, G. Ramaswamy, Targeting Apolipoprotein E for Alzheimer's Disease: An Industry Perspective. Int J Mol Sci 20, (2019).
319. A. M. Di Battista, N. M. Heinsinger, G. W. Rebeck, Alzheimer's Disease Genetic Risk Factor APOE-epsilon4 Also Affects Normal Brain Function. Curr Alzheimer Res 13, 1200-1207 (2016).
320. K. Blennow, M. J. de Leon, H. Zetterberg, Alzheimer's disease. Lancet (London, England) 368, 387-403 (2006).
321. E. J. Coulthard, S. Love, A broader view of dementia: multiple co-pathologies are the norm. Brain : a journal of neurology 141, 1894-1897 (2018).
322. L. Bain, N. I. Keren, C. Stroud, Developing Multimodal Therapies for Brain Disorders. (2017).

323. J. Foraker et al., The APOE Gene is Differentially Methylated in Alzheimer's Disease. Journal of Alzheimer's disease : JAD 48, 745-755 (2015).
324. V. Theendakara et al., Direct Transcriptional Effects of Apolipoprotein E. J Neurosci 36, 685-700 (2016).
325. A. Di Francesco et al., Global changes in DNA methylation in Alzheimer's disease peripheral blood mononuclear cells. Brain, behavior, and immunity 45, 139-144 (2015).
326. T. T. T. Tran et al., APOE genotype influences the gut microbiome structure and function in humans and mice: relevance for Alzheimer's disease pathophysiology. FASEB J 33, 8221-8231 (2019).
327. D. Saita et al., Adaptive immunity against gut microbiota enhances apoE-mediated immune regulation and reduces atherosclerosis and western-diet-related inflammation. Scientific reports 6, 29353 (2016).

Chapter 3

ATP impedes the inhibitory effect of Hsp90 on Aβ40 fibrillation

Hongzhi Wang[1], Max Lallemang[2,3], Bianca Hermann[2], Cecilia Wallin[4], Rolf Loch[1], Alain Blanc[5], Bizan N. Balzer[2,3], Thorsten Hugel[2,3], Jinghui Luo[1]

1. Department of Biology and Chemistry, Paul Scherrer Institute, 5232 Villigen, Switzerland.
2. Institute of Physical Chemistry, University of Freiburg, Albertstraße 21, 79104 Freiburg, Germany.
3. Cluster of Excellence livMatS @ FIT – Freiburg Center for Interactive Materials and Bioinspired Technologies, University of Freiburg, Georges-Köhler-Allee 105, D-79110 Freiburg, Germany.
4. Department of Biochemistry and Biophysics, Stockholm University, 10691 Stockholm, Sweden.
5. Center for Radiopharmaceutical Sciences, Paul Scherrer Institute, 5232 Villigen, Switzerland.
Corresponding author: Jinghui.luo@psi.ch, +41 56 310 47 64

Published in Journal of molecular biology. DOI: 10.1016/j.jmb.2020.11.016

3.1 Abstract

Heat shock protein 90 (Hsp90) is a molecular chaperone that assists protein folding in an Adenosine triphosphate (ATP)-dependent way. Hsp90 has been reported to interact with Alzheimer´s disease associated amyloid-β(Aβ) peptides and to suppress toxic oligomer- and fibril formation. However, the mechanism remains largely unclear. Here we use a combination of atomic force microscopy (AFM) imaging, circular dichroism (CD) spectroscopy and biochemical analysis to quantify this interaction and put forward a microscopic picture including rate constants for the different transitions towards fibrillation. We show that Hsp90 binds to Aβ40 monomers weakly but inhibits Aβ40 from growing into fibrils at substoichiometric concentrations. ATP impedes this interaction, presumably by modulating Hsp90's conformational dynamics and reducing its hydrophobic surface. Altogether, these results might indicate alternative ways to prevent Aβ40 fibrillation by manipulating chaperones that are already abundant in the brain.

Keywords: Hsp90, Aβ40, fibrillation, conformation, hydrophobic interaction

3.2 Introduction

Heat shock protein 90 (Hsp90) is a ubiquitously expressed, evolutionarily conserved, and highly dynamic molecular chaperone, which mainly consists of three structural domains: an N-terminal ATP-binding domain, a middle domain for client protein binding, and a C-terminal dimerization domain (1). Hsp90, including yeast Hsp90 (Hsp82) used in this study (Table.S1), usually locate intracellularly (2, 3), but can also be secreted into extracellular space (4). It participates in a variety of cellular processes including cell survival, hormone signaling, cell cycle control and response to cellular (heat) stress (5-9), as well as in assisting folding, maturation and degradation of more than 200 'client proteins' in eukaryotes (10-13). These functions of Hsp90 are achieved in concert with different co-chaperones and adaptor proteins and often with the help of ATP (8, 14).

Amyloid-β (Aβ) peptide fibrillation and accumulation are usually triggered by a conformational transition from random coil to β-sheet secondary structures and progresses via the classical lag-, elongation-, and plateau- phases, in which hydrophobic interactions are involved (15, 16). These processes usually take place extracellularly and play central roles in the progression of Alzheimer's disease according to the amyloid cascade hypothesis (15, 17). However, Aβ can be produced intracellularly or taken up from extracellular space to the cytoplasm through receptor binding and subsequent internalization and accumulates intracellularly including in mitochondria (18). Intracellular Aβ

accumulation influences a variety of physiological activities like autophagy, degradation and apoptosis, indicative of the crucial role of intracellular Aβ in Alzheimer's disease (19, 20). Recent evidence suggests that lipid raft and lipid membranes play crucial roles in Alzheimer's disease by promoting the production and oligomer formation of Aβ peptides, while Aβ oligomers can bind to lipid membranes and induce the aberrant clustering of lipid raft and membranes (21, 22). As the disease progresses, intracellular Aβ oligomers may interact with lipid membranes, induce neuronal dysfunction, or pass into the extracellular space as a source of fibril deposits (18). Changes in the raft-lipid composition or membranes of the cells can induce the release of heat shock proteins, like Hsp90, from cytoplasm to modulate intercellular signaling (23, 24). In vivo studies indicate that intracellular chaperones can play a role in modulating intracellular Aβ metabolism and toxicity (25). Thus interactions between Hsp90 and Aβ can possibly take place both extracellularly and intracellularly, while Aβ aggregation mainly occur extracellularly. The In vivo interaction between Hsp90 and Aβ and the physiological relevance of this interaction remain to be explored. Molecular chaperones such as Hsp90 are in the first line of the cellular defense system against protein aggregation. A growing body of evidence indicates that Hsp90 inhibits amyloid protein aggregation, cellular toxicity, or clearance of Alzheimer's Aβ (10, 26-29), but the molecular mechanism of Hsp90 modulating Aβ remains unknown. For instance, does Hsp90 interfere with Aβ fibrillation in an ATP-dependent and/or specific way? How do different Hsp90 conformations influence Aβ fibrillation? In which phase does Hsp90 interfere with Aβ fibrillation?

To answer these questions, we investigated how Aβ40 fibrillation is affected by dimeric wild type Hsp90 (WT), Hsp90 tetramer, and the ATPase defective mutant E33A also lacking the charged linker region between the N-terminal and middle domains (30). We assumed that each one has a different dynamics in equilibrium, therefore exposing varied time-dependent hydrophobic surfaces as possible client binding sites. The fibrillation of Aβ was observed with atomic force microscopy (AFM) imaging under various environmental conditions, by Thioflavin T (ThT) fluorescence, circular dichroism (CD) spectroscopy and SDS-PAGE. AFM imaging has already revealed a variety of structural information about Aβ40 aggregation (31-34) and its interaction with small molecules (35-37). Furthermore, AFM imaging was also previously used to support that the chaperones Hsp60 (38), GroEL (39) and HspB1 (40) inhibit Aβ40 aggregation. However, to the best of our knowledge neither the role of Hsp90 on the Aβ40 aggregation, nor the effect of ATP on this system have been studied by AFM experiments yet. In addition, our specific modulation of Hsp90 allows us to put forward a mechanism for the inhibition of fibril growth. We observed that all three Hsp90 forms inhibit Aβ40 fibrillation to different degrees and this effect of Hsp90 can be impeded by the addition of ATP, which can induce a change in the conformation dynamics and hydrophobicity of Hsp90. We

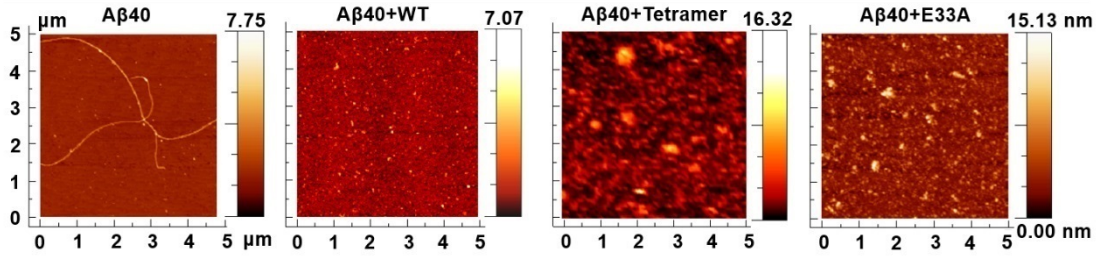

FIGURE 1: Hsp90 inhibits fibril formation of Aβ40. AFM images of 10 μM Aβ40 in the presence or absence of 0.5 μM Hsp90 forms (WT, tetramer, or E33A mutant) after incubation at 37 °C for 24 h at 300 rpm, show that Hsp90 morphologically inhibits the fibril formation of Aβ40. The color scales indicate height values.

therefore suggest that Hsp90 inhibits Aβ40 fibrillation through the modulation of conformational dynamics and hydrophobic surfaces. Our results provide a new perspective for the mechanism of inhibition of amyloid fibrillation by Hsp90 and other chaperones.

3.3 Results

3.3.1 Hsp90 inhibits Aβ40 fibrillation

We used AFM in air to investigate the morphology changes of the Aβ40 peptides in the absence or presence of Hsp90 dimers (wild type), tetramers, and an ATPase-deficient E33A mutant. **Fig.1** shows the AFM images recorded after an incubation of 10 μM Aβ40 alone or with 0.5 μM Hsp90 variants at 37 °C for 24 h. The Aβ40 sample alone forms fibrils in an unbranched, twisted helical morphology while the Aβ40 samples in the presence of the three Hsp90 forms display other distinct morphologies. In the presence of Hsp90 proteins, the Aβ40 peptides aggregated into irregular small amorphous aggregates. Likely, the larger Aβ40 aggregates observed in the presence of the Hsp90 tetramer may result from the co-aggregation with the Aβ40 peptides and the aggregation-prone tetramer. This result indicates that Hsp90 proteins suppress the formation of Aβ40 fibrils, but to different degrees depending on their forms, WT induced the formation of smaller amorphous aggregates compared with tetramer and E33A, suggesting that WT is probably the most efficient one to inhibit the Aβ40 fibrillation.

3.3.2 Hsp90 inhibits Aβ40 peptide secondary structure transitions during fibrillation

To investigate the influence of Hsp90 proteins on the Aβpeptide secondary structures, we carried out CD spectroscopy measurements. CD spectra were recorded over time to

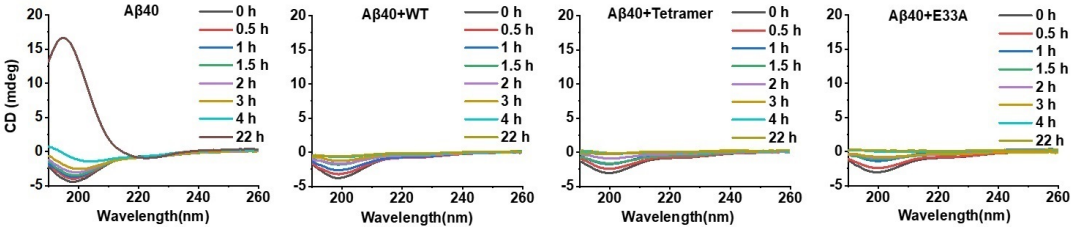

FIGURE 2: Hsp90 inhibits secondary structure transition of Aβ40. CD spectroscopy of 10 μM Aβ40 in the presence or absence of 0.04 μM Hsp90 (WT, tetramer, and E33A mutant) after incubation at 37 °C and measured immediately after mixing with a pipette, indicates that Hsp90 prevents the secondary structural transition of Aβ40 from random coil to β-sheets.

quantify the secondary structure transition of the Aβ40 peptides with or without the different Hsp90 forms. The aggregation of 10 μM Aβ40 in the presence or absence of 0.04 μM Hsp90 were monitored in the far-UV region from 190 to 260 nm after 0, 0.5, 1, 1.5, 2, 3, 4, 5, 6, 7, 8, and 22 h incubation at 37 °C. **Fig.2** and **Fig.S1** illustrate that the CD spectrum of Aβ40 at time zero is characterized by a typical random coil conformation, with a characteristic minimum at ˜198 nm. As the incubation time increases, the random coil conformation of Aβ40 converts gradually into the typical β-sheet structure showing the characteristic curve with a minimum at ˜220 nm and a maximum at ˜195 nm via an isodichroic point at ˜210 nm, similar to the result in our previous study (41). However, in the presence of Hsp90 proteins, no signal corresponding to a β-sheet secondary structure conformation is observed and the signal of the initial Aβ40 random coil secondary structure conformation decreases step by step as the incubation carries on and finally disappears. The latter might, to a large extent, be caused by some large aggregates formed by Hsp90 and Aβ40. Three Hsp90 forms at a low concentration of 0.04 μM are similarly efficient in inhibiting the secondary structure transition of the Aβ40 peptides. Based on our AFM and CD spectroscopy results, we suggest that Hsp90 structurally modulates the transition pathway of Aβ40 aggregation and morphologically impedes the formation of Aβ40 fibrils.

3.3.3 Hsp90 impedes the secondary pathways

By using a ThT kinetics assay, we investigated how Aβ40 amyloid fibrillation kinetics is modulated by Hsp90 proteins. ThT is a commonly used fluorescence dye to monitor the formation of amyloid fibrils, as its fluorescence intensity sharply increases when bound to amyloid fibrils (42). **Fig.3** and **Fig.S2A** show the results of the ThT kinetic fluorescence assays. In non-agitating condition, all Hsp90 proteins inhibit Aβ40 fibrillation in a concentration-dependent manner, with WT being the most efficient, probably because it is more dynamic than the other forms. The general aggregation course of amyloid

protein aggregation is shown in **Fig.3A**. Calculated from sigmoidal curve fitting, the phenomenological parameters t_{lag} and $t_{1/2}$ of the fibrillation of 10 μM Aβ40 alone were estimated to t_{lag} = 8.6±1.56 h and $t_{1/2}$ = 10.8±0.95 h and Hsp90 significantly prolongs the t_{lag} and $t_{1/2}$ of the fibrillation, as the concentration of Hsp90 increases (**Fig.3B** and **C**).

To get further insight into the microscopic mechanisms of Aβ40 fibrillation in the presence of Hsp90, global fit analysis of the kinetic data was performed with an integrated rate law (43-46) by using the AmyloFit online software server (47). It has been reported that amyloid proteins usually aggregate through either primary or secondary dominated pathways (44, 48) and Aβ40 undergoes fibrillation mainly via secondary nucleation processes (41, 48). Therefore, we selected the secondary nucleation dominated model and first fitted the ThT data of Aβ40 alone, obtaining a set of parameters including the primary nucleation rate constant k_n = 0.00174 in concentration^{-nc+1}time^{-1} (nc is the reaction order of primary nucleation that simply interpretates a nucleus size), the secondary nucleation rate constant (k_2)=7.11e^{+7} in concentration^{-n2} time^{-1} (n2 is the reaction order of secondary nucleation that simply interpretates a nucleus size), and the elongation rate constant (k_+) = 9.22e^{+6} in concentration^{-1} time^{-1} of Aβ40 fibrillation process, which were used as the initial guess values for the following fit. Each one of the three rate constants (k_n, k_2, k_+) was fitted freely, while the other two were kept as initial guess values. The result of the global fit analysis is shown in **Fig.3D** and the relative rate constants derived from the global fit are presented in **Fig.3E**. The global fit analysis depicts that if the rate constants k_2 and k_+, rather than the k_n, were freely fitted, the results can describe the Hsp90-dependent aggregation data, suggesting that the secondary pathways (the secondary nucleation and/or elongation processes) of Aβ40 aggregation are the ones mostly affected by Hsp90 proteins.

3.3.4 Hsp90 modulates the hydrophobic surface of Aβ40 peptides

To determine which microscopic rate constant, k_2 or k_+, of Aβ40 is most influenced by Hsp90, we performed seeding experiments of Aβ40 peptide fibrillation kinetics in the presence and absence of Hsp90 proteins. Pre-formed Aβ40 seeds were added at time zero to the samples with Aβ40 monomers and Hsp90 proteins. In the presence of seeds, the primary nucleation processes are nearly negligible compared to the secondary processes. At a high seed concentration, with a concave ThT aggregation kinetic curve, the growth of fibrillary aggregates mainly originates from elongation processes. The results of the seeding assays in **Fig.4A** and **Fig.S2B** show the absolute and normalized signal corresponding to the aggregation concentration, respectively. It illustrates that the addition of Aβ40 seeds to Aβ40 monomers (the Aβ40+seeds curve) significantly

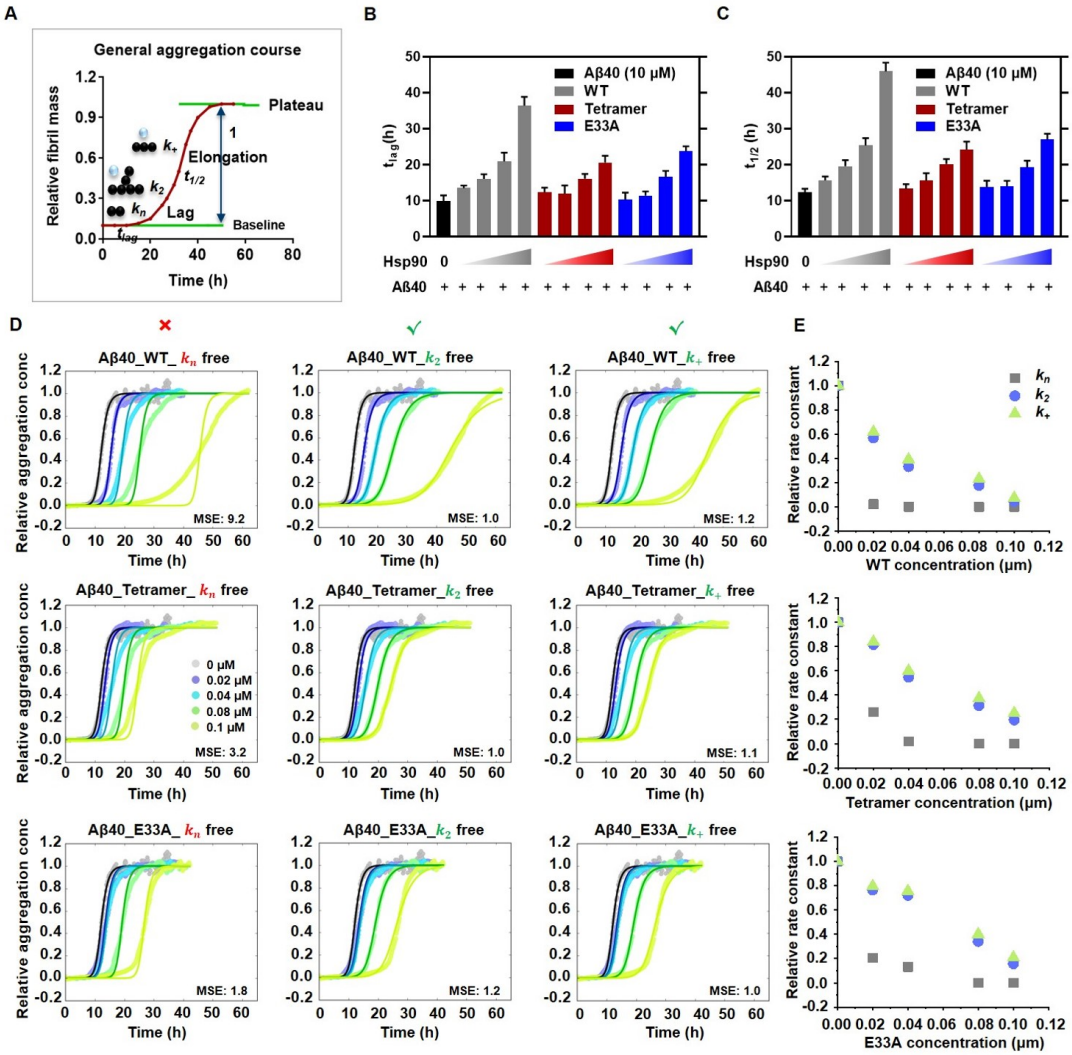

FIGURE 3: Aβ40 aggregation kinetics. **(A)** General aggregation course of amyloid protein fibrillation. Typically, this process goes through the lag-, elongation-, and plateau-phases, in which primary nucleation (rate constant k_n and t_{lag}), secondary nucleation (rate constant k_2), and/or elongation (k_+ and $t_{1/2}$) processes are involved, respectively. **(B)** and **(C)** The t_{lag} and $t_{1/2}$ of the fibrillation of 10 μM Aβ40 in the absence or presence of different Hsp90 forms (WT, tetramer, and E33A) at concentrations of 0.02, 0.04, 0.08, and 0.1 μM, were derived from sigmoidal fitting of ThT data of each repeat. Error bars represent standard deviation of at least three replicates **(D)** Secondary processes of Aβ40 fibrillation are influenced by Hsp90. Aggregation kinetics of 10 μM Aβ40 in the absence or presence of different Hsp90 forms were monitored by ThT fluorescence over time (the raw data can be found in **Fig.S2A**) and then globally fitted by using the AmyloFit online software server (47).For the fitting procedure, the data of Aβ40 alone were first fitted (the result is shown in **Fig.S3**) with a secondary nucleation dominated model, from which a set of parameters including $k_n = 0.00174$ in concentration^{-nc+1}time^{-1},$k_2 = 7.11\text{e}^{+7}$ in concentration^{-n2} time^{-1}, and $k_+ = 9.22\text{e}^{+6}$ in concentration^{-1}time^{-1} of Aβ40 fibrillation were obtained and used as the initial guess values for the following global fit. Each one of the rate constants k_n, k_2, or k_+ was fitted freely, while the other two were set as initial guess values, by choosing the secondary nucleation dominated model. When k_2 and k_+, but not k_n, were freely fitted then the data was well described (see main text for details). The mean square error (MSE) values for each set of Aβ40 and Hsp90 samples were normalized against the one with the best fit (lowest MSE value). **(E)** Relative rate constants (relative to the rate constants of Aβ40 alone) derived from global fitting for different concentrations of Hsp90

speeds up the Aβ40 fibrillation, reaching the plateau phase within the time the unseeded Aβ40 sample remains in the lag phase. Notably, the seeded kinetic curve shows a concave shape in opposite to the sigmoidal curve for unseeded Aβ40. The unseeded samples with Aβ40 supplemented with Hsp90 proteins dramatically slow down the process with slower aggregation kinetics with sigmoidal curves. This is consistent with the results of ThT assay in **Fig.3** that all variants inhibit Aβ40 fibrillation, with WT being the most efficiently. In both **Fig.3D** and **4A**, the mutant E33A without ATPase activity inhibits Aβ40 fibrillation, suggesting that Aβ40 may not only bind to one specific site on Hsp90, and that the ATPase activity is also not the only determinant in the effect of Hsp90 on Aβ40 fibrillation. In the presence of both Aβ40 seeds and Hsp90, the fibrillation process of Aβ40 is prolonged as compared to Aβ40 alone without seeds. This indicates that the elongation process of Aβ40 fibrillation with seeds is significantly inhibited by Hsp90.

As both hydrophobic and electrostatic interactions play an important role in the aggregation process of amyloid proteins (16), we performed ANS (8-anilino-1-naphthalenesulfonic acid) (49) fluorescence studies (see methods) to understand the effect of Hsp90 protein on the surface hydrophobic reorganization of Aβ40 peptides. The ANS assay was conducted for10 μM Aβ40 in the presence or absence of 0.1 μM Hsp90 protein forms, to check how Hsp90 influence the hydrophobic surface and the fibrillation behavior of Aβ40 (**Fig.4B**). The decrease of the fluorescence signal after the addition of Hsp90 WT, tetramer or mutant (E33A) compared to that of Aβ40 alone, suggests that the hydrophobic surface of Aβ40 to interact with ANS is decreased. Among these Hsp90 proteins, Hsp90 WT is the most effective one to reduce the hydrophobic surface of Aβ40, which is in line with our ThT data, with Hsp90 WT as the most effective inhibitor against the fibrillation. This suggests that the accessible hydrophobic surfaces of Aβhave a crucial role in Aβ fibrillation (50). But if this was the only effect, a red-shift of the emission peak would have been expected. Therefore, some electrostatic interaction will also be involved (51).

To further investigate the aggregation behavior, a photo-induced cross-linking experiment was carried out to stabilize 90 μM Aβ40, in the absence or presence of 2 μM Hsp90. The data in **Fig.4C** and **D** suggest that Aβ40 alone aggregates into a series of different oligomer sizes, but that Hsp90 significantly retains Aβ40 as monomers on the SDS-PAGE gel, with the wild type Hsp90 being the most efficient.

Therefore, we can propose that the Hsp90 slows down the elongation process of Aβ40 fibrillation presumably by decreasing the accessible hydrophobic surfaces of Aβ40 and thus keeping the peptides as monomers or small oligomers.

To further confirm this observation, we continued with a photo-induced cross-linking assay (52, 53) to stabilize Aβ40 samples but this time at the end point of the ThT assay (**Fig.4E**, results of reference experiments conducted with samples at 0 h are shown in

Fig.S4B, indicating that Hsp90s almost show no effect on Aβ40 fibrillation at time zero of ThT experiment). In the presence of Hsp90, Aβ40 monomers were observed, while almost no Aβ40 monomers were found in the absence of Hsp90 on the SDS-PAGE gel after the cross-linking assay, which might be caused by the formation of the fibrils that are too large to go through the SDS-PAGE gel. **Fig. 4C** shows also shows some higher-molecular-weight proteins, which probably are Hsp90 aggregates after the cross-linking at a high concentration (2 μM), which is less present at a low concentration (0.5 μM) (**Fig.4E**). In **Fig.4E**, the bands above 170 kDa can be SDS-resistant wild-type or E33A Hsp90 tetramers and Aβ40 fibrils do not run into the page because of the insolubility. 10 μM Aβ40 peptides in the presence of 0.5 μM Hsp90 likely remain as monomers before (**Fig.S4B**) or after (**Fig.4E**) the ThT assay, supporting that 0.5 μM Hsp90 WT or variant completely suppresses Aβ40 fibrillation in **Fig.S4A**. These results also show that Hsp90 retains Aβ40 as mainly monomeric species and slows down the fibril formation in vitro.

3.3.5 ATP modulates the hydrophobic surface of Hsp90 and thereby Aβ40 fibrillation

To investigate the potential mechanism by which ATP affects the protective activity of Hsp90 protein against Aβ40 fibrillation, we conducted kinetic aggregation studies with 10 μM Aβ40 and 0.1 μM Hsp90 (WT) in the absence or presence of 2 mM ATP or AMP-PNP. It is well known that ATP slightly shifts Hsp90 towards a closed conformation and AMP-PNP mainly locks Hsp90 in the closed conformation (1, 54). The aggregation kinetics observed in **Fig.5A** and **Fig.S2C** indicate that ATP or AMP-PNP on its own (i.e. in the absence of Hsp90) does not significantly influence Aβ40 fibrillation, but that both negatively regulate the effect of Hsp90 on Aβ40 fibrillation.

Again, we used the ANS fluorescence assay to test for hydrophobic surfaces, this time of 6 μM Hsp90 (WT) on its own, in the absence or presence of 2 mM ATP or AMP-PNP. **Fig.5B** shows the reduction of the hydrophobic surface of Hsp90 upon the addition of the nucleotides, which likely has the negative regulatory inhibition efficiency of Hsp90 against Aβ40 fibrillation. Our hydrophobicity assay agrees with the observed fibrillation kinetics: the accessible hydrophobic surface decreases from apo Hsp90 to ATP/Hsp90 to AMP-PNP/Hsp90, similar to the inhibitory effects of Hsp90 on Aβ40 fibrillation in **Fig.5A**. The decrease of Hsp90 inhibition by AMP-PNP is not as strong as for ATP, indicating that the hydrophobicity is not the only determinant, but that conformational dynamics likely also plays a significant role.

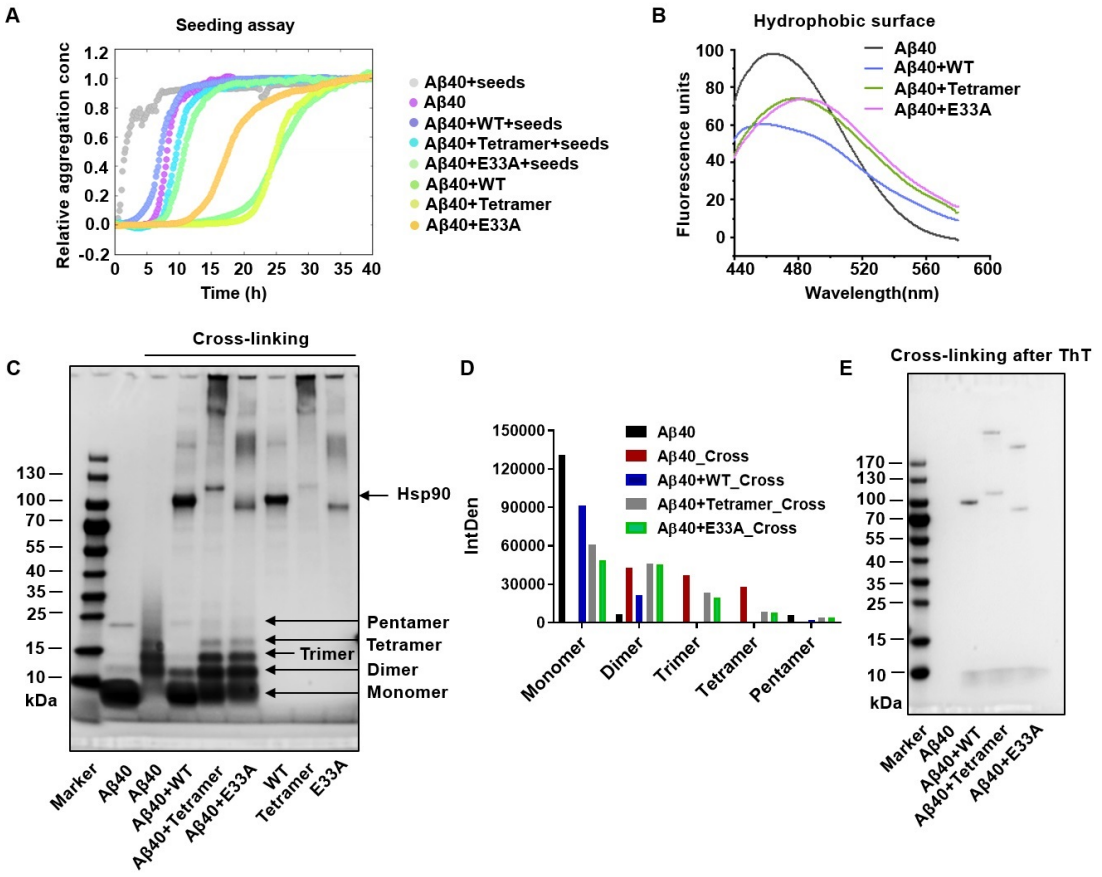

FIGURE 4: Hsp90 inhibits the elongation process of Aβ40 fibrillation by attenuating hydrophobic interactions among the Aβ40 peptides. **(A)** The seeding experiments of 10 μM Aβ40 in the presence of 1 μM Aβ40 seeds without (gray) or with 0.1 μM Hsp90 protein WT (blue), tetramer (cyan) or mutant E33A (light green), monitored by ThT fluorescence at 37 °C without agitation. As controls, 10 μM Aβ40 fibrillation kinetic assays were conducted without the seeds in the absence (purple) or presence of 0.1 μM Hsp90 protein WT (green), tetramer (yellow) or mutant E33A (orange). **(B)** ANS fluorescence assay performed with 10 μM Aβ40 in the presence or absence of 0.1 μM Hsp90 protein variants at 37 °C. **(C)** SDS page of the photo-induced cross-linking samples of 90 μM Aβ40 in the presence or absence of 2 μM Hsp90 after 15 min incubation at room temperature. **(D)** Quantitative comparison of oligomers from the cross-linking experiment. (E) SDS page of the photo-induced cross-linking samples of 10 μM Aβ40 with or without 0.5 μM Hsp90 after the ThT assay shown in **Fig.S4A**.

We then further confirm the inhibitory effect of Hsp90 on Aβ40 fibrillation and the influence of ATP on this effect by using AFM imaging in aqueous environment under various conditions. First Aβ40 was incubated for 92 h at 300 rpm and 30 °C at a concentration of 75 μM to form mature fibrils (**Fig.5C**). The same experiment was repeated in the presence of Hsp90 (Aβ40:Hsp90 ratio of 10:1). **Fig.5D** shows that no fibrils were formed, i.e. that Hsp90 efficiently inhibited Aβ40 fibrillation at substoichiometric concentrations, consistent with previously reported experiments (28). Finally, the same experiment was repeated with Hsp90 in the presence of 5 mM ATP. In this case, some fibrils could be observed, but to a much lower extent as with Aβ40 alone (**Fig.5E**).

Fig.5F-H show the heights and contour lengths of Aβ40 aggregates under the various conditions. The AFM images show straight and spiral fibrils, with contour lengths around 500 nm, which were formed in the absence of Hsp90 and ATP. The height of the fibrils is around 5 nm in agreement with previous reports (32, 34). In the presence of Hsp90 and absence of ATP, mainly monomers and oligomers with contour lengths below 50 nm were observed representing most likely monomers or small co-aggregates of Aβ40 and Hsp90. In the presence of Hsp90 and ATP, monomers, oligomers as well as fibrils were observed, indicating a suppressing effect of ATP on the capability of Hsp90 to inhibit the fibrillation process.

3.3.6 Binding mode between Hsp90 and the Aβ40 peptides

To investigate the binding affinity between Hsp90 and Aβ peptides, fluorescence polarization (FP) experiment was carried out. The result shown in **Fig.6A** indicates that Hsp90 does not display any strong affinity (Kd is estimated to be lower than 100 μM) for the Aβ40 peptides (monomers) in the absence or presence of AMP-PNP. Both closed and open Hsp90 proteins presumably protect the Aβ40 peptides from the fibrillation via surface hydrophobic solubilization rather than a specific interaction, in agreement with our ANS assays where Hsp90 stabilizes Aβwith changed hydrophobic surface. As shown in **Fig.S6**, Hsp90 with open conformation offers more hydrophobic surfaces than that in closed state, supporting **Fig.5A-B** where Hsp90 without AMP-PNP has more hydrophobic surfaces and better inhibition efficiency than the one with AMP-PNP (closed state). The weak/unspecific interaction between Hsp90 and Aβ40 can be converted to covalent connection through PICUP (55). To further investigate if Hsp90 offers the surfaces for Aβ solubilization, the PICUP experiments were conducted (**Fig.6B**), followed by the LC/MS analysis in **Fig.S7A-B**. Hsp90 forms more higher-molecular-weight bands in the presence of Aβ40 on the SDS-page gel than these without Aβ40 in **Fig.6B**, suggesting that Hsp90 forms several complexes with different numbers of Aβ40 monomers. Followed by liquid chromatography, ESI–time-of-flight (TOF) mass spectrometry enables to determine the spectrum m/z of the Hsp90 complexes from the PICUP assay. As shown in **Fig.S7A**, PICUP products eluted from the column with different elution times indicate the formation of Hsp90 complexes with different polarities. Hsp90 without PICUP gives a single peak in the m/z spectra in **Fig.S7B**. After PICUP, Hsp90 with the Aβ40 peptides (in green and red curve, **Fig.S7B**) seems to form more complexes in comparison to the one without the peptides (in purple curve, **Fig.S7B**). Altogether this data indicates that Hsp90 solubilizes Aβpeptides to large degree through hydrophobic surfaces as suggested by the ANS assay, although the binding to monomers is weak, which we conclude from our fluorescence polarization assay. This is consistent with the

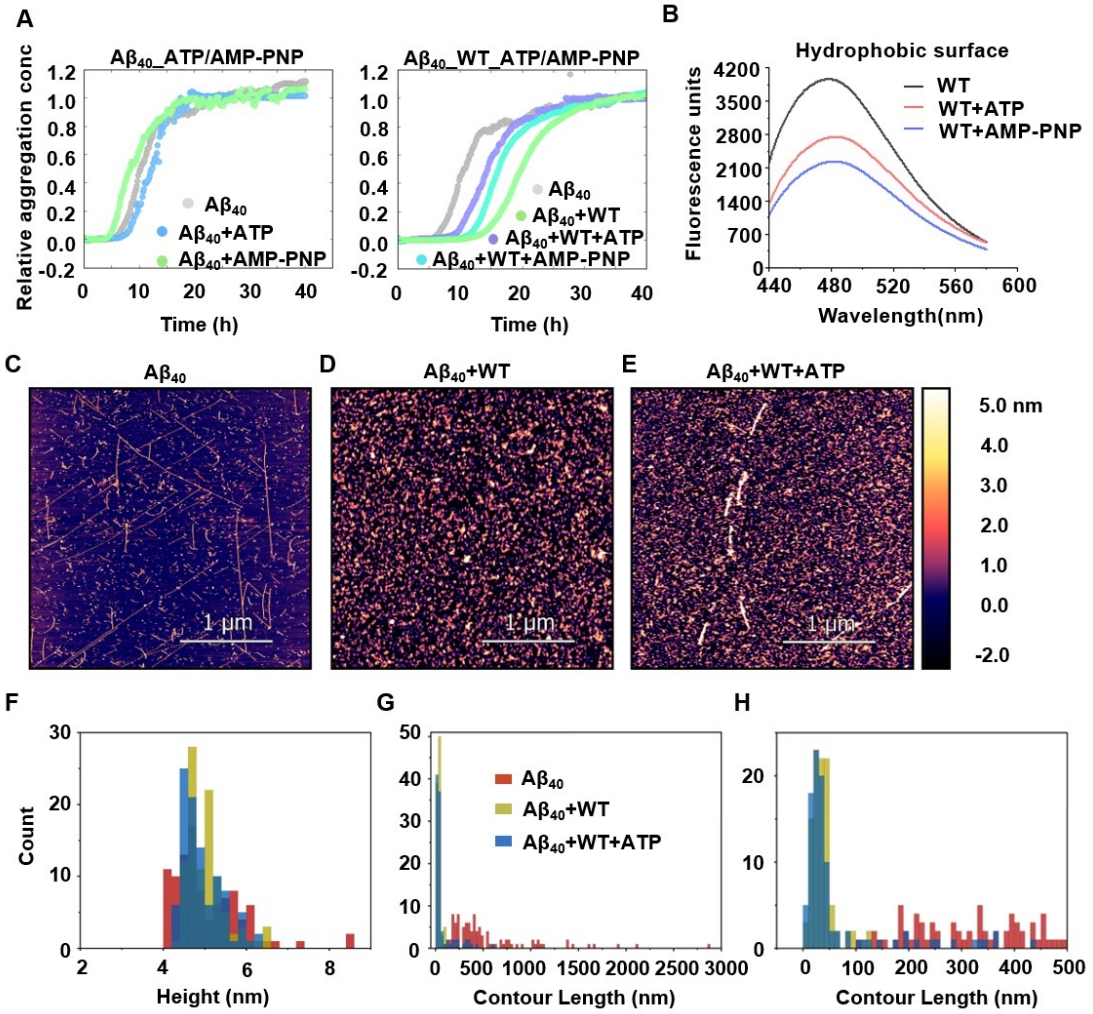

FIGURE 5: **(A-B)** ATP negatively regulates the inhibitory efficiency of Hsp90 against Aβ40 fibrillation by modulating the conformation dynamics and reducing hydrophobic surfaces of Hsp90. **(A)** Aggregation kinetics of Aβ40 fibrillation monitored by ThT fluorescence. The experiment was conducted with 10 μM Aβ40 and 0.1 μM Hsp90, in the presence or absence of 2 mM ATP or AMP-PNP at 37°C without agitation, and the averaged data were normalized with *AmyloFit*. The normalized data of individual curves were shown in **Fig.S5**. **(B)** ANS fluorescence experiment performed with 6 μM WT Hsp90 in the presence or absence of 2 mM ATP or AMP-PNP at 37°C. (C-H) Results of AFM imaging in liquid. **(C)** Aβ40 peptides only. **(D)** Aβ40 peptides with Hsp90 (10:1). **(E)** Aβ40 peptides with Hsp90 (10:1) and ATP (5.0 mM). All samples (Aβ40 concentration: 75 μM) were incubated for 92 h at 300 rpm at 30 °C. The respective sample was deposited on a flat mica surface and measured in HEPES pH 7.0 with 10 mM $MgCl_2$ with a scan size of 3 μm × 3 μm and a scan rate of 2.44 Hz. In total, about 5 images of each sample were taken and the experiments were performed twice. **(F)** Height histograms of Aβ40 structures, showing height values of 5 ($\pm$1) nm in all cases. **(G)** Contour length histogram (bin width 28 nm) of the Aβ40 structures, showing values of (546 $\pm$464) nm (Aβ40 incubation only), (37$\pm$23) nm (Aβ40 peptides incubated with Hsp90), (72$\pm$106) nm (Aβ40 peptides incubated with Hsp90 and ATP). The large error for the latter is due to the bimodal distribution (monomers and oligomers). **(H)** Zoom into the first part of **(G)** with a bin width of 10 nm. Please note that longer structures (>100nm) are only visible in the absence of Hsp90 (red) or if Hsp90+ATP are present (blue).

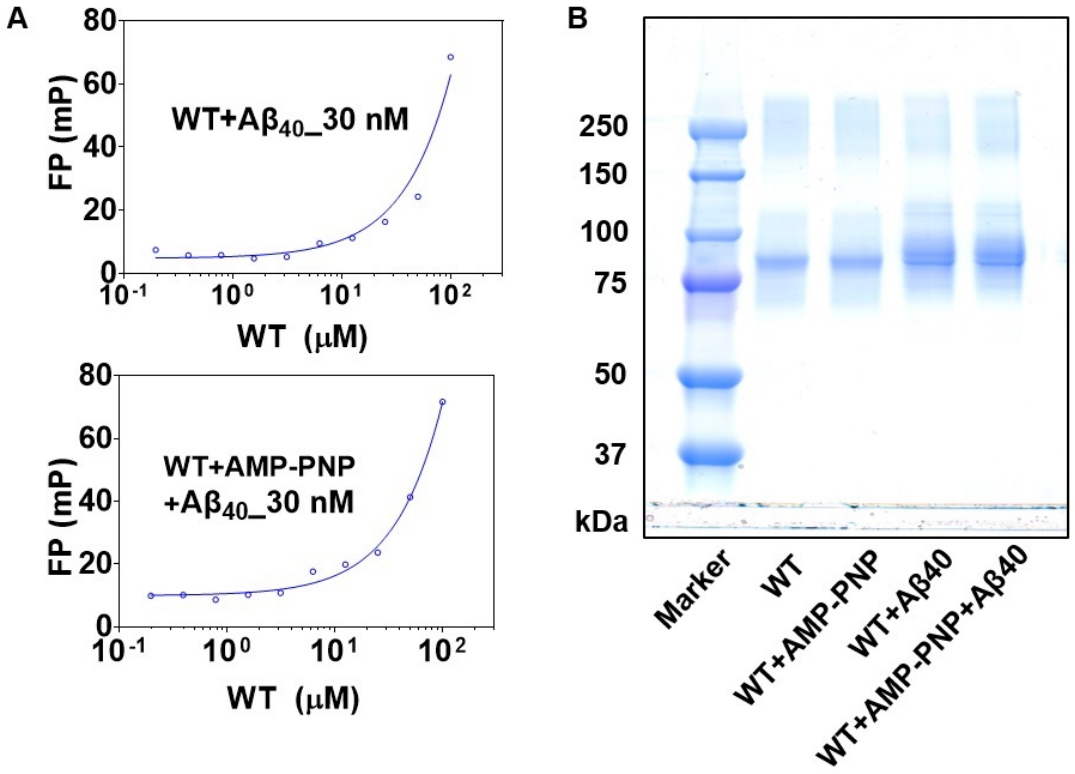

FIGURE 6: **(A)** Fluorescence polarization (FP) assays conducted with 30 nM HL488-Aβ40 and Hsp90 (WT, 0-100 μM, two-fold serial dilution) in the absence or presence of AMP-PNP. **(B)** SDS-page of the photo-induced cross-linking samples of 2 μM Hsp90 (WT) and 90 μM Aβ40 with or without AMP-PNP after 15 min incubation at room temperature. Hsp90 and Aβ40 form complexes in the presence or absence of 2mM AMP-PNP.

interaction of Hsp90 with several disordered proteins like tau via a transient and weak binding on the extended substrate binding surfaces that crosses the domain boundaries (14).

3.4 Discussion

Here we report how wild type Hsp90 and Hsp90 variants slow down Aβ40 peptide fibril formation at substoichiometric ratios *in vitro*. Our AFM and CD experiments further show that Hsp90 proteins alter the conversion of secondary structure conformations of Aβ40 during fibrillation and induce formation of amorphous Aβ40 aggregates. Our global fit analysis of the kinetic data suggests that Hsp90 proteins influence both the secondary nucleation and elongation processes. The seeding assay confirms the finding that the elongation process of Aβ40 is significantly modulated by Hsp90. The cross-linking assay further shows that, in the presence of Hsp90, Aβ40 even remains predominantly

in its monomeric state compared to in the absence of Hsp90 proteins. In order to elucidate the molecular mechanisms behind the interaction between Hsp90 and Aβ40, an ANS fluorescence assay was conducted, from which we conclude that Hsp90 decreases the accessible hydrophobic surfaces of the Aβ40 peptides.

The Hsp90 protein is intrinsically flexible with a number of accessible hydrophobic surfaces (56) and coexists in various conformations. Furthermore, the conformational transition of Hsp90 can be modulated upon the binding of diverse substrates, co-chaperones, adaptor proteins, or nucleotides (10, 57-60). Here we investigated the effect of nucleotides by repeating the experiments in the presence of ATP or the non-hydrolysable AMP-PNP. In particular, our ThT kinetics experiments show that ATP alone hardly inhibits the aggregation of Aβ40, which is consistent with a previous study (61). On the contrary, the inhibitory effect of Hsp90 on Aβ40 fibrillation is significantly attenuated by the addition of ATP, while AMP-PNP reduces this effect of Hsp90 to a lower extent, confirming that our observations are related to the conformational dynamics of Hsp90 proteins. To study the influence of ATP on the hydrophobicity and electrostatic interactions of Hsp90, an ANS fluorescence assay was conducted, which shows that ATP or AMP-PNP decreases the total hydrophobic surface of Hsp90. Thus, ATP diminishes the inhibitory effect of Hsp90 on Aβ40 fibrillation also by decreasing the hydrophobic surface of Hsp90. Nevertheless, this is likely not the only effect, as ATP reduces the inhibitory effect of Hsp90 more than AMP-PNP, despite AMP-PNP having a larger effect on the hydrophobic surface (**Fig.5A** and **B**). Therefore, we speculate that also the large conformational dynamics of Hsp90s plays a crucial role. In addition, ATP hydrolysis might displace Aβ40 monomers from Hsp90, further reducing the inhibitory potency of Hsp90.

We briefly summarize in a schematic model in **Fig.7** how Aβ40 fibrillation can be influenced by Hsp90 as well as ATP at the microscopic and molecular levels: (1) Hsp90 inhibits the fibrillation (mostly the elongation process) of Aβ40 monomers by interfering with the hydrophobic interactions between Aβ40 monomers and/or oligomers; (2) ATP suppresses the inhibitory effect of Hsp90 on Aβ40 fibrillation. Conceivably, ATP triggers a conformational conversion of Hsp90's quaternary structure even in the presence of Aβ40 and thus reduces the global hydrophobic surfaces of Hsp90, leading to the release of the Hsp90-bound Aβ40 peptides and/or less binding of free Aβ40. In other words, ATP hydrolysis would lead to something considered as a 'clean cycle' to leave the relatively bare Hsp90 and more unbound Aβ40 available for fibrillation. AMP-PNP on the other hand is k $_n$ own to close the Hsp90 dimer and therefore stably reduce the accessible hydrophobic surface of Hsp90. This is consistent with the concept that Hsp90 usually interacts with its clients via a large number of low energy contacts in a dynamic and transient way (62). Similar to the hydrophobic surfaces of Hsp90 for Aβ40, the binding

site of Tau on the Hsp90 mainly consists of hydrophobic residues (10). The binding surface of Aβ40 or Tau (10) on Hsp90 are generally in accordance with how Hsp90 interacts with the other amyloid proteins, like the misfolded transthyretin monomer (63), the GR-LBD (glucocorticoid receptor-ligand binding domain) (58), or the unfolded kinase Cdk4 (64). Since Aβ40 is 10 times size smaller than Tau, Hsp90 may stoichiometrically bind to more Aβ40 compared to Tau or other amyloid protein. Tau takes 106-Å-long binding patch of Hsp90 for the low-affinity interaction (10), while Hsp90 forms several complexes with different numbers of Aβ40 monomers as observed by the PICUP in Fig.6B and the following LC-MS assay (**Fig.S7A-B)** with low binding affinity (**Fig.6A**).

We still do not fully understand the molecular action of the tetramer and E33A mutant, as shown in **Fig.4A** and **B**, because the tetramer and E33A show similar effects regarding the reduction of Aβ40 hydrophobicity but a different acceleration of Aβ40 fibrillation, but this is not the intension of this paper. Nevertheless, the tetramer and E33A helped us to delineate factors that determine the interaction between Hsp90 and Aβ40. It became clear, that the ATPase activity is very important, but not the only determinant. One other determinant is a reduction of Hsp90 hydrophobicity. Besides, we are convinced that a third determinant is the conformational dynamics/flexibility of Hsp90, but this is a point of further investigation.

Taken together, the different behaviors of Aβ40 fibrillation in the presence of wild type Hsp90 and the variants are presumably caused by Hsp90 conformation dynamics, ATPase activity, hydrophobicity, and the heterogeneity of Aβ40 aggregation process. This can also explain the differences in the behavior of Aβ40 aggregation kinetics in the presence of different Hsp90 isoforms in **Fig.3D** and **Fig.4A**. Like other oligomeric proteins (65), tetrameric Hsp90 may equilibrate to dimer or monomer. The equilibria might cause the interface change (66) of tetrameric Hsp90, therefore changing the different hydrophobic surfaces for Aβ40 and leading to the similar effect with that of E33A mutant. The tetrameric equilibria and Aβ40 aggregation can be further explored but are not an aim of our study. Oligomer equilibria can be dependent of environmental conditions, like temperature and pH. The different equilibrium of Hsp90 tetramer may explain the slight different effects of the tetramer on Aβ40 fibrillation shown in **Fig.3D** and **Fig.4A**.

On the physiological relevance, we can only speculate. In Alzheimer's disease, mitochondrial electron transport chain is severely affected by Aβ aggregation, leading to a decrease of ATP production (67). With less ATP, there might be less Hsp90-client complexes. Instead, there could be more accessible hydrophobic surfaces on client-free Hsp90 available for binding Aβ, inhibiting the aggregation, and further restoring the function of ATP production. Although the direct physiological relevance of Hsp90 and ATP for modulating Aβ fibrillation remain to be explored, increasing evidence indicates

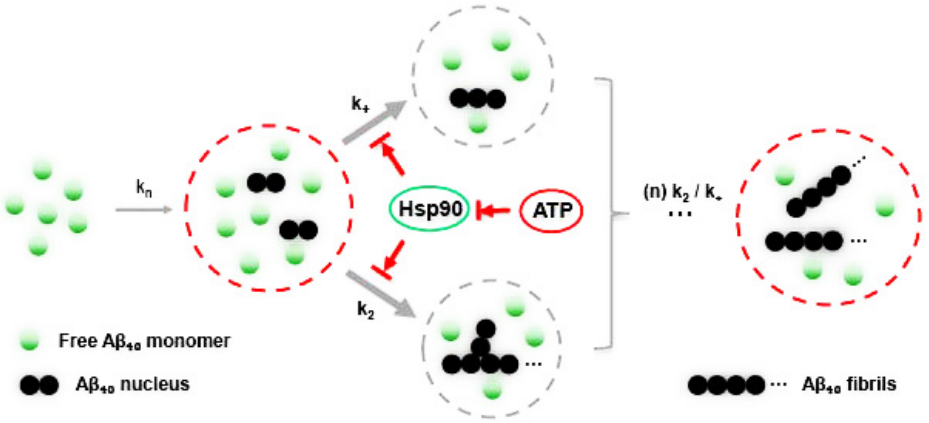

FIGURE 7: Schematic diagram of the inhibitory effect of Hsp90 on Aβ40 fibrillation in the presence and absence of ATP. The fibrillation of Aβ40 peptides occur via primary nucleation, elongation and secondary nucleation mechanisms, here described as the rate constants, k_n, k_+, and k_2. Secondary nucleation is the dominating process for an increase of aggregate mass during Aβ40 amyloid formation, after which the pre-fibrils undergo several (n) elongation/secondary nucleation processes, to become mature fibrils. The presence of Hsp90 provides exposed hydrophobic surfaces to which various Aβ40 species can bind, leading to a decrease of free Aβ40 monomers and/or oligomers that are available to form new nuclei and for the subsequent elongation and secondary nucleation processes. ATP modulates the global conformation and surface hydrophobicity of Hsp90, and therefore reduces the activity of Hsp90 against, mostly, the elongation process of Aβ40 fibrillation.

that Aβ can be produced and can aggregate inside cells and that there is a communication between the extracellular and intracellular Aβ pools (68-71). Furthermore, our study provides a potential mechanism how Hsp90 and variants may regulate Aβ fibrillation. These shed light on the multiple facets of the chaperone Hsp90 interaction with amyloid proteins.

3.5 Materials and methods

3.5.1 Purification of recombinant Hsp90 from *E.coli*

Gene expression and subsequent protein purification was performed following established protocols with minor modification (72). The construct used in this study were yeast Hsp90 WT carrying an N-terminal *His6-tag* and yeast Hsp90_E33A with a substituted charged linker region and a cleavable *His6-SUMO-tag* (1). In short, pET28 derived expression constructs were transformed with BL21 Star (DE3) cells. Gene expression was induced at OD600=0.7 with 1 mM IPTG in cells grown in lysogeny broth media at 37°C. The cells were harvested 4 h after induction.

Cells were resuspended in HEPES buffer pH 7.5 containing 150 mM NaCl and 20 mM Imidazole and lysed with a Cell Disrupter (Constant Systems) at 1.6 kbar. Cleared lysate was then applied to HisTrap HP column followed by anion exchange chromatography with HiTrap Q and gel filtration on S200 (all columns GE Healthcare). Fractions corresponding to the dimer and to a higher oligomer were pooled separately. The protein was flash frozen in liquid nitrogen in concentrations of 130 - 315 μM and stored at – 80°C. Cleavage of the SUMO-tag was done by dialysis of the HisTrap eluate in the presence of 1/100 mol SENP protease against imidazole free buffer and removal of free SUMO and uncleaved fusion-protein by a second HisTrap.

The oligomeric state of the higher oligomer was examined with right angle light scattering and refractive index analysis (Viscotek TDA 305) after separation on a S200 10/300 GL increase column (GE Healthcare) confirming a predominantly tetrameric composition.

3.5.2 Materials and sample preparation

Concentrated Hsp90 protein stock solutions were diluted to working concentration in 40 mM Hepes buffer supplemented with 150 mM KCl, pH 7.5. Aβ40 was purchased from (Alexo Tech) and Adenosine 5'-triphosphate disodium salt hydrate (ATP, CAS: 34369-07-8), Adenylyl-imidodiphosphate (AMP-PNP, CAS: 25612-73-1), 8-Anilino-1-naphthalenesulfonic acid (ANS, CAS: 82-76-8), Thioflavin T (ThT, CAS: 2390-54-7), Tris(2,2'-bipyridyl) dichlororuthenium(II) hexahydrate (Ru(Bpy), CAS: 50525-27-4), and Ammonium persulfate (APS, CAS: 7727-54-0) were purchased from Sigma-Aldrich. Aβ40 stock solutions were prepared by dissolving the lyophilized powder in 10 mM NaOH to a concentration of 2 mg/mL and then sonicated in an ice-water bath for 1 min. ATP and AMP-PNP stock solutions were prepared at a concentration of 100 mM in 50 mM Tris-HCL, pH 7.5. ThT and ANS stocks were prepared to 3 and 10 mM in

50 mM Tris buffer pH 7.4 and DMSO, respectively. The concentrations of Ru(Bpy) and APS were 1 and 20 mM in 10 mM sodium phosphate buffer, pH 7.4, respectively. All of the buffers, 10 mM NaOH, ThT and ANS stocks were filtered with 0.2 μM syringe-driven filters.

3.5.3 ThT fluorescence assays

To study the effect of Hsp90 (WT, tetramer, and E33A mutant) on the fibrillation kinetics of the Aβ40 peptides, Hsp90 solutions at the different concentrations (0, 0.02, 0.04, 0.08, and 0.1 μM) were prepared with 40 μM ThT and 10 μM Aβ40 in the assay buffer (20 mM sodium phosphate buffer, pH 7.4, 0.2 mM EDTA, 0.02% NaN3) on ice. 40 μL of each sample was then transferred into a 384-well black plate with transparent bottom (NUNC) and sealed with a piece of foil film. The plate was incubated in a microplate reader (PHERAstar FSX, BMG LABTECH, Germany) and the fluorescence kinetics of Aβ40 was monitored at 37°C without agitation every 5 min, using wavelengths of 430 nm and 480 nm for excitation and emission, respectively.

To investigate how ATP and AMP-PNP affect the activity of Hsp90 on Aβ40 fibril formation, we conducted another ThT assay with 40 μM ThT, 10 μM Aβ40, 0.1 μM Hsp90 (WT, tetramer, or E33A mutant), in the presence or absence of 2 mM ATP and AMP-PNP. The samples were prepared and the kinetics was monitored in the same way as mentioned above. As a control, the effect of ATP and AMP-PNP on Aβ40 fibrillation kinetics was studied as well.

In a seeding assay, 10 μM Aβ40 seeds were freshly prepared from a monomeric solution allowed to incubate for 15 h at 37 °C in a 384-well black plate (NUNC) without agitation. The seeds were then sonicated in ice-water bath for 2 min. The samples were prepared as described above in the presence of 1 μM Aβ40 seeds.

These ThT assays were conducted with at least three replicates.

All of the original ThT data were plotted with Prism7.0 (GraphPad Software). The averaged ThT data were normalized with **equation (1)** and globally fitted in *AmyloFit* (47), the sigmodial fitting were performed with data of individual curves by using **equation (2)**. The averaged data of seeding assays and the data of individual curves obtained from ThT assays with ATP or AMP-PNP were normalized with **equation (1)** in *AmyloFit*.

$$\boldsymbol{y_{norm,i} = (1\text{-}M_{0,frac})*(y_i\text{-}y_{baseline})/(y_{plateau}\text{-}y_{baseline})+M_{0,frac}} \quad \textbf{(1)}$$

$$\boldsymbol{y = (y_{baseline}\text{-}y_{plateau})/(1+e^{(t\text{-}t_0)/dt})+y_{plateau}} \quad \textbf{(2)}$$

where $y_{baseline}$ and $y_{plateau}$ are the values of the data at the baseline and the plateau, $M_{0,frac}$ is the relative initial concentration of aggregates (i.e., a value between 0 and 1). t is the time of amyloid aggregation course and t_0 is the time when the fluorescence intensity reaches half of the plateau value, while dt is the time constant. $y_{norm,i}$ is the normalized value of y_i, the original value of the ith data point, and y was the fitted value of the data at time t. The lag time t_{lag} and aggregation half time $t_{1/2}$ were given as follows.

$$\boldsymbol{t_{1/2} = t_0} \textbf{ (3)}$$

$$\boldsymbol{t_{lag} = t_{1/2}\text{-}2dt} \textbf{ (4)}$$

The normalized data, t_{lag} and $t_{1/2}$ were plotted with Prism7.0 (GraphPad software).

3.5.4 Global fitting

To identify which microscopic rate processes of Aβ40 aggregation are the ones most influenced by Hsp90, the ThT data of Aβ40/Hsp90 (0, 0.02, 0.04, 0.08, 0.1 and 0.5 μM) were fitted globally with an integrated rate law (43, 44) in *AmyloFit* online software server (47). The secondary nucleation dominated model was selected, the data of Aβ40 alone was first fitted, obtaining a set of parameters, which were used as the initial guess values for the following fits. Among these obtained parameters, the primary nucleation rate constant (k_n, with units of concentration^{-nc+1}time^{-1}, where nc is the reaction order of primary nucleation that simply interpretates a nucleus size), the secondary nucleation rate constant (k_2, with units of concentration^{-n2} time^{-1}, where n2 is the reaction order of secondary nucleation that simply interpretates a nucleus size), or the elongation rate constant (k_+, with units of of concentration^{-1}time^{-1}) was fitted freely while the other two rate constants were set as fixed initial values. For detailed definitions of these parameters and fitting procedure, please refer to the nature protocol (47).

3.5.5 Atomic force microscopy (AFM) imaging in air

For AFM measurement in air, 10 μM Aβ40, with or without 0.5 μM Hsp90 (WT, tetramer, or E33A mutant) were incubated at 37 °C in 1.5 mL microcentrifuge tubes for 24 h at 300 rpm. 15 μL of each sample was then added onto the freshly cleaved muscovite mica (Electron Microscopy Sciences) and incubated for 5 min at room temperature. The excess sample was removed with filter paper and the mica plate with the sample was rinsed once with 150 μL of Milli-Q water. The excess water was removed with filter paper and the mica plate with the sample was dried under nitrogen gas. The images

were obtained with the Bruker Dimension Icon Scanning Station (Bruker, USA) in intermittent contact mode in air and processed with the WSxM 4.0 software (73).

3.5.6 Atomic Force Microscope imaging in liquid

For AFM imaging, Aβ40 peptides were diluted with PBS buffer (Dulbecco's Phosphate Buffered Saline, pH 7.2, 500 mL, Sigma-Aldrich, USA) to a final concentration of 75 μM with 7.5 μM Hsp90 (WT), 5.0 mM ATP or 7.5 μM BSA. The peptides were incubated at 30°C for 92 h at 300 rpm (Eppendorf Thermotop, Germany). A flat mice surface (muscovite, diameter 10-12 mm, Plano, Germany) was cleaved, immobilized on an AFM specimen (diameter: 15 mm) using UV curable glue (NOA 63, Norland Products, USA) and washed with ultrapure water (30 μL, 18.2 MΩ cm, Purelab Chorus 1, Elga LabWater, Germany) and the Aβ40 solution was incubated on the mica surface at 60°C for 30 min. Finally, the surface was washed with ultrapure water (30 μL).

AFM imaging was performed on a Cypher ES (Asylum Research, an Oxford Instruments Company, USA) using a heating/cooling sample stage set to 25°C and AC mode based on the blueDrive (photothermal excitation). The measurements were performed in HEPES buffer (pH 7.0) with 10 mM $MgCl_2$. The images were obtained with the BioLever-AC40TS cantilevers (Olympus, Japan) with a resonance frequency of about 20-25 kHz in liquid. The following parameters were chosen for the measurements: a scan size of 5 μm, a scan rate of 2.44 Hz, a setpoint of 300-400 mV and a scan angle of 0°.

The images were processed with the Gwyddion Free SPM analysis software (Petr Klapetek, version 2.53) (74). To correct the recorded height image (using the trace image), the data was levelled by mean plane subtraction, the rows were aligned to the median value and the minimum data value was shifted to 0.

Grain analysis using Gwyddion Free SPM analysis software was performed to obtain height values of the imaged structures. First, the threshold of grain-like features was marked. Then, the generated grain data was exported and the height values of the grains were taken to provide histograms, mean and error values using Origin (Version 2019, OriginLab, USA).

The contour length of the structures was determined by Easyworm 1 (75). The respective AFM images were loaded into the software and 100 individual chains were marked using cursors. Then, Easyworm 2 was used to generate the contour length values for each individual chain marked in Easyworm 1 and the raw data was exported to provide histograms, mean and error values using Origin.

3.5.7 Circular dichroism (CD) spectroscopy

In CD spectroscopy, the sample was performed with 10 μM Aβ40 supplemented with or without 0.04 μM Hsp90 proteins (WT, tetramer, or E33A mutant) in 20 mM potassium phosphate buffer, pH 7.0. The CD spectra were recorded in the far-UV region from 190 to 260 nm with a Chirascan plus CD spectrometer (Applied Photophysics Limited, U.K.). The samples were measured in a quartz cuvette with a pathlength of 10 mm at 37°C immediately after stirred manually with a pipette, using a step size of 1.0 nm, a bandwidth of 1.0 nm, and a time per point of 0.5 s. The spectra were recorded at 0, 0.5, 1, 1.5, 2, 3, 4, 5, 6, 7, 8, and 22 h. The curves were replotted and smoothed by 20 times with the Origin (Version 2018, OriginLab, USA).

3.5.8 Photo-induced cross-linking of unmodified proteins (PICUP)

In the PICUP experiment, 18 μl of 90 μM Aβ40 with or without 2 μM Hsp90 (WT, tetramer, or E33A mutant) in 10 mM sodium phosphate buffer, pH 7.4, were incubated for 15 min at room temperature, followed by the addition of 1 μL of 1 mM Ru(Bpy) and 1 μL of 20 mM APS, obtaining a reaction volume of 20 μL in PCR tubes. The samples were then irradiated for 2 s and quenched by the addition of 2 μL of 0.5 M 1,4-Dithiothreitol (DTT). These cross-linked samples, together with the 90 μM unlinked Aβ40, were subjected to the SDS-PAGE with a 4%-20% gel and imaged with the Amersham Imager 600 (GE Healthcare Life Sciences, US). The bands corresponding to Aβ40 monomers and different kinds of oligomers were quantified and plotted with ImageJ and Prism 7.0 (GraphPad software), respectively.

The same experiments were carried out for 10 μM Aβ40 in the presence or absence of 0.5 μM Hsp90 proteins (WT, tetramer, or E33A mutant) after the ThT kinetics experiments in **Fig.S4A**, as well as for control samples (at time zero of Aβ40 aggregation kinetics), the results of which are shown in **Fig.S4B**.

The similar experiment was also carried out for 2 μM Hsp90 and 90 μM Aβ40 in the absence or presence of 2 mM AMP-PNP with irradiation time of 5 s. The cross-linked samples were then subjected to the SDS-PAGE with a 4%-20% gel and imaged with the EPSON Scanner.

3.5.9 LC-MS experiemnts

To check how Hsp90 interacts with Aβ40 and how conformation dynamics will influence this interaction, Liquid chromatography-mass spectrometry (LC-MS) experiments were

Table 1: HPLC Method description.

Time (min)	Solvent A (acetonitrile with 0.1% formic acid)	Solvent B (water with 0.1 % formic acid)	Flow (mL/min)
0	2%	98%	0.5
2	25%	75%	0.5
25	50%	50%	0.5
30	80%	20%	0.5

performed with 10 μM Hsp90 in native state, 2 μM Hsp90/2 mM AMP-PNP (cross-linked), 2 μM Hsp90/90 μM Aβ40 (cross-linked), and 2 μM Hsp90/2 mM AMP-PNP /90 μM Aβ40 (cross-linked). LC/MS analysis was performed on a LCT Premier mass spectrometer and HPLC Waters 2795 (Waters, US). Samples were chromatographed on a Reprosil-PUR 2000 C18-AQ column (3 μm, 100mmX2mm) heated to 50°C using the following condition:

The result of MS experiment was given as the spectrum m/z.

3.5.10 Fluorescence polarization (FP) assay

To investigate the binding affinity of Hsp90 with Aβ40. FP assays were performed with Hsp90 (WT, two-fold serial dilution, with a highest concentration of 100 μM, the results are shown in **Fig.6A**) and 30 nM HL488-Aβ40 in the absence or presence of 2 mM AMP-PNP with 480 nm and 520 nm as the excitation and emission wavelengths, respectively. The measurements were performed with a microplate reader (PHERAstar FSX, BMG LABTECH, Germany) at 37°C. The data were plotted with Prism7.0 (GraphPad software). To confirm these results, we performed the experiments once more with WT at the highest concentration of 160 μM with the same method, and obtained similar results (data not shown).

3.5.11 ANS experiments

To study the effect of ATP and AMP-PNP on the hydrophobic surface of the Hsp90 proteins, the samples were prepared in the presence or absence of 6 μM WT Hsp90 with 2 mM ATP or AMP-PNP and then incubated for 1 h at room temperature. ANS fluorescence dye was added to the prepared samples at a final concentration of 30 μM. ANS is believed to binding to (buried) hydrophobic sites of proteins. The observed features of ANS, a blue shift of fluorescence emission maxima and the increase of fluorescence intensity and lifetime, are generally attributed to the hydrophobicity of a binding site

and the restricted mobility of ANS. 40 μL of each mixed sample was then transferred into a 384-well white plate (PerkinElmer, USA). The samples were measured using a multi-mode microplate reader from BioTek at 37°C, with an excitation wavelength of 400 nm and an emission wavelength region of 440-580 nm. The obtained values were averaged, plotted and smoothed with Origin (Version 2018, OriginLab).

We also conducted the ANS experiment to investigate whether Hsp90 (WT, tetamer, and E33A) influence the hydrophobic surface of Aβ40. Samples containing 10 μM Aβ40 in the presence of 0.1 μM Hsp90 (WT, tetamer, or E33A) were prepared, incubated, and measured in the same way as mentioned above.

3.6 Abbreviations

Hsp90 - heat shock protein 90; **ATP** - adenosine triphosphate; **AFM** - atomic force microscopy; **CD** - circular dichroism; **ThT** - Thioflavin T; **ANS** - 8-anilino-1-naphthalenesulfonic acid; **A**β- amyloid-β; **WT** - wild type Hsp90; **GR-LBD** - glucocorticoid receptor-ligand binding domain; **ETC** - mitochondrial electron transport chain; **UPR** - unfolded protein response; **ER** - endoplasmic reticulum; **AMP-PNP** - Adenylyl-imidodiphosphate; **APS** - Ammonium persulfate.

3.7 Declarations of interest

None.

3.8 Funding

M.L., B.N.B. and T.H. were funded by the Deutsche Forschungsgemeinschaft (DFG, German Research Foundation) under Germany's Excellence Strategy – EXC-2193/1 – 390951807. H.W. was sponsored by the State Scholarship Fund (China Scholarship Council (CSC): 201806200097) and J.L. was supported by the Brightfocus foundation (A20201759S).

3.9 Author contributions

HW, BNB, TH, JL: conceptualisation. HW, ML, BH: investigation. HW, ML, CW, RL, BNB, TH, JL: analysis and validation. HW, JL: the original draft writing and project administration. HW, ML, BH, CW, RL, BNB, TH, JL: review and editing.

3.10 References

1. M. M. Ali et al., Crystal structure of an Hsp90-nucleotide-p23/Sba1 closed chaperone complex. Nature 440, 1013-1017 (2006).
2. W. K. Huh et al., Global analysis of protein localization in budding yeast. Nature 425, 686-691 (2003).
3. C. Didelot et al., Interaction of heat-shock protein 90 beta isoform (HSP90 beta) with cellular inhibitor of apoptosis 1 (c-IAP1) is required for cell differentiation. Cell death and differentiation 15, 859-866 (2008).
4. S. Suzuki, A. B. Kulkarni, Extracellular heat shock protein HSP90beta secreted by MG63 osteosarcoma cells inhibits activation of latent TGF-beta1. Biochemical and biophysical research communications 398, 525-531 (2010).
5. K. A. Borkovich, F. W. Farrelly, D. B. Finkelstein, J. Taulien, S. Lindquist, hsp82 is an essential protein that is required in higher concentrations for growth of cells at higher temperatures. Molecular and cellular biology 9, 3919-3930 (1989).
6. P. Csermely, T. Schnaider, C. Soti, Z. Prohaszka, G. Nardai, The 90-kDa molecular chaperone family: structure, function, and clinical applications. A comprehensive review. Pharmacology & therapeutics 79, 129-168 (1998).
7. K. Richter, M. Haslbeck, J. Buchner, The heat shock response: life on the verge of death. Molecular cell 40, 253-266 (2010).
8. F. H. Schopf, M. M. Biebl, J. Buchner, The HSP90 chaperone machinery. Nature reviews. Molecular cell biology 18, 345-360 (2017).
9. R. Zhao et al., Navigating the chaperone network: an integrative map of physical and genetic interactions mediated by the hsp90 chaperone. Cell 120, 715-727 (2005).
10. G. E. Karagoz et al., Hsp90-Tau complex reveals molecular basis for specificity in chaperone action. Cell 156, 963-974 (2014).
11. A. J. McClellan et al., Diverse cellular functions of the Hsp90 molecular chaperone uncovered using systems approaches. Cell 131, 121-135 (2007).
12. D. Picard, Heat-shock protein 90, a chaperone for folding and regulation. Cellular and molecular life sciences : CMLS 59, 1640-1648 (2002).
13. W. B. Pratt, D. O. Toft, Steroid receptor interactions with heat shock protein and immunophilin chaperones. Endocrine reviews 18, 306-360 (1997).
14. G. E. Karagöz, S. G. Rüdiger, Hsp90 interaction with clients. Trends in biochemical sciences 40, 117-125 (2015).
15. P. R. Bharadwaj, A. K. Dubey, C. L. Masters, R. N. Martins, I. G. Macreadie, Abeta aggregation and possible implications in Alzheimer's disease pathogenesis. Journal of cellular and molecular medicine 13, 412-421 (2009).
16. M. C. Owen et al., Effects of in vivo conditions on amyloid aggregation. Chemical Society reviews 48, 3946-3996 (2019).

17. D. J. Selkoe, J. Hardy, The amyloid hypothesis of Alzheimer's disease at 25 years. EMBO molecular medicine 8, 595-608 (2016).
18. F. M. LaFerla, K. N. Green, S. Oddo, Intracellular amyloid-beta in Alzheimer's disease. Nature reviews. Neuroscience 8, 499-509 (2007).
19. C. Ripoli et al., Intracellular accumulation of amyloid-β(Aβ) protein plays a major role in Aβ-induced alterations of glutamatergic synaptic transmission and plasticity. J Neurosci 34, 12893-12903 (2014).
20. M. Li, L. Chen, D. H. S. Lee, L.-C. Yu, Y. Zhang, The role of intracellular amyloid βin Alzheimer's disease. Progress in Neurobiology 83, 131-139 (2007).
21. J. V. Rushworth, N. M. Hooper, Lipid Rafts: Linking Alzheimer's Amyloid-βProduction, Aggregation, and Toxicity at Neuronal Membranes. International journal of Alzheimer's disease 2011, 603052 (2010).
22. F. Tofoleanu, N.-V. Buchete, Alzheimer Aβpeptide interactions with lipid membranes: fibrils, oligomers and polymorphic amyloid channels. Prion 6, 339-345 (2012).
23. S. K. Calderwood, S. S. Mambula, P. J. Gray, J. R. Theriault, Extracellular heat shock proteins in cell signaling. FEBS Letters 581, 3689-3694 (2007).
24. I. Horváth, G. Multhoff, A. Sonnleitner, L. Vígh, Membrane-associated stress proteins: more than simply chaperones. Biochimica et biophysica acta 1778, 1653-1664 (2008).
25. V. Fonte et al., Interaction of intracellular beta amyloid peptide with chaperone proteins. Proc Natl Acad Sci U S A 99, 9439-9444 (2002).
26. S. Ansar et al., A non-toxic Hsp90 inhibitor protects neurons from Abeta-induced toxicity. Bioorganic & medicinal chemistry letters 17, 1984-1990 (2007).
27. Y. Chen et al., Hsp90 chaperone inhibitor 17-AAG attenuates Abeta-induced synaptic toxicity and memory impairment. The Journal of neuroscience : the official journal of the Society for Neuroscience 34, 2464-2470 (2014).
28. C. G. Evans, S. Wisen, J. E. Gestwicki, Heat shock proteins 70 and 90 inhibit early stages of amyloid beta-(1-42) aggregation in vitro. The Journal of biological chemistry 281, 33182-33191 (2006).
29. K. Takata et al., Heat shock protein-90-induced microglial clearance of exogenous amyloid-beta1-42 in rat hippocampus in vivo. Neurosci Lett 344, 87-90 (2003).
30. W. M. Obermann, H. Sondermann, A. A. Russo, N. P. Pavletich, F. U. Hartl, In vivo function of Hsp90 is dependent on ATP binding and ATP hydrolysis. The Journal of cell biology 143, 901-910 (1998).
31. J. Adamcik, R. Mezzenga, Study of amyloid fibrils via atomic force microscopy. Current Opinion in Colloid & Interface Science 17, 369–376 (2012).
32. S. Banerjee, Z. Sun, E. Y. Hayden, D. B. Teplow, Y. L. Lyubchenko, Nanoscale Dynamics of Amyloid beta-42 Oligomers As Revealed by High-Speed Atomic Force Microscopy. ACS nano 11, 12202-12209 (2017).

33. E. Drolle, F. Hane, B. Lee, Z. Leonenko, Atomic force microscopy to study molecular mechanisms of amyloid fibril formation and toxicity in Alzheimer's disease. Drug metabolism reviews 46, 207-223 (2014).

34. T. Watanabe-Nakayama et al., High-speed atomic force microscopy reveals structural dynamics of amyloid beta1-42 aggregates. Proceedings of the National Academy of Sciences of the United States of America 113, 5835-5840 (2016).

35. M. A. Downey et al., Inhibiting and Remodeling Toxic Amyloid-Beta Oligomer Formation Using a Computationally Designed Drug Molecule That Targets Alzheimer's Disease. Journal of the American Society for Mass Spectrometry 30, 85-93 (2019).

36. F. Hane, G. Tran, S. J. Attwood, Z. Leonenko, Cu(2+) affects amyloid-β(1-42) aggregation by increasing peptide-peptide binding forces. PLoS One 8, e59005-e59005 (2013).

37. B. Y. Lee, S. J. Attwood, S. Turnbull, Z. Leonenko, Effect of Varying Concentrations of Docosahexaenoic Acid on Amyloid Beta (1(-)42) Aggregation: An Atomic Force Microscopy Study. Molecules 23, (2018).

38. M. R. Mangione et al., Hsp60, amateur chaperone in amyloid-beta fibrillogenesis. Biochim Biophys Acta 1860, 2474-2483 (2016).

39. M. A. Walti et al., Probing the mechanism of inhibition of amyloid-beta(1-42)-induced neurotoxicity by the chaperonin GroEL. Proceedings of the National Academy of Sciences of the United States of America 115, E11924-e11932 (2018).

40. J. Ojha, G. Masilamoni, D. Dunlap, R. A. Udoff, A. G. Cashikar, Sequestration of toxic oligomers by HspB1 as a cytoprotective mechanism. Molecular and cellular biology 31, 3146-3157 (2011).

41. C. Wallin et al., The Neuronal Tau Protein Blocks in Vitro Fibrillation of the Amyloid-beta (Abeta) Peptide at the Oligomeric Stage. Journal of the American Chemical Society 140, 8138-8146 (2018).

42. M. Biancalana, S. Koide, Molecular mechanism of Thioflavin-T binding to amyloid fibrils. Biochimica et biophysica acta 1804, 1405-1412 (2010).

43. S. I. Cohen, M. Vendruscolo, C. M. Dobson, T. P. Knowles, Nucleated polymerization with secondary pathways. II. Determination of self-consistent solutions to growth processes described by non-linear master equations. The Journal of chemical physics 135, 065106 (2011).

44. S. I. Cohen, M. Vendruscolo, C. M. Dobson, T. P. Knowles, From macroscopic measurements to microscopic mechanisms of protein aggregation. Journal of molecular biology 421, 160-171 (2012).

45. S. I. Cohen et al., Proliferation of amyloid-beta42 aggregates occurs through a secondary nucleation mechanism. Proceedings of the National Academy of Sciences of the United States of America 110, 9758-9763 (2013).

46. T. P. Knowles et al., An analytical solution to the kinetics of breakable filament

assembly. Science (New York, N.Y.) 326, 1533-1537 (2009).
47. G. Meisl et al., Molecular mechanisms of protein aggregation from global fitting of kinetic models. Nature protocols 11, 252-272 (2016).
48. G. Meisl et al., Differences in nucleation behavior underlie the contrasting aggregation kinetics of the Abeta40 and Abeta42 peptides. Proceedings of the National Academy of Sciences of the United States of America 111, 9384-9389 (2014).
49. E. Schönbrunn, S. Eschenburg, K. Luger, W. Kabsch, N. Amrhein, Structural basis for the interaction of the fluorescence probe 8-anilino-1-naphthalene sulfonate (ANS) with the antibiotic target MurA. Proceedings of the National Academy of Sciences 97, 6345 (2000).
50. P. R. Bharadwaj, A. K. Dubey, C. L. Masters, R. N. Martins, I. G. Macreadie, Abeta aggregation and possible implications in Alzheimer's disease pathogenesis. J Cell Mol Med 13, 412-421 (2009).
51. O. K. Gasymov, B. J. Glasgow, ANS fluorescence: potential to augment the identification of the external binding sites of proteins. Biochim Biophys Acta 1774, 403-411 (2007).
52. G. Bitan, Structural study of metastable amyloidogenic protein oligomers by photo-induced cross-linking of unmodified proteins. Methods in enzymology 413, 217-236 (2006).
53. G. Bitan, A. Lomakin, D. B. Teplow, Amyloid beta-protein oligomerization: prenucleation interactions revealed by photo-induced cross-linking of unmodified proteins. The Journal of biological chemistry 276, 35176-35184 (2001).
54. M. Mickler, M. Hessling, C. Ratzke, J. Buchner, T. Hugel, The large conformational changes of Hsp90 are only weakly coupled to ATP hydrolysis. Nature Structural & Molecular Biology 16, 281-286 (2009).
55. G. W. Preston, A. J. Wilson, Photo-induced covalent cross-linking for the analysis of biomolecular interactions. Chemical Society reviews 42, 3289-3301 (2013).
56. K. A. Krukenberg, T. O. Street, L. A. Lavery, D. A. Agard, Conformational dynamics of the molecular chaperone Hsp90. Quarterly reviews of biophysics 44, 229-255 (2011).
57. J. Li, J. Soroka, J. Buchner, The Hsp90 chaperone machinery: conformational dynamics and regulation by co-chaperones. Biochim Biophys Acta 1823, 624-635 (2012).
58. O. R. Lorenz et al., Modulation of the Hsp90 chaperone cycle by a stringent client protein. Molecular cell 53, 941-953 (2014).
59. A. K. Shiau, S. F. Harris, D. R. Southworth, D. A. Agard, Structural Analysis of E. coli hsp90 reveals dramatic nucleotide-dependent conformational rearrangements. Cell 127, 329-340 (2006).
60. B. Hellenkamp, P. Wortmann, F. Kandzia, M. Zacharias, T. Hugel, Multidomain

structure and correlated dynamics determined by self-consistent FRET networks. Nature methods 14, 174-180 (2017).

61. O. Coskuner, I. V. Murray, Adenosine triphosphate (ATP) reduces amyloid-beta protein misfolding in vitro. Journal of Alzheimer's disease : JAD 41, 561-574 (2014).

62. M. Radli, S. G. D. Rudiger, Dancing with the Diva: Hsp90-Client Interactions. Journal of molecular biology 430, 3029-3040 (2018).

63. J. Oroz, J. H. Kim, B. J. Chang, M. Zweckstetter, Mechanistic basis for the recognition of a misfolded protein by the molecular chaperone Hsp90. Nature structural & molecular biology 24, 407-413 (2017).

64. K. A. Verba et al., Atomic structure of Hsp90-Cdc37-Cdk4 reveals that Hsp90 traps and stabilizes an unfolded kinase. Science (New York, N.Y.) 352, 1542-1547 (2016).

65. D. M. Kanno, M. Levitus, Protein oligomerization equilibria and kinetics investigated by fluorescence correlation spectroscopy: a mathematical treatment. J Phys Chem B 118, 12404-12415 (2014).

66. M. H. Ali, B. Imperiali, Protein oligomerization: how and why. Bioorg Med Chem 13, 5013-5020 (2005).

67. P. Picone, D. Nuzzo, D. Giacomazza, M. Di Carlo, β-Amyloid Peptide: the Cell Compartment Multi-faceted Interaction in Alzheimer's Disease. Neurotoxicity research 37, 250-263 (2020).

68. F. M. LaFerla, K. N. Green, S. Oddo, Intracellular amyloid-βin Alzheimer's disease. Nature Reviews Neuroscience 8, 499-509 (2007).

69. S. Oddo, A. Caccamo, I. F. Smith, K. N. Green, F. M. LaFerla, A dynamic relationship between intracellular and extracellular pools of Abeta. Am J Pathol 168, 184-194 (2006).

70. R. P. Friedrich et al., Mechanism of amyloid plaque formation suggests an intracellular basis of Abeta pathogenicity. Proc Natl Acad Sci U S A 107, 1942-1947 (2010).

71. O. Wirths, G. Multhaup, T. A. Bayer, A modified β-amyloid hypothesis: intraneuronal accumulation of the β-amyloid peptide – the first step of a fatal cascade. 91, 513-520 (2004).

72. M. Gotz, P. Wortmann, S. Schmid, T. Hugel, A Multicolor Single-Molecule FRET Approach to Study Protein Dynamics and Interactions Simultaneously. Methods in enzymology 581, 487-516 (2016).

73. I. Horcas et al., WSXM: A software for scanning probe microscopy and a tool for nanotechnology. Review of Scientific Instruments 78, 013705 (2007).

74. D. Nečas, P. Klapetek, Gwyddion: an open-source software for SPM data analysis. Central European Journal of Physics 10, 181-188 (2012).

75. G. Lamour, J. B. Kirkegaard, H. Li, T. P. J. Knowles, J. Gsponer, Easyworm: an open-source software tool to determine the mechanical properties of worm-like chains.

Source Code for Biology and Medicine 9, 16 (2014).

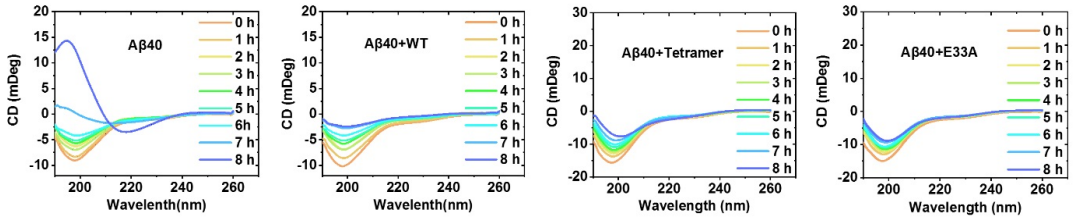

FIGURE S1: Hsp90 inhibits secondary structure transition of Aβ40. CD spectroscopy of 10 μM Aβ40 in the presence or absence of 0.04 μM Hsp90 (WT, tetramer, or E33A mutant) measured immediately after incubation for 0, 1, 2, 3, 4, 5, 6, 7, or 8 h at 37°C, indicates that Hsp90 prevents the secondary structural transition of Aβ40 from random coil to β-sheets.

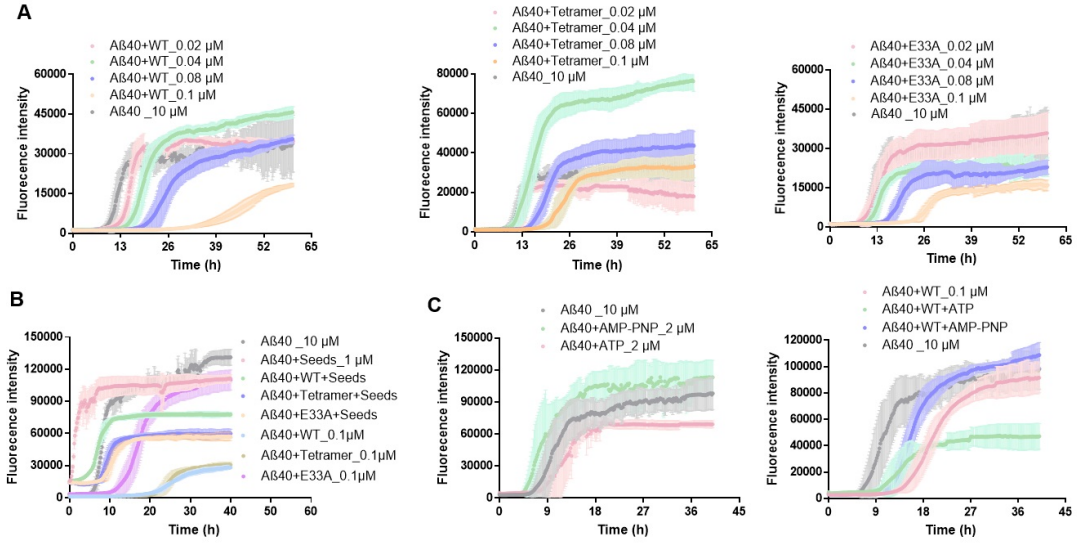

FIGURE S2: Original results of ThT assays. (A) Aggregation kinetics of Aβ40, in dependence on Hsp90 at different concentrations (0, 0.02, 0.04, 0.08, and 0.1μM). (B) Aggregation kinetics of Aβ40, with or without 1 μM Aβ40 seeds in the presence or absence of 0.1 μM Hsp90. (C) Aggregation kinetics of Aβ40, with or without 0.1μM Hsp90 in the presence or absence of 2 mM ATP or AMP-PNP. The error ranges are composed of error bars (SD values) of each data point.

3.11 Supporting information

Reference 1. B. Hellenkamp, P. Wortmann, F. Kandzia, M. Zacharias, T. Hugel, Multidomain structure and correlated dynamics determined by self-consistent FRET networks. Nature methods 14, 174-180 (2017).

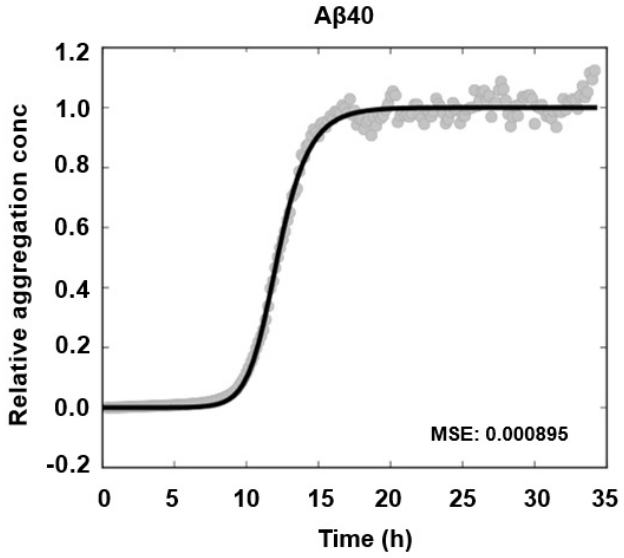

FIGURE S3: Result of fitting with ThT data from Aβ40 alone. Aβ40 fibrillation is a secondary nucleation dominated process. Following this fit, a set of parameters were obtained: k_n= 0.00174 in concentration^{-nc+1}time^{-1}; k_2= 7.11e^{+7} in concentration^{-n2} time^{-1}; k_+= 9.22e^{+6} in concentration^{-1}time^{-1}, which were uses as the initial guess values for the following fitting of Aβ40 +Hsp90.

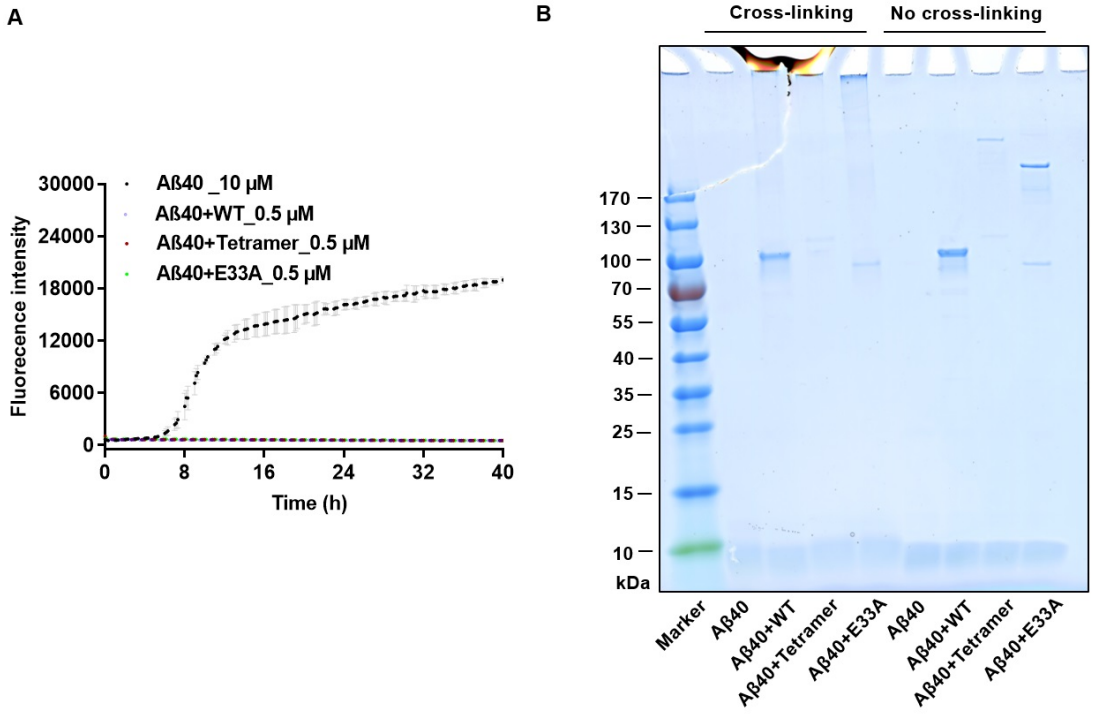

FIGURE S4: (A) ThT assay of 10 μM Aβ40 in the presence or absence of 0.5 μM Hsp90. The samples after 40 hours incubation at 37 degree were used for the photo-induced cross-linking assay in Fig. 4E. (B) A reference SDS page (with samples at 0 h of the ThT assays) to cross-linking experiment conducted with end point samples after ThT assay shown in Fig.4E. 10 μM Aβ40 in the absence or presence of 0.5 μM Hsp90 (WT, Tetramer, and E33A) were subjected to cross-linking and then SDS-page gel, or go directly to SDS-page gel. At time 0 h, Hsp90s show almost no effect on Aβ40, while keep more Aβ40 as monomers after ThT assay (Fig.4E).

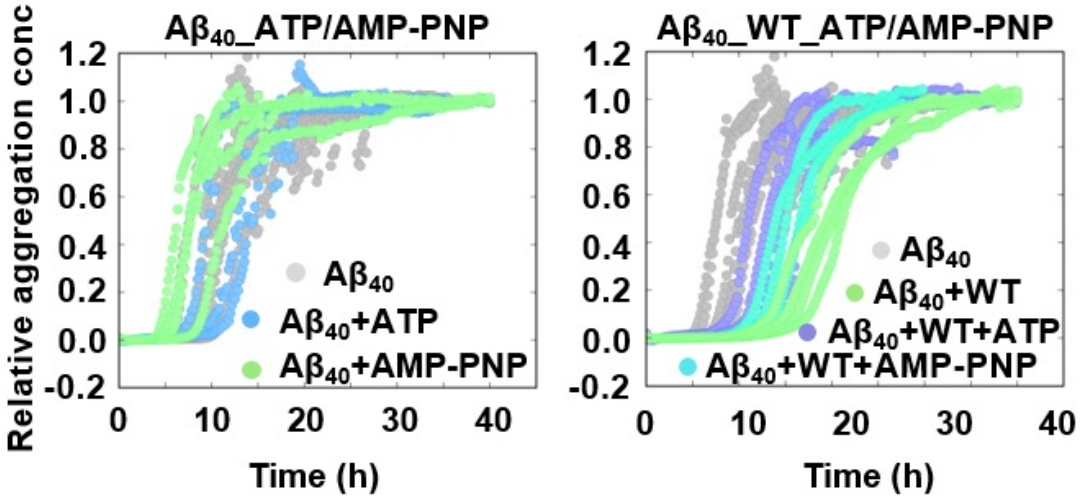

FIGURE S5: Aggregation kinetics of Aβ40 fibrillation monitored by ThT fluorescence. The experiment was conducted with 10 μM Aβ40 and 0.1 μM Hsp90, in the presence or absence of 2 mM ATP or AMP-PNP at 37°C without agitation, and the data of each repeat was normalized with AmyloFit online server.

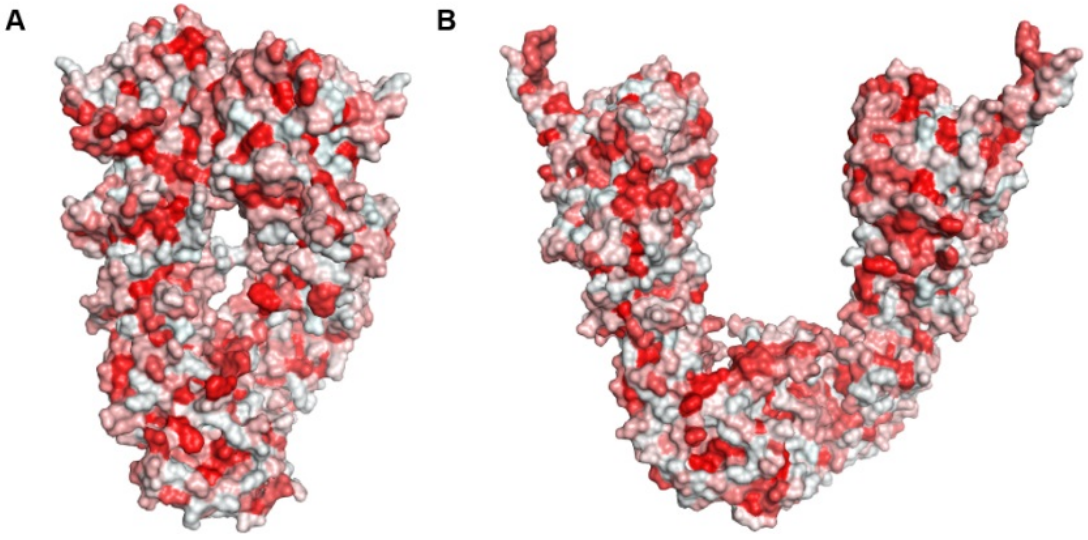

FIGURE S6: Potential hydrophobic surfaces of Hsp90 in closed (PDB ID: 2CG9) (A) and open (1) (B) states for Aβ40 binding. These show that the variation in conformational dynamics of Hsp90, such as open-to-closed transition, changes the exposed hydrophobic surfaces of Hsp90 for Aβ40 binding, apparently with more exposed hydrophobic surfaces for the open state. The hydrophobic surfaces of Hsp90 were determined with the 'PyMOL wiki Color h' script and shown in red.

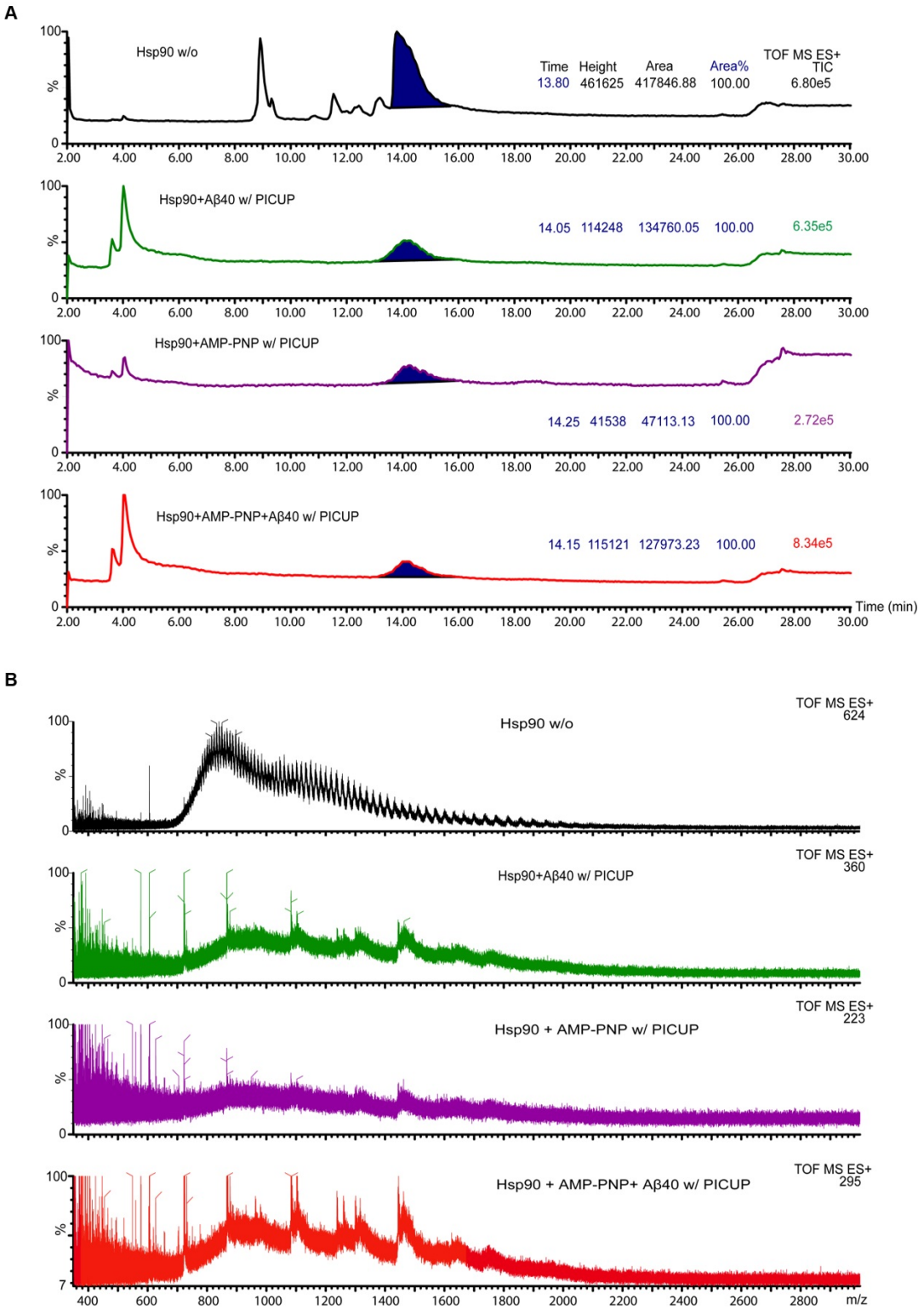

FIGURE S7: The interaction of 2 μM Hsp90 (WT) with 90 μM Aβ40 in the absence or presence of 2mM AMP-PNP. (A) and (B) LC-MS assays show that Hsp90 and Aβ40 form complexes, consistent with the result of cross-linking experiment in Fig.6B. The concentration of Hsp90 in native state (blue curve) is 10 μM. m/z is the mass-to-charge ratio of ions.

TABLE S1: The sequence of yeast Hsp90 (Hsp82) used in our study (Uniprot code: P02829).

MASETFEFQAEITQLMSLIINTVYSNKEIFLRELISNASDALDKIRYKSLSDPKQLETEP
DLFIRITPKPEQKVLEIRDSGIGMTKAELINNLGTIAKSGTKAFMEALSAGADVSMIGQF
GVGFYSLFLVADRVQVISKSNDDEQYIWESNAGGSFTVTLDEVNERIGRGTILRLFLKDD
QLEYLEEKRIKEVIKRHSEFVAYPIQLVVTKEVEKEVPIPEEEKKDEEKKDEEKKDEDDK
KPKLEEVDEEEEKKPKTKKVKEEVQEIEELNKTKPLWTRNPSDITQEEYNAFYKSISNDW
EDPLYVKHFSVEGQLEFRAILFIPKRAPFDLFESKKKKNNIKLYVRRVFITDEAEDLIPE
WLSFVKGVVDSEDLPLNLSREMLQQNKIMKVIRKNIVKKLIEAFNEIAEDSEQFEKFYSA
FSKNIKLGVHEDTQNRAALAKLLRYNSTKSVDELTSLTDYVTRMPEHQKNIYYITGESLK
AVEKSPFLDALKAKNFEVLFLTDPIDEYAFTQLKEFEGKTLVDITKDFELEETDEEKAER
EKEIKEYEPLTKALKEILGDQVEKVVVSYKLLDAPAAIRTGQFGWSANMERIMKAQALRD
SSMSSYMSSKKTFEISPKSPIIKELKKRVDEGGAQDKTVKDLTKLLYETALLTSGFSLDE
PTSFASRINRLISLGLNIDEDEETETAPEASTAAPVEEVPADTEMEEVD

Chapter 4

Multivariate effects of pH, salt, and Zn^{2+} ions on Aβ fibrillation

Hongzhi Wang[1], Jinming Wu[1], Rebecca Sternke-Hoffmann[1], Axel Abelein[2], Cecilia Mörman[3], Jinghui Luo[1]*

1. Department of Biology and Chemistry, Paul Scherrer Institute, 5232 Villigen, Switzerland.
2. Department of Neurobiology, Care Sciences and Society, Center for Alzheimer Research, Division of Neurogeriatrics, Karolinska Institutet, 141 57, Huddinge, Sweden.
3. Department of Biochemistry and Biophysics, the Arrhenius Laboratories, Stockholm University, 106 91 Stockholm, Sweden.
*Corresponding author: Jinghui.luo@psi.ch, Tel: +41 56 310 47 64

under submission

4.1 Abstract

Abnormal amyloid beta (Aβ) peptide aggregation plays a central role in the progress of Alzheimer's disease (AD), of which Aβ-deposited extracellular amyloid plaque is a major hallmark. Observed in AD patients, the brain micro-environmental variation, like local acidification, increased ionic strength, or elevated metal ion level, modulates the aggregation of the Aβ peptides. Although the effects of pH, ionic strength, or metal ions on Aβ aggregation have been individually studied, the multivariate effects on the aggregation remain to be further explored. Here, we investigate the multivariate effects on Aβ fibrillation kinetics by using a buffer matrix with varied pH, ionic strength, with or without 40 μM Zn^{2+} ions. Our results reveal that Aβ fibrillation kinetics are not only controlled by pH but also synergistically modulated by Zn^{2+} ions and/or ionic strength: (1) pH decrease inhibits amyloid formation of Aβ40 in the absence of Zn^{2+} ions, but promotes in the presence of Zn^{2+} ions, which is further modulated by ionic strength; (2) ionic strength promotes Aβ40 fibrillation without Zn^{2+} ions across the whole pH range, while in the presence of Zn^{2+} ions, inhibits at pH 6.5-7.1 and promotes at pH 7.4-8.0 Aβ40 fibrillation; (3) the promotive effects of Zn^{2+} ions on Aβ40 fibrillation convert into the inhibitory ones as pH increases, and ionic strength shifts the conversion to a lower pH; (4) pH and ionic strength influence the fibrillation kinetics of Aβ 40 mainly by regulating the elongation process; and (5) ionic strength modulates the morphology of Aβ40 aggregates. Given the commonly observed changes in pH values and the levels of salt and Zn^{2+} ions in AD patients, the reported complex covariate effects of pH, salt, and Zn^{2+} ions will deepen our understanding of the molecular pathology and the local brain microenvironment in AD.

Keywords: Aβ40 fibrillation, pH, ionic strength, Zn^{2+} ions, electrostatics

4.2 Introduction

Alzheimer's disease (AD) is the most prevalent form of devastating neurodegenerative diseases and contributes to 60%-70% of cases of dementia, whilst the therapeutics is under evaluation (1). The abnormal aggregation of the amyloid beta (Aβ) peptides and the tau protein play an essential role in the development of AD, that is pathogenically manifested by Aβ senile plaques (2) and tau neurofibrillary tangles (3). Aβ peptide fibrillation occurs through the typical lag-, elongation-, and plateau- phases, during which the secondary structure converts from random coil to β-sheet (4, 5). The brain micro-environmental constituents, like pH, salt, and metal ions, play a vital role to

modulate the secondary conversion, fibril formation, as well as toxicity of Aβaggregates (5, 6).

Alterations of micro-environmental constituent, like pH, ionic strength, and metal ions, have been clinically observed in AD brain. The pH varied from 6.3 to 6.8 in AD brains (7) is lower than that of the healthy ones ranged from 7.1 to 7.3 (8). The low pH is assumed to an acidosis and linked to inflammatory processes in AD. Zn^{2+} ions increase up to 1 mM within amyloid plaques (9), so does an increased ionic strength of sodium, potassium, or chloride ions in AD (10). The effects of pH, Zn^{2+} ions, or ionic strength (salt) on Aβ aggregation have been already individually investigated. The fibrillation rate of Aβ42 drops as pH decreases below pH at 7, whilst the rate is independent of the pH ranging from 7 to 9 (11). A low pH at 6 has a strong stabilizing effect on the fibrillary assembly of Aβ(12). It reveals that low pH may slow down Aβ fibrillation but stabilize the end-product fibril. Ionic strength can promote Aβ40 fibrillation and modulate the morphology and structure of Aβ40 aggregates presumably through electrostatic interactions [16]. Under near-physiological conditions (pH 7.2-7.4), substoichiometric amounts of Zn^{2+} effectively retard Aβ40 fibrillation by reducing the elongation rate through the transient formation of Aβ40-Zn^{2+} complex within the N-terminus (13). On the contrary, the binding of Zn^{2+} ions to Aβ40 under physiological conditions (pH 7.4) rapidly destabilize the peptide, inducing formation of larger aggregates (14). This discrepancy could be explained by the different experimental conditions. That emphasizes the importance of investigating the covariate/multivariate effects systematically. The covariate effect of these brain constituents on amyloid aggregation behavior will provide comprehensive knowledge for the understanding of complicated Aβaggregation as well as the molecular pathogenesis in AD.

In this study, we implemented protein crystallization robotics to create a buffer matrix including 96 different conditions with a range of pH values from 6.5 to 8.0, and varied ionic strengths (0 M to 0.1 M NaCl) in the absence or presence of 40 μM Zn^{2+} ions. With this buffer matrix, we investigated the covariate effects of micro-environmental factors, like pH, Zn^{2+} ions, and ionic strength, on Aβ40 fibrillation kinetics and the morphologies of Aβ40 aggregates. Depending on the concentration of Zn^{2+} ions, a low pH, i.e., pH 6.5, can both promote and inhibit Aβaggregation of which can be further modulated by ionic strength. At a high concentration, NaCl promotes Aβ aggregation, except those at pH 6.5-7.1 in the presence of Zn^{2+} ions, which inhibit Aβ aggregation. In the absence of NaCl, Zn^{2+} ions promotes Aβ40 aggregation at low pH values (6.5 and 6.8) but inhibits at high pH values (7.1, 7.4, 7.7, and 8.0). This change in the effects of Zn^{2+} ions on Aβ40 aggregation can be achieved at lower pH values in the presence of increasing concentrations of NaCl. pH and ionic strength influence Aβ aggregation by interfering with the elongation process. The complex covariate effects of pH, salt,

and Zn^{2+} ions on Aβ40 aggregation reported here can, to some extent, explain the inconsistency in this field, which might be induced by the difference in the experiment conditions, and provide us with better understanding of the pathology of AD.

4.3 Results

4.3.1 Buffer matrix design

To investigate how the micro-environmental constituents modulate Aβ40 fibrillation process, Thioflavin T (ThT) fluorescence assay was used to monitor the aggregation kinetics of 10 μM Aβ40. ThT is a commonly used fluorescence dye to monitor the formation of amyloid fibrils, as its fluorescence intensity sharply increases upon binding to amyloid fibrils (15). The buffer matrix was programmed and dispensed with the protein crystallography screen builder (Formulator). The builder accurately generates 96-condition buffer matrix shown in Table 1 with a series of pH values from 6.5 to 8.0 and NaCl concentrations from 0 M to 0.1 M in the presence or absence of 40 μM Zn^{2+} ions. By conducting ThT fluorescence assays in a buffer matrix, we were able to observe the covariate/multivariate effects of two or three constitutes on Aβ40 fibrillation kinetics in **Fig.1**. The fibrillation kinetics assays in the buffer matrix have been repeated separately for four times, samples were tested in triplicate each time, and one representative are selected in **Fig.1** for the following analysis.

4.3.2 Covariate effects of pH, ionic strength and Zn^{2+} ions on Aβ40 fibrillation

The effects of pH on Aβ40 fibrillation were investigated by varying NaCl concentrations from 0 M to 0.1 M in the absence or presence of 40 μM Zn^{2+} ions with ThT assays shown in **Fig.1**. In the absence of Zn^{2+} ions, as shown by the half-time $t_{1/2}$ of Aβ 40 fibrillation obtained by sigmoidal fitting in **Fig.2A**, pH decrease from 7.4 to 6.5 inhibits Aβ40 fibrillation at all given NaCl concentrations. In the absence of NaCl, pH increase from 7.4 to 8 inhibits Aβ40 fibrillation. In the presence of NaCl, pH increase from 6.5 to 8 promotes Aβ40 fibrillation. In the absence of Zn^{2+} ions, NaCl promotes Aβ40 fibrillation as its concentration increases from 0 M to 0.1 M, which is confirmed by the $t_{1/2}$ obtained by sigmoidal fitting in **Fig.2B**. The promoting effect of NaCl on Aβ40 fibrillation is slightly enhanced as pH values increase. Briefly, a reduction of $t_{1/2}$ is observed at higher NaCl concentrations compared to those at lower NaCl concentrations at a specific pH value, and the reduction is promoted as pH increases.

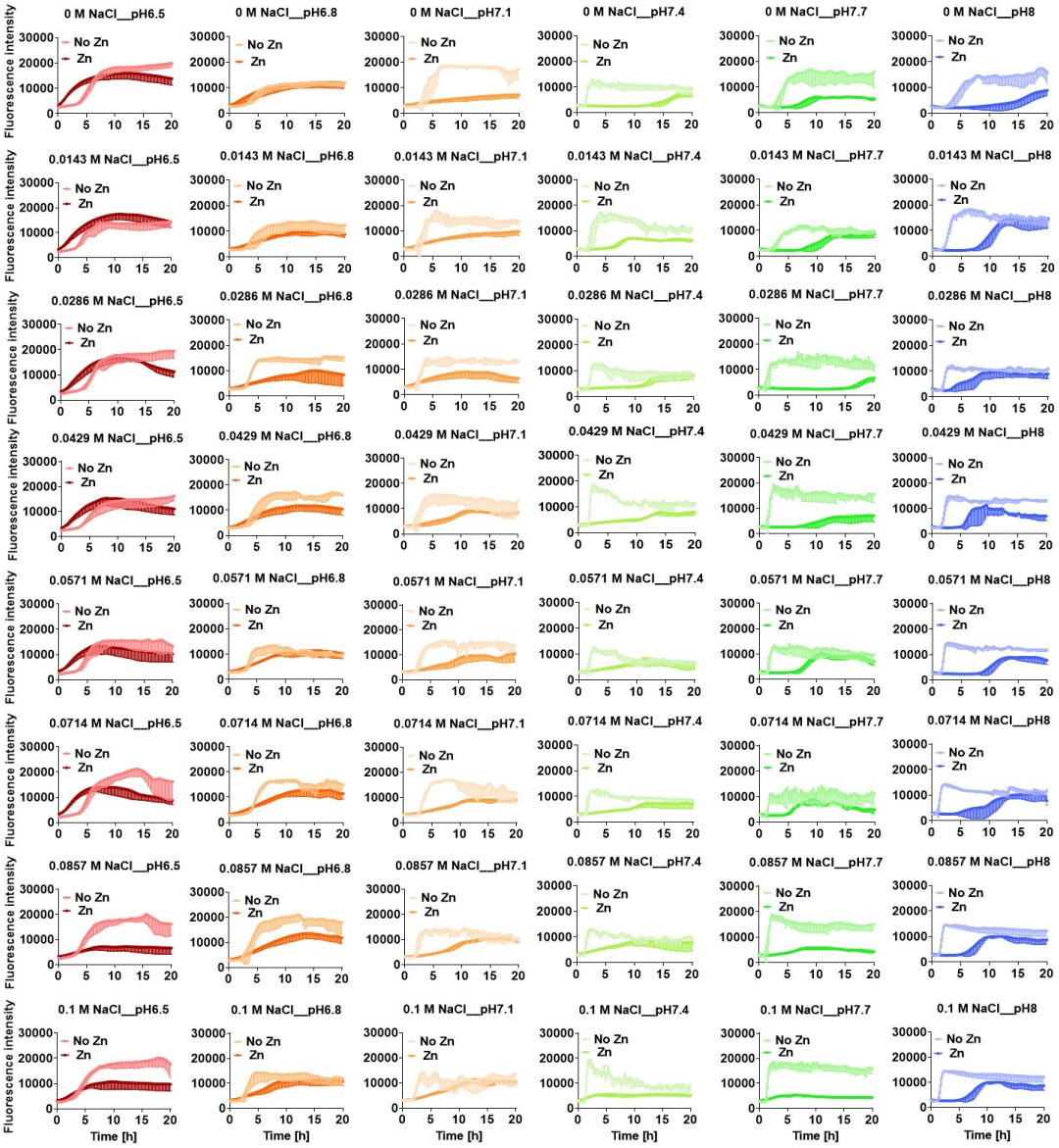

FIGURE 1: Covariate/multivariate effects of pH, NaCl, and Zn^{2+} ions on Aβ40 fibrillation. Aggregation kinetics of 10 μM Aβ40 were monitored by ThT assays at 37°C under quiescent conditions. The results indicate that effects of pH, salt, and Zn^{2+} ions on Aβ40 aggregation are influenced mutually. In the absence of Zn^{2+} ions, decreasing in pH values from 7.4 inhibits Aβ40 fibrillation, while above 7.4, pH values have no significant influence in Aβ40 fibrillation. Increasing in salt concentrations can promotes Aβ40 fibrillation and the similar promotion effect of salt on Aβ40 fibrillation can be achieved at lower salt concentration as pH increases. In the presence of Zn^{2+} ions, decreasing in pH values from 7.4 promotes Aβ40 fibrillation, while higher pH (7.7, 8.0) inhibits Aβ40 fibrillation with no obvious difference; salt has almost no effect on Aβ40 fibrillation at lower concentrations, but as concentration increases, inhibits Aβ40 fibrillation at lower pH (6.5, 6.8, 7.1) and promotes Aβ40 fibrillation at higher pH (7.4, 7.7, 8). Zn promotes Aβ40 fibrillation at low pH and gradually inhibits Aβ40 fibrillation as pH increases, besides, the change (from promotion to inhibition) in the effect of Zn on Aβ40 fibrillation appears earlier at higher salt concentrations compared to those at lower salt concentrations.

The covariate effects of pH and ionic strength were also investigated in the presence of Zn^{2+} ions. As shown in**Fig.2A** and **2B**, pH decrease from 7.1 to 6.5 promotes Aβ40 fibrillation, whereas Aβ40 fibrillation is independent of pH changes at pH over 7.1. Both effects, the promoting effect of pH values from 7.1 to 6.5 and the erratic inhibitory effects of pH values above 7.1 are weakened as the ionic strength of NaCl increases. In the presence of Zn^{2+} ions, pH affects Aβ40 fibrillation, which can be further altered by the ionic strength. NaCl has no obvious effect on Aβ40 fibrillation at low concentrations. As the concentration increases, the effects of NaCl are dependent on the particular pH values: at lower pH values (6.5, 6.8, and 7.1) NaCl inhibits Aβ40 fibrillation with increasing concentrations, while this inhibitory effect of high concentrations of NaCl is converted into a promotive effect at higher pH values (7.4, 7.7 and 8).

The effects of 40 μM Zn^{2+} ions on Aβ40 fibrillation were studied at varied pHs from 6.5 to 8 and varied ionic strength from 0 M to 0.1 M NaCl by ThT assays, and the results are shown in **Fig.1**. Zn^{2+} ions has opposite effects on Aβ40 fibrillation depending on pH values, which can be further modulated by the variation in the concentrations of NaCl. The promotive effect of Zn^{2+} ions converts to inhibitory one on Aβ40 fibrillation as pH values change from 6.5 to 8, and this change in the effects of Zn^{2+} ions on Aβ40 fibrillation occur at lower pH values as the concentrations of NaCl increase from 0 M to 0.1 M.

In summary, Aβ40 fibrillation behaves differently under various conditions with specific combination of pH value, salt concentration, and Zn^{2+} ions, suggesting that it would be better to take other microenvironmental factors into consideration when interpret the effect of one specific factor.

4.3.3 Covariate effects of pH and ionic strength on the kinetics of Aβ40 fibrillation

To get further insight into the microscopic mechanisms of Aβ40 fibrillation at different pHs and NaCl concentrations in the absence of Zn^{2+} ions, global fit analysis of the kinetic data was conducted with an integrated rate law (16-19) by using the *AmyloFit* online software server (20). Amyloid proteins usually undergo aggregation via either primary or secondary dominated pathways (17, 21) and Aβ40 fibrillation is mainly dominated by secondary nucleation process (21, 22). Therefore, we selected the secondary nucleation dominated model and first fitted the ThT data of Aβ40 at pH 7.4 in the absence of NaCl and Zn^{2+} ions. A set of parameters, including the primary nucleation rate constant (k_n) = 0.00047 in concentration^{nc+1} time^{-1} (nc is the reaction order of primary nucleation that simply interprets a nucleus size), the secondary nucleation rate constant (k_2) = 4e^{+7}

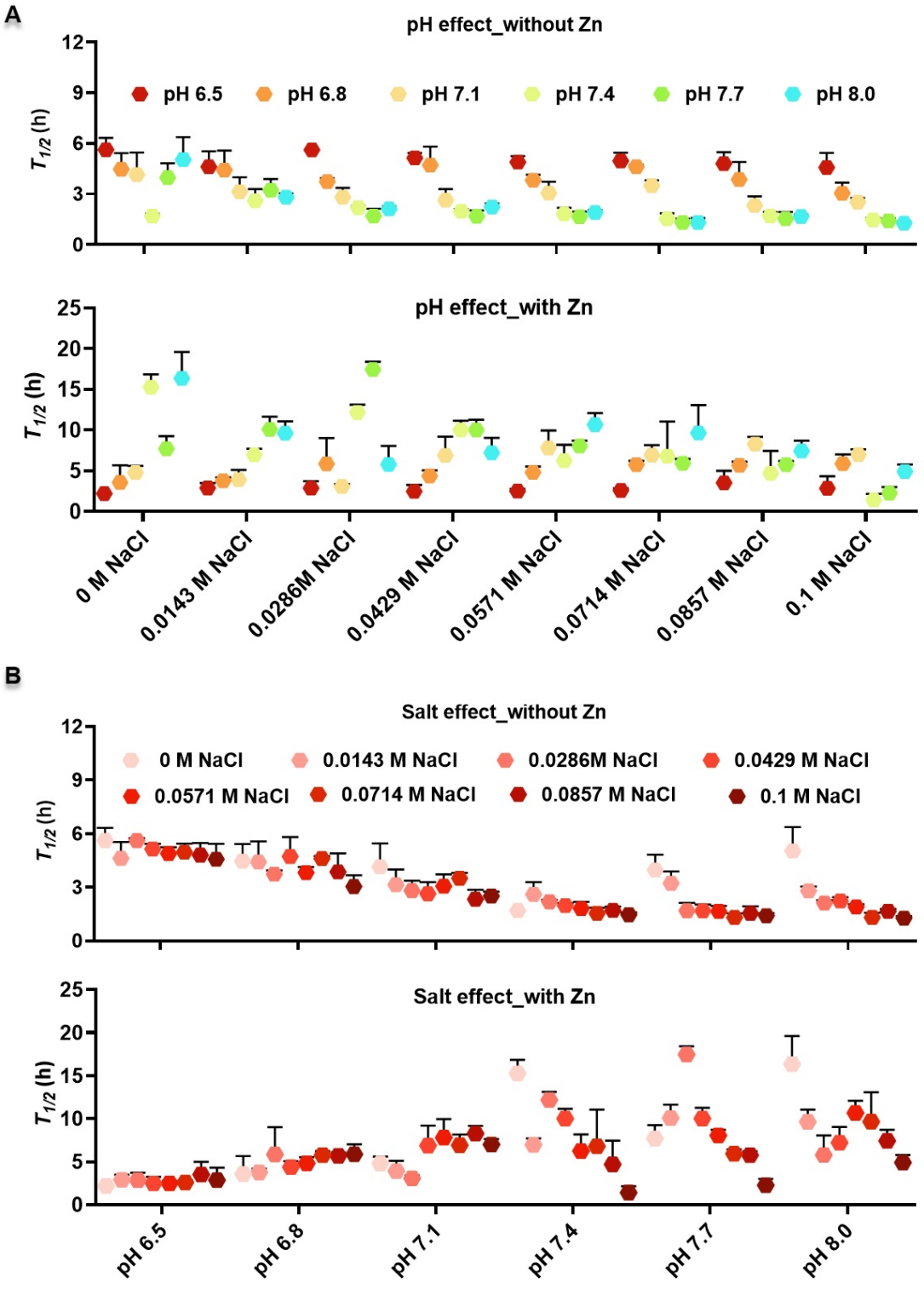

FIGURE 2: Covariate effects of pH, ionic strength and Zn^{2+} ions on Aβ40 fibrillation. The $t_{1/2}$ of the fibrillation of 10 µM Aβ40 at various pH values (6.5, 6.8, 7.1, 7.4, 7.7, and 8) and NaCl concentrations (0, 0.0143, 0.0285, 0.0429, 0.0571, 0.0714, 0.0857, and 0.1 M), were derived from sigmoidal fitting of ThT data of each repeat in the absence or presence of Zn^{2+} ions. (A) pH effects and (B) salt effects on Aβ40 fibrillation are shown separately for comparison (check text for details).

in concentration^{-n2} time^{-1} (n2 is the reaction order of secondary nucleation), and the elongation rate constant (k_+) = 9.49e^{+8} in concentration^{-1}time^{-1} of Aβ40 fibrillation process were obtained and used as the initial guess values for the following fit. Each one of the three rate constants (k_n, k_2, k_+) was fitted freely, while the other two were kept as initial guess values. Then, the fitting for all data was performed by both pH effect and salt effect. The results of the global fit analysis shown in **Fig.3A** and **Fig.S1A** indicate that if the rate constants k_2 and k_+, especially k_+, rather than thek_n, were freely fitted, the fitting results can reproduce the curve shapes and the dependence of Aβ40 fibrillation on pH and NaCl, suggesting that the secondary pathways (mostly the elongation processes) of Aβ40 aggregation are modulated by pH and NaCl. In addition, the relative rate constants derived from the global fit shown in **Fig.3B** and **Fig.S1B** are consistent with the half-times $t_{1/2}$ in **Fig.2**. For instance, an increased relative rate constant in **Fig.3B** and **Fig.S1B** matches with a decreased $t_{1/2}$ in **Fig.2**, corresponding to the promotive effect of this specific pH value and concentration of NaCl on Aβ40 aggregation in **Fig.1**. To sum up, pH and salt modulate the fibrillation of Aβ40 peptide via interfering with its elongation processes in the absence of Zn^{2+} ions.

4.3.4 Covariate effects of pH, ionic strength, and Zn^{2+} ions on the morphologies of Aβ40 aggregates

To investigate the influence of pH, NaCl, and Zn^{2+} ions in the morphology of Aβ40 aggregates, 10 μM Aβ40 samples taken from ThT assays at various pH values, 0.1 M NaCl and in the absence or presence of 40 μM Zn^{2+} ions were visualized using TEM. The TEM images shown in **Fig.5** reveal two different kinds of Aβ40 aggregates, fibrils and amorphous aggregates. In the absence of NaCl, Aβ40 peptide forms fibrils while in the presence of 0.1 M NaCl, amorphous aggregates were observed independent of pH values and the presence of Zn^{2+} ions. This indicates that NaCl, not pH and Zn^{2+} ions plays a role in changing the morphology of Aβ40 aggregates.

4.4 Discussion

Employing the protein crystallization robotics, we prepared a buffer matrix including 96 different conditions with the varied pH values and ionic strengths in the absence or presence of 40 μM Zn^{2+} ions. With this buffer matrix, we investigated the covariate effects of the disease relevant micro-environmental constitutes on Aβ40 fibrillation kinetics and the morphological changes of Aβ40 aggregates. We found that Aβ40 fibrillation can be affected by not only pH, but ionic strength (NaCl) and Zn^{2+} ions simultaneously,

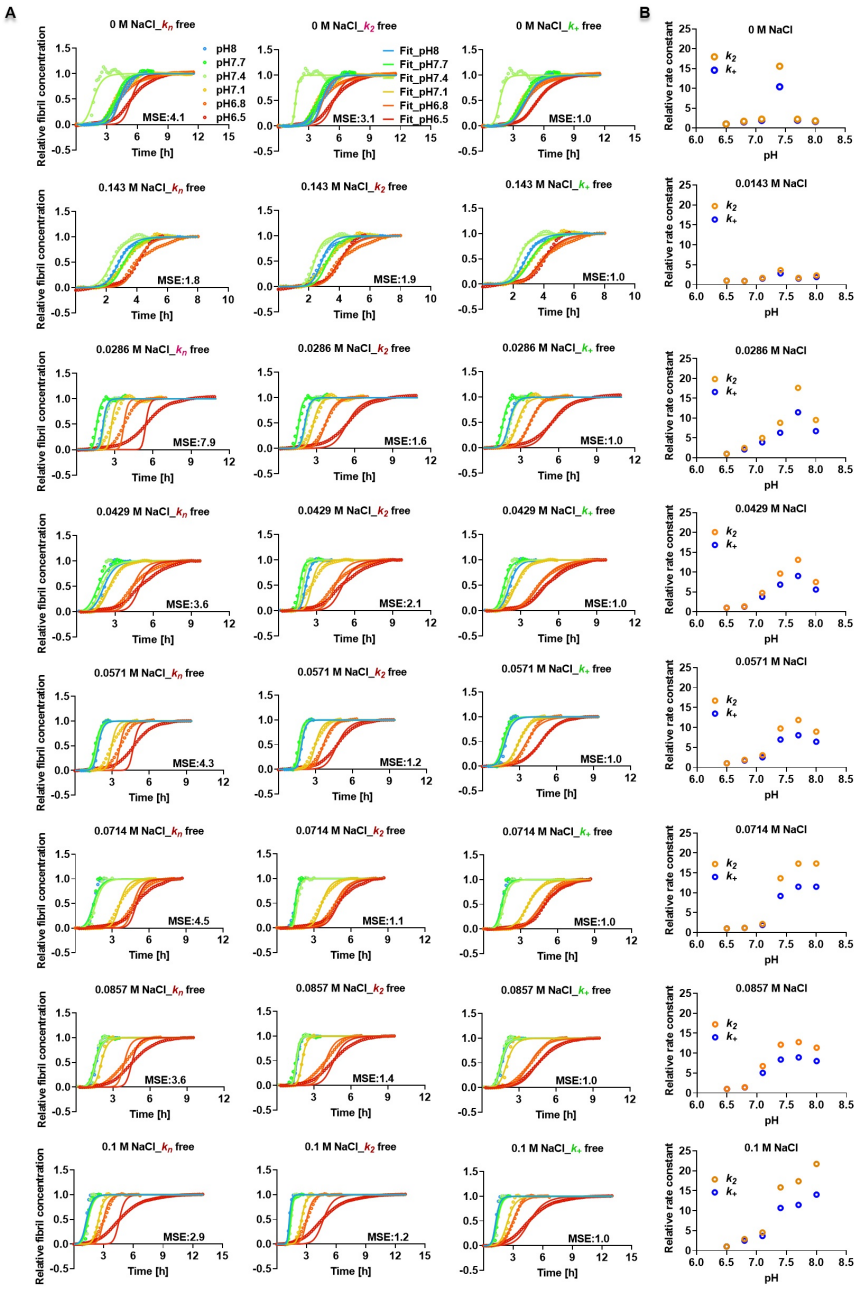

FIGURE 3: pH values mainly influence the elongation process of the kinetics of Aβ40 fibrillation in the absence of Zn^{2+} ions. (A) Elongation processes of Aβ40 fibrillation are influenced by pH values at various concentrations of NaCl. Aggregation kinetics of 10 µM Aβ40 at different pH values (6.5, 6.8, 7.1, 7.4, 7.7, and 8) and concentrations of NaCl (0, 0,0143, 0.0285, 0.0429, 0.0571, 0.0714, 0.0857, and 0.1 M) were monitored by ThT fluorescence over time (the raw data can be found in Fig.1). The ThT data were then globally fitted by using the *AmyloFit* online software server (20). For the fitting procedure, the data of Aβ40 at pH 7.4 in the absence of NaCl were first fitted with a secondary nucleation dominated model, from which a set of parameters including k_n = 0.00047 in concentration^{-nc+1} time^{-1}, k_2 = 4e^{+7} in concentration^{-n2} time^{-1}, and k_+ = 9.49e^{+8} in concentration^{-1} time^{-1} of Aβ40 fibrillation were obtained and used as the initial guess values for the following global fit. Each one of the rate constants k_n, k_2, or k_+ was fitted freely, while the other two were set as initial guess values, by choosing the secondary nucleation dominated model. When k_+ and/or k_2, but not k_n, were freely fitted then the data was well described (see main text for details). The mean square error (MSE) values for each set of Aβ40 samples were normalized against the one with the best fit (lowest MSE value). (B) Relative rate constants (relative to the rate constants of Aβ40 at pH 6.5) derived from global fitting for Aβ40 samples at different pH values and salt concentrations.

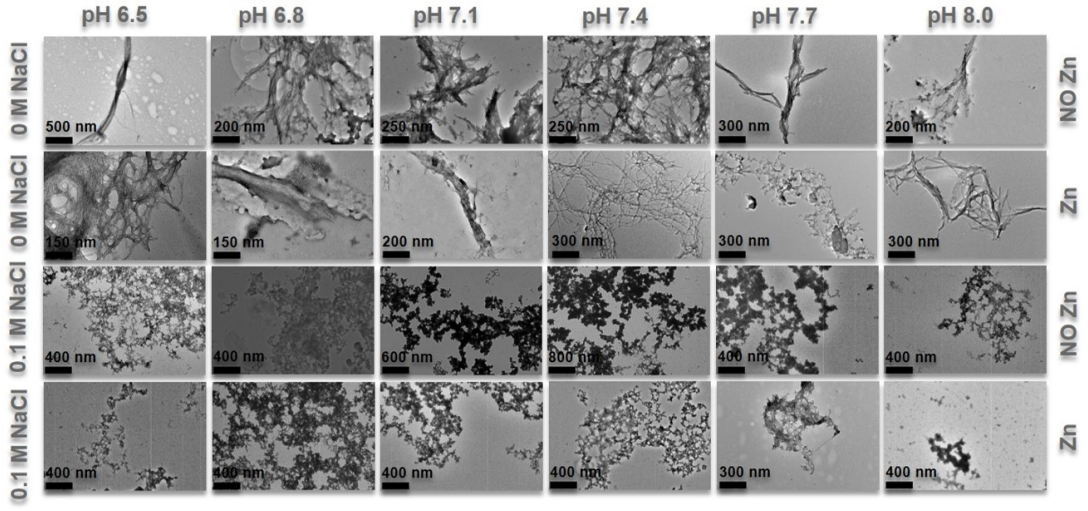

FIGURE 4: TEM images of 10 μM Aβ40 in the presence or absence of NaCl and/or Zn^{2+} ions at different pHs obtained after incubation at 37°C for 20 h without agitation, show that salt, but not pH and Zn^{2+} ions influence the morphology of Aβ40 aggregates.

as shown in **Fig.1** and summarized in **Fig.5**. Decreasing in pH values to 6.5 possesses both promotive and inhibitory effects on Aβ40 fibrillation, depending on the presence of Zn^{2+} ions. In addition, the effect of pH on Aβ40 fibrillation can be further modulated by different concentrations of NaCl. Increasing in concentrations of NaCl generally promote Aβ40 aggregation. However, high concentrations of NaCl inhibit Aβ40 aggregation at pH 6.5-7.1 in the presence of Zn^{2+} ions. Zn^{2+} ions exert opposite effects on Aβ40 aggregation at lower and higher pH values used in this study. These effects may be achieved by regulating the elongation process of Aβ40 fibrillation, as shown by the global fitting results in **Fig.3** and **Fig.S1**. Besides, the morphology of Aβ40 aggregates change in the presence of NaCl.

The isoelectric point (pI) of Aβ40 is pH 5.4 (23) and the effective pI changes as interacting with specific ions (24). The histidines (H13/H14) on Aβsequence have a pKa at around 6.0 (25). The fibrillation rate of Aβ42 drops as pH decreases under pH 7, whilst the rate is independent of pH 7-9 (11). The concurrent protonation of H13/H14 at low pH contributes to positive charges that repel each other, thereby stabilizing the peptides and preventing the fibril formation (11). Our study further agreed that in the absence of Zn^{2+} ions, the lower pH in the range from 7.4 to 6.5, the less yield of amyloid fibrils. Higher pH values (7.7 and 8.0) cannot significantly affect Aβ40 fibrillation compared with that at pH 7.4 (**Fig.1** and **Fig.2A**). An exception is the effect of pH on Aβ40 fibrillation in the absence of NaCl, where decreasing in pH from 8.0 to 7.4 promotes Aβ40 fibrillation (**Fig.1** and **Fig.2A**). And this promotive effect of pH decrease agrees with another study that reducing pH from 8.0 to 7.4 enhances the secondary nucleation of Aβ42 peptides, due to the attenuated electrostatic repulsion among Aβ42 peptides (26).

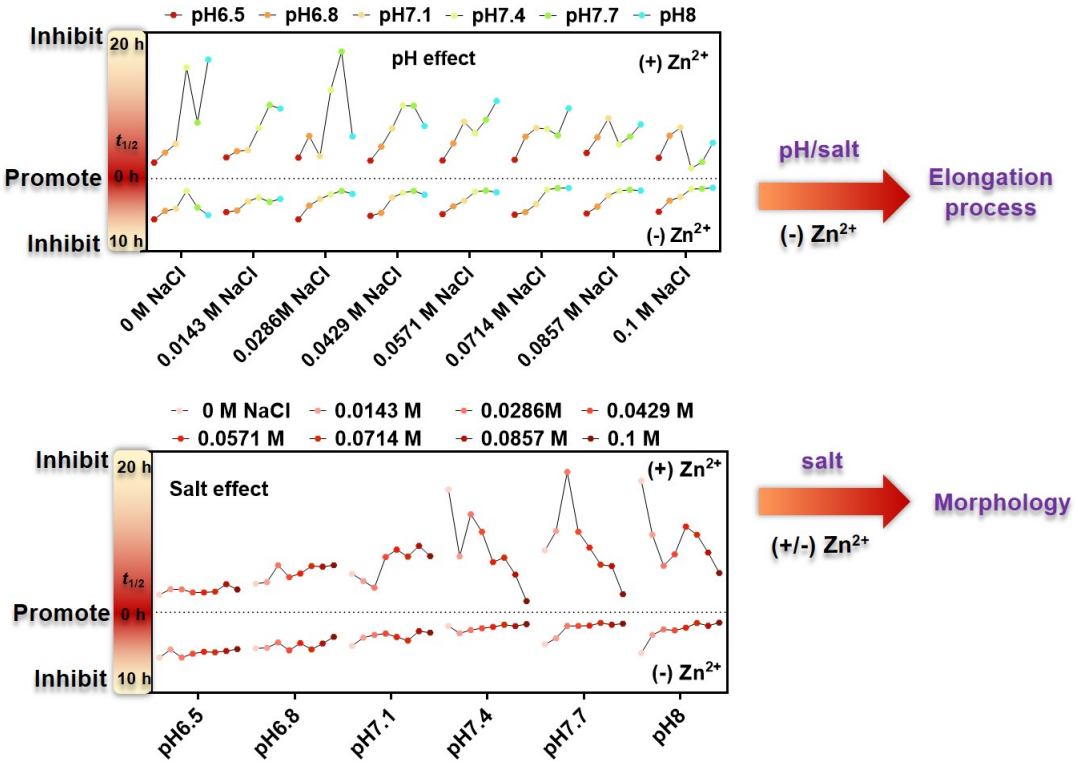

FIGURE 5: Covariate effects of pH, ionic strength, and Zn^{2+} ions on Aβ40 fibrillation kinetics and the morphology of Aβ40 aggregates

The aggregation of Aβ42 can be induced by the intra- and intermolecular salt bridges formed at pH 6-8, but not at pH <5 and >9.0 (27). In addition, a rearrangement of the salt bridge network is involved in the misfolding of ApoE4 protein (28). This agrees with the pH effect on Aβ40 fibrillation in the absence of NaCl and Zn^{2+} ions that both pH decrease and increase from 7.4 inhibit Aβ40 fibrillation **(Fig.1** and **Fig.2A**), which may be induced by the attenuation of the salt bridges between the side chains of D23 and K28. Zn^{2+}ions may compete with H^{+} ions at lower pH values (6.5, 6.8, and 7.1) for the H13 and H14 residues, thereby reducing their levels of protonation and leading to decreased repulsion force among the Aβ40 peptides. Consequently, pH decrease from 7.1 to 6.5 promotes Aβ40 fibrillation compared with that at pH 7.1, in opposite of the effect of lower pH values in the absence of Zn^{2+} ions (**Fig.1** and **Fig.2A**). These results are consistent with previous study showing that low pH at 6 has a strong stabilizing effect on the fibrillary assembly of Aβ (12, 29). pH 7.4-8.0 in the presence of Zn^{2+} ions shows irregular effects on Aβ40 fibrillation. This irregularity may due to the integrated effect of pH on the protonation of side chains, salt on shielding electrostatic repulsion, and Zn^{2+} ions on binding to H13/H14 of Aβ40 peptide

Ionic strength can shield the charge repulsion and may promote amyloid formation (6). This is backed by studies (24, 30) showing that salts accelerate Aβ40 aggregation and modulate the morphological and structural changes of Aβ40 aggregates, presumably

through electrostatic interactions, which may yield more heterogeneous fibrils. Consistent with these studies, our results in the absence of Zn^{2+} ions indicate that increasing the concentration of NaCl from 0 M to 0.1 M promotes Aβ40 fibrillation (**Fig.1** and **Fig.2B**) and the presence of 0.1 M NaCl converts Aβ40 fibrils into amorphous aggregates (**Fig.4**). Salt can promote fibrils formation, however, it can also inhibit fibril formation, leading to amorphous aggregates, depending on the concentration of salt (31). The fibrils formed in the presence of 0.1 M NaCl probably converted into amorphous aggregates as the incubation time goes on in ThT assays. In addition, the promotive effect of NaCl on Aβ40 fibrillation is generally enhanced by the increase in pH values from 6.5 to 8.0, which may be due to the reduction of electrostatic repulsion at higher pH values. In the presence of Zn^{2+} ions, increasing the concentrations of NaCl inhibits Aβ40 fibrillation at pH 6.5-7.1, while promotes Aβ40 fibrillation at pH 7.4-8.0. The different effects of NaCl on Aβ40 fibrillation at low and high pH values, may be explained that Zn^{2+} ions complement with ionic strength differently for shielding the electrostatic repulsion among the Aβ40 peptides at different pHs. It still remains to be further explored.

Zn^{2+} ions bind to the N-terminus (aa1-16) of the Aβ peptides involving the H13/H14 residues (32, 33). One study shows that under near-physiological conditions (pH 7.2-7.4), substoichiometric amounts of Zn^{2+} effectively retard Aβ40 fibrillation by reducing the elongation rate through the transient formation of Aβ40-Zn^{2+} complex within N-terminus (13). In this study, Zn^{2+} ions at a final concentration of 40 μM possess opposite effects on Aβ40 fibrillation as pH values increase from 6.5 to 8.0. For instance, Zn^{2+} ions promote Aβ40 fibrillation at lower pH values like pH 6.5 and inhibit Aβ40 fibrillation at higher pH values like pH 8.0, compared with those at pH 7.4. This might be caused by the protonation of H13/H14 at lower pH values (6.5, 6.8, and 7.1), leading to the reduction of Zn^{2+} ions binding to the H13/H14 residues and consequently the decreased efficiency in inhibiting Aβ40 fibrillation. While at higher pH values (7.7 and 8.0), the H13/H14 residues may be further deprotonated compared to those at pH 7.4 and more Zn^{2+} ions can bind to H13/H14, leading to enhanced inhibitory effect of Zn^{2+} ions on Aβ40 fibrillation. The change in the effect of Zn^{2+} ions on Aβ40 fibrillation as pH increases from 6.5 to 8.0 occurs at lower pH values with the concentrations of NaCl increasing from 0 M to 0.1 M. This can be explained that the Cl- ions may counteract the effect of protonation of H13/H14 residues at relatively lower pH values, at which the change in the effect of Zn^{2+} ions on Aβ40 fibrillation were achieved. However, Zn^{2+} ions have also been reported, under physiological conditions (pH 7.4), to rapidly induce the aggregation of the Aβpeptides in vitro (14). The discrepancy compared with above-mentioned studies could be explained by the different conditions used in different studies, as has been shown in this study that Zn^{2+} ions have different effects under various conditions.

Besides, our global fitting results indicate that pH and NaCl influence Aβ40 fibrillation by mainly interfering with the elongation process in the absence of Zn^{2+} ions (**Fig.3** and **Fig.S1**), which is in line with previous study (30). The addition of salt may shield the charge repulsion between the ends of the existing fibrils and free Aβ40 monomers that are about to be added to the fibril ends.

The micro-environmental constituents, like pH, salt, and metal ions in the brain change during the progression of AD (7-10, 34). This change can modulate the abnormal aggregation of the Aβ40 peptide (5, 6). Though the effects of pH, salt, and Zn^{2+} ions on Aβ40 aggregation have been individually investigated, neither has the consensus been reached (11-14), nor have the covariate effects been studied. However, Aβ40 fibrillation kinetics is prone to alteration even with minor micro-environmental change. In this study, although we have not yet investigated the pH effect in the whole range, pH 6.5-8 substantially covers the micro-environmental changes in AD's brain. Low pH values used in vitro can mimic the acidosis, which is usually linked to inflammatory processes in vivo. The covariate effects of pH, ionic strength, and Zn^{2+} ions on Aβ40 fibrillation may clarify the discrepancy in this field and deepen our understanding of the molecular pathogenesis of AD.

4.5 Materials and methods

4.5.1 Materials and sample preparation

Aβ40 was purchased from Alexo Tech and the stock solutions were prepared by dissolving the lyophilized powder in 10 mM NaOH to a concentration of 2 mg/mL and then sonicated in an ice-water bath for 1 min, filtered with a 0.2 μm centrifugal filter unit at 4°C. All other agents, including potassium phosphate dibasic and potassium phosphate monobasic stocks, were purchased from Sigma-Aldrich. ThT stock solution was prepared to 3 mM in Milli-Q water. Zinc chloride and sodium chloride stock solutions were prepared by dissolving in Milli-Q water to concentrations of 1 M and 5 M, respectively. All of buffers and stock solutions including 10 mM NaOH were filtered with 0.2 μm syringe-driven filters.

4.5.2 ThT buffer preparation with Formulator

To prepare buffers used in ThT assays, potassium phosphate dibasic and potassium phosphate monobasic stocks were mixed at two different volume ratios, yielding potassium phosphate stocks at final concentrations of 1 M and pH values of 6 and 8, respectively.

TABLE 1: ThT buffers prepared with Formulator in a 96-deep well plate.

ThT buffers	20 mM potassium phosphate with 40 µM ThT in the absence of 40 µM Zn						20 mM potassium phosphate with 40 µM ThT in the presence of 40 µM Zn					
	1	2	3	4	5	6	7	8	9	10	11	12
A	pH 6.5 0M NaCl	pH 6.8 0M NaCl	pH 7.1 0M NaCl	pH 7.4 0M NaCl	pH 7.7 0M NaCl	pH 8.0 0M NaCl	pH 6.5 0M NaCl	pH 6.8 0M NaCl	pH 7.1 0M NaCl	pH 7.4 0M NaCl	pH 7.7 0M NaCl	pH 8.0 0M NaCl
B	pH 6.5 0.0143 M NaCl	pH 6.8 0.0143 M NaCl	pH 7.1 0.0143 M NaCl	pH 7.4 0.0143 M NaCl	pH 7.7 0.0143 M NaCl	pH 8.0 0.0143 M NaCl	pH 6.5 0.0143 M NaCl	pH 6.8 0.0143 M NaCl	pH 7.1 0.0143 M NaCl	pH 7.4 0.0143 M NaCl	pH 7.7 0.0143 M NaCl	pH 8.0 0.0143 M NaCl
C	pH 6.5 0.0286 M NaCl	pH 6.8 0.0286 M NaCl	pH 7.1 0.0286 M NaCl	pH 7.4 0.0286 M NaCl	pH 7.7 0.0286 M NaCl	pH 8.0 0.0286 M NaCl	pH 6.5 0.0286 M NaCl	pH 6.8 0.0286 M NaCl	pH 7.1 0.0286 M NaCl	pH 7.4 0.0286 M NaCl	pH 7.7 0.0286 M NaCl	pH 8.0 0.0286 M NaCl
D	pH 6.5 0.0429 M NaCl	pH 6.8 0.0429 M NaCl	pH 7.1 0.0429 M NaCl	pH 7.4 0.0429 M NaCl	pH 7.7 0.0429 M NaCl	pH 8.0 0.0429 M NaCl	pH 6.5 0.0429 M NaCl	pH 6.8 0.0429 M NaCl	pH 7.1 0.0429 M NaCl	pH 7.4 0.0429 M NaCl	pH 7.7 0.0429 M NaCl	pH 8.0 0.0429 M NaCl
E	pH 6.5 0.0571 M NaCl	pH 6.8 0.0571 M NaCl	pH 7.1 0.0571 M NaCl	pH 7.4 0.0571 M NaCl	pH 7.7 0.0571 M NaCl	pH 8.0 0.0571 M NaCl	pH 6.5 0.0571 M NaCl	pH 6.8 0.0571 M NaCl	pH 7.1 0.0571 M NaCl	pH 7.4 0.0571 M NaCl	pH 7.7 0.0571 M NaCl	pH 8.0 0.0571 M NaCl
F	pH 6.5 0.0714 M NaCl	pH 6.8 0.0714 M NaCl	pH 7.1 0.0714 M NaCl	pH 7.4 0.0714 M NaCl	pH 7.7 0.0714 M NaCl	pH 8.0 0.0714 M NaCl	pH 6.5 0.0714 M NaCl	pH 6.8 0.0714 M NaCl	pH 7.1 0.0714 M NaCl	pH 7.4 0.0714 M NaCl	pH 7.7 0.0714 M NaCl	pH 8.0 0.0714 M NaCl
G	pH 6.5 0.0857 M NaCl	pH 6.8 0.0857 M NaCl	pH 7.1 0.0857 M NaCl	pH 7.4 0.0857 M NaCl	pH 7.7 0.0857 M NaCl	pH 8.0 0.0857 M NaCl	pH 6.5 0.0857 M NaCl	pH 6.8 0.0857 M NaCl	pH 7.1 0.0857 M NaCl	pH 7.4 0.0857 M NaCl	pH 7.7 0.0857 M NaCl	pH 8.0 0.0857 M NaCl
H	pH 6.5 0.1 M NaCl	pH 6.8 0.1 M NaCl	pH 7.1 0.1 M NaCl	pH 7.4 0.1 M NaCl	pH 7.7 0.1 M NaCl	pH 8.0 0.1 M NaCl	pH 6.5 0.1 M NaCl	pH 6.8 0.1 M NaCl	pH 7.1 0.1 M NaCl	pH 7.4 0.1 M NaCl	pH 7.7 0.1 M NaCl	pH 8.0 0.1 M NaCl

1 mM zinc chloride was prepared by diluting the 1 M stock solution with Milli-Q water. ThT buffers were then prepared with the Formulator by dispensing the potassium phosphate stocks at pH 6 and pH 8 at 6 volume ratios, 8 different volumes of 5 M sodium chloride stock solution, and 3 mM ThT stock and 1 mM zinc chloride at constant volumes. The yielded ThT buffers (20 mM potassium phosphate) contain ThT at a final concentration of 40 μM in the absence or presence of zinc chloride (40 μM), while pH values change from pH 6.5 to pH 8 along the columns and sodium concentrations vary from 0 M to 0.1 M along the rows in a plate with 96 deep wells. The detailed information on the ThT buffers is shown in **Table.1**.

4.5.3 ThT fluorescence assays

To study the covariate effects of pH, salt (NaCl) and Zn^{2+}ions on the fibrillation kinetics of Aβ40 peptide, ThT assays were conducted immediately after the buffers were prepared with the Formulator. Samples were prepared by dispensing Aβ40 stock solution into the wells of a transparent 96-well plate manually, and then mixing thoroughly with the freshly prepared ThT buffers with a multiple channel pipette, yielding Aβ40 samples at a final concentration of 10 μM in 96 different ThT buffers as described in Table.1. 30 μL of each sample was then transferred from the 96-well plate into a 384-well, non-treated black plate with transparent bottom (NUNC) and sealed with a piece of foil film.

All samples were prepared in triplicate on ice. The 384-well plate was incubated in a microplate reader (PHERAstar FSX, BMG LABTECH, Germany) and the fluorescence kinetics of Aβ40 was monitored at 37°C without agitation every 5 min, using wavelengths of 430 nm and 480 nm for excitation and emission, respectively.

All of the original ThT data were smoothed by choosing the Savitzky-Golay method with a Points of Window from 5 to 30 using Origin (Version 2018, OriginLab, USA). The smoothed data were then plotted with Prism (Version 8.0, GraphPad Software), as shown in **Fig.1**.

4.5.4 Sigmodial fitting

To obtain the half time $t_{1/2}$ of Aβ40 aggregation kinetics, the sigmodial fitting with smoothed data of individual curves obtained was performed by using equation (1) with Origin (Version 2018, OriginLab, USA).

$$\boldsymbol{y = (y_{baseline}\text{-}y_{plateau})/(1+e^{(t\text{-}t_0)/dt})+y_{plateau}} \quad \textbf{(1)}$$

where $y_{baseline}$ and $y_{plateau}$ are the values of the data at the baseline and the plateau, t is the time of amyloid aggregation course and t_0 is the time when the fluorescence intensity reaches half of the plateau value, while dt is the time constant. And y is the fitted value of the data at time t. $t_{1/2}$ of aggregation kinetics was given as follow and plotted with Prism (Version 8.0, GraphPad Software), as shown in **Fig.2**.

$$\boldsymbol{t_{1/2} = t_0} \quad \textbf{(2)}$$

4.5.5 Global fitting

To identify how pH and salt affect the microscopic rate processes of Aβ40 aggregation, the averaged ThT data obtained in the absence of Zn^{2+}ions were smoothed with the same method used for the smooth process of individual curves and fitted globally with an integrated rate law (16, 17) in *AmyloFit* online software server (20) by using the method in our previous study (35). Briefly, the secondary nucleation dominated model was selected, the data of Aβ40 at pH 7.4 in the absence of NaCl was first fitted, obtaining a set of parameters, which were used as the initial guess values for the following fits. Among these obtained parameters, the primary nucleation rate constant k_n, secondary nucleation rate constant k_2, or the elongation rate constant k_+ was fitted freely while the other two rate constants were set as fixed initial values. For detailed definitions of these parameters and fitting procedure, please refer to the nature protocol (20) and our previous study (35). The fitting results are shown in **Fig.3** and **Fig.S1**.

4.5.6 Transmission electron microscopy (TEM)

For TEM assay, the Formvar-coated, carbon-stabilized copper grids (400 mesh, from Ted Pella Inc., Redding CA) were glow-discharged (20 mA for 20 s). 10 μM Aβ40 samples were taken from ThT assays conducted at different pH values in the absence or presence of Zn^{2+} ions and/or NaCl. 4 μL of each sample was loaded on the discharged grid and incubated for 30 s, the excess samples on the grids were blotted with a piece of filter paper. 3.5 μL of 2% uranyl acetate was immediately added onto the grid and the excess stain solution was blotted after incubation for 30 s. The staining process was performed twice. The grids were then washed with 6 μL of Milli-Q water and air-dried. The negatively stained samples were imaged on a transmission electron microscope (PSI, Switzerland) operating with an accelerator voltage of 80 kV. Typical magnifications ranged from 20,000 to 60,000.

4.6 References

1. A. Burns, S. Iliffe, Alzheimer's disease. BMJ 338, b158 (2009).
2. D. J. Selkoe, Alzheimer's disease: genes, proteins, and therapy. Physiol Rev 81, 741-766 (2001).
3. T. C. Gamblin et al., Caspase cleavage of tau: linking amyloid and neurofibrillary tangles in Alzheimer's disease. Proc Natl Acad Sci U S A 100, 10032-10037 (2003).
4. P. R. Bharadwaj, A. K. Dubey, C. L. Masters, R. N. Martins, I. G. Macreadie, Abeta aggregation and possible implications in Alzheimer's disease pathogenesis. Journal of cellular and molecular medicine 13, 412-421 (2009).
5. M. C. Owen et al., Effects of in vivo conditions on amyloid aggregation. Chemical Society reviews 48, 3946-3996 (2019).
6. Y. Goto, M. Adachi, H. Muta, M. So, Salt-induced formations of partially folded intermediates and amyloid fibrils suggests a common underlying mechanism. Biophys Rev 10, 493-502 (2018).
7. C. M. Yates, J. Butterworth, M. C. Tennant, A. Gordon, Enzyme activities in relation to pH and lactate in postmortem brain in Alzheimer-type and other dementias. J Neurochem 55, 1624-1630 (1990).
8. M. Chesler, Regulation and modulation of pH in the brain. Physiol Rev 83, 1183-1221 (2003).
9. M. A. Lovell, J. D. Robertson, W. J. Teesdale, J. L. Campbell, W. R. Markesbery, Copper, iron and zinc in Alzheimer's disease senile plaques. Journal of the Neurological Sciences 158, 47-52 (1998).
10. V. M. Vitvitsky, S. K. Garg, R. F. Keep, R. L. Albin, R. Banerjee, Na+ and K+

ion imbalances in Alzheimer's disease. Biochim Biophys Acta 1822, 1671-1681 (2012).
11. A. Tiiman, J. Krishtal, P. Palumaa, V. Tõugu, In vitro fibrillization of Alzheimer's amyloid-βpeptide (1-42). AIP Advances 5, 092401 (2015).
12. K. Brannstrom, T. Islam, L. Sandblad, A. Olofsson, The role of histidines in amyloid beta fibril assembly. FEBS Lett 591, 1167-1175 (2017).
13. A. Abelein, A. Graslund, J. Danielsson, Zinc as chaperone-mimicking agent for retardation of amyloid beta peptide fibril formation. Proc Natl Acad Sci U S A 112, 5407-5412 (2015). 14. A. I. Bush et al., Rapid induction of Alzheimer A beta amyloid formation by zinc. Science 265, 1464-1467 (1994).
15. M. Biancalana, S. Koide, Molecular mechanism of Thioflavin-T binding to amyloid fibrils. Biochim Biophys Acta 1804, 1405-1412 (2010).
16. S. I. Cohen, M. Vendruscolo, C. M. Dobson, T. P. Knowles, Nucleated polymerization with secondary pathways. II. Determination of self-consistent solutions to growth processes described by non-linear master equations. The Journal of chemical physics 135, 065106 (2011).
17. S. I. Cohen, M. Vendruscolo, C. M. Dobson, T. P. Knowles, From macroscopic measurements to microscopic mechanisms of protein aggregation. Journal of molecular biology 421, 160-171 (2012).
18. S. I. Cohen et al., Proliferation of amyloid-beta42 aggregates occurs through a secondary nucleation mechanism. Proceedings of the National Academy of Sciences of the United States of America 110, 9758-9763 (2013).
19. T. P. Knowles et al., An analytical solution to the kinetics of breakable filament assembly. Science (New York, N.Y.) 326, 1533-1537 (2009).
20. G. Meisl et al., Molecular mechanisms of protein aggregation from global fitting of kinetic models. Nature protocols 11, 252-272 (2016).
21. G. Meisl et al., Differences in nucleation behavior underlie the contrasting aggregation kinetics of the Abeta40 and Abeta42 peptides. Proceedings of the National Academy of Sciences of the United States of America 111, 9384-9389 (2014).
22. C. Wallin et al., The Neuronal Tau Protein Blocks in Vitro Fibrillation of the Amyloid-beta (Abeta) Peptide at the Oligomeric Stage. Journal of the American Chemical Society 140, 8138-8146 (2018).
23. B. H. Kim et al., Single-molecule atomic force microscopy force spectroscopy study of Abeta-40 interactions. Biochemistry 50, 5154-5162 (2011).
24. K. Klement et al., Effect of different salt ions on the propensity of aggregation and on the structure of Alzheimer's abeta(1-40) amyloid fibrils. Journal of molecular biology 373, 1321-1333 (2007).
25. S. Zhang, J. P. Lee, Selectively 2H-labeled Glu/Asp: application to pKa measurements in Abeta amyloid peptides. J Pept Res 55, 1-6 (2000).
26. G. Meisl, X. Yang, B. Frohm, T. P. Knowles, S. Linse, Quantitative analysis of

intrinsic and extrinsic factors in the aggregation mechanism of Alzheimer-associated Abeta-peptide. Sci Rep 6, 18728 (2016).

27. S. Kobayashi et al., Dependence pH and proposed mechanism for aggregation of Alzheimer's disease-related amyloid-β(1–42) protein. Journal of Molecular Structure 1094, 109-117 (2015).

28. J. Luo, J. D. Marechal, S. Warmlander, A. Graslund, A. Peralvarez-Marin, In silico analysis of the apolipoprotein E and the amyloid beta peptide interaction: misfolding induced by frustration of the salt bridge network. PLoS Comput Biol 6, e1000663 (2010).

29. K. Brannstrom et al., The N-terminal region of amyloid beta controls the aggregation rate and fibril stability at low pH through a gain of function mechanism. Journal of the American Chemical Society 136, 10956-10964 (2014).

30. A. Abelein, J. Jarvet, A. Barth, A. Graslund, J. Danielsson, Ionic Strength Modulation of the Free Energy Landscape of Abeta40 Peptide Fibril Formation. Journal of the American Chemical Society 138, 6893-6902 (2016).

31. M. Adachi, M. So, K. Sakurai, J. Kardos, Y. Goto, Supersaturation-limited and Unlimited Phase Transitions Compete to Produce the Pathway Complexity in Amyloid Fibrillation. J Biol Chem 290, 18134-18145 (2015).

32. S. A. Kozin, S. Zirah, S. Rebuffat, G. H. Hoa, P. Debey, Zinc binding to Alzheimer's Abeta(1-16) peptide results in stable soluble complex. Biochem Biophys Res Commun 285, 959-964 (2001).

33. N. T. Watt, I. J. Whitehouse, N. M. Hooper, The role of zinc in Alzheimer's disease. Int J Alzheimers Dis 2011, 971021 (2010).

34. H. Prasad, R. Rao, Amyloid clearance defect in ApoE4 astrocytes is reversed by epigenetic correction of endosomal pH. Proc Natl Acad Sci U S A 115, E6640-E6649 (2018).

35. H. Wang et al., ATP Impedes the Inhibitory Effect of Hsp90 on Abeta40 Fibrillation. J Mol Biol 433, 166717 (2021).

4.7 Supporting information

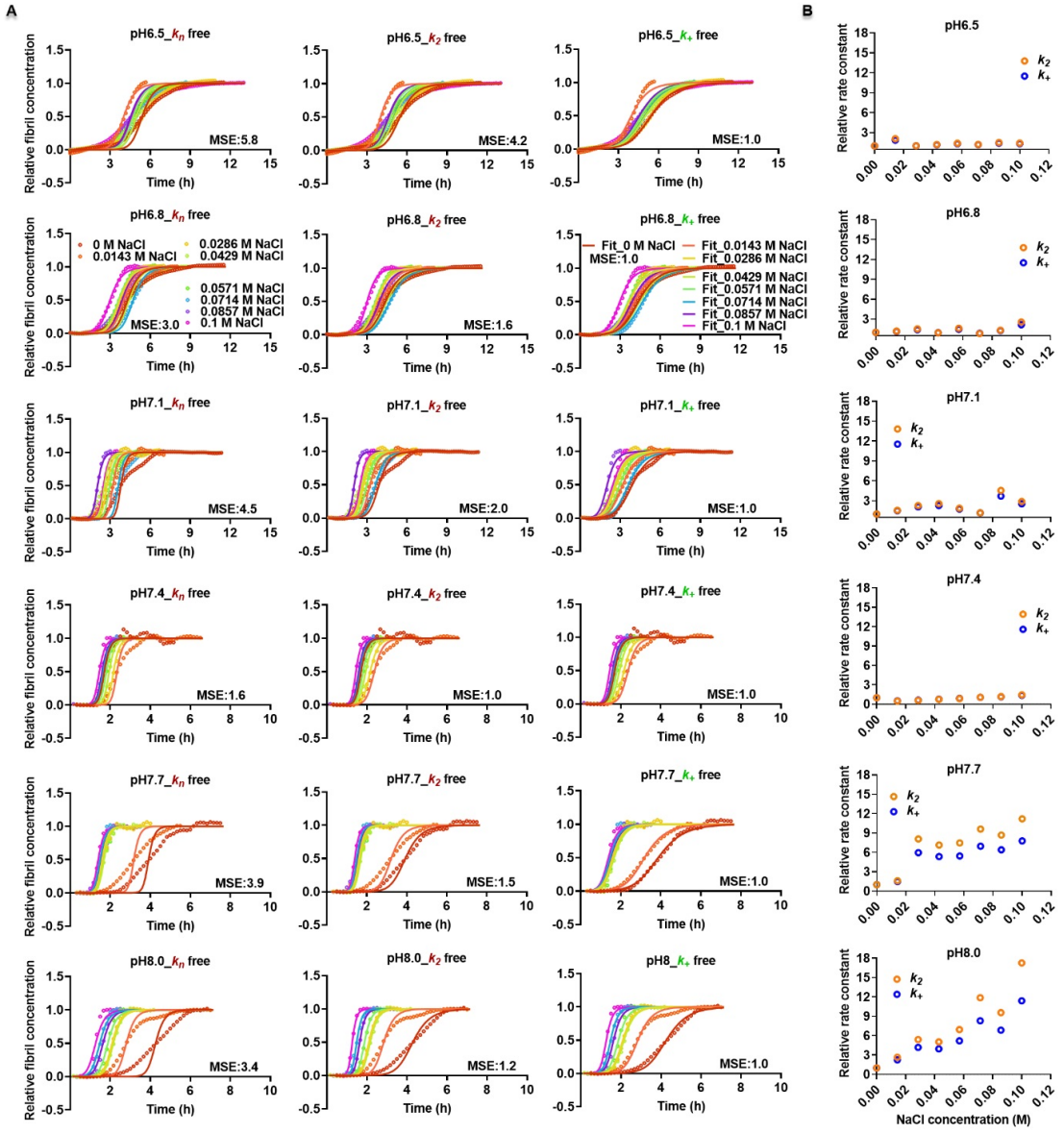

FIGURE S1: Salts mainly influence the elongation process of Aβ40 fibrillation in the absence of Zn^{2+}ions. (A) Elongation processes of Aβ40 fibrillation are influenced by changes in concentrations of NaCl at different pH values. Aggregation kinetics of 10 µM Aβ 40 at different pH values (6.5, 6.8, 7.1, 7.4, 7.7, and 8) and NaCl concentrations (0, 0,0143, 0.0285, 0.0429, 0.0571, 0.0714, 0.0857, and 0.1 M) were monitored by ThT fluorescence over time (the raw data can be found in Fig.1). The ThT data were then globally fitted with the same method used in Fig.3 by using the AmyloFit online software server (20). The mean square error (MSE) values for each set of Aβ40 samples were normalized against the one with the best fit (lowest MSE value). (B) Relative rate constants (relative to the rate constants of Aβ40 at 0 M NaCl) derived from global fitting for Aβ40 samples at different pH values and salt concentrations.

Chapter 5

Cu^{2+} ions modulate the interaction between α-synuclein and lipid membranes

Hongzhi Wang[1], Cecilia Mörman[2], Rebecca Sternke-Hoffmann[1], Chia-Ying Huang[3], Andrea Prota[1], Pikyee Ma[1], Jinghui Luo[1]*

1. Department of Biology and Chemistry, Paul Scherrer Institute, 5232 Villigen, Switzerland.

2. Department of Biochemistry and Biophysics, Stockholm University, 10691 Stockholm, Sweden.

3. Laboratory for Macromolecules and Bioimaging, Paul Scherrer Institute, 5232 Villigen, Switzerland.

*Corresponding author: Jinghui.luo@psi.ch +41 56 310 47 64

Under revision in Journal of Inorganic Biochemistry

5.1 Abstract

Alpha-synuclein (α-Syn) is the major constituent of Lewy bodies, which is a main pathogenic hallmark of Parkinson's disease (PD). Interactions with lipids are essential for α-Syn physiologically and pathologically and have been extensively investigated. Cu^{2+} ions bind to α-Syn protein and modulate its aggregation propensity and toxicity. However, the covariant effect of copper ions and lipid membranes on α-Syn remains to be explored. Using a combination of methods including small-angle X-ray scattering (SAXS), circular dichroism (CD), and nuclear magnetic resonance (NMR), we investigated the interaction of α-Syn with different lipid models including lipid vesicles, lipidic cubic phase (LCP) matrix, and cellular membranes, and how Cu^{2+} ions modulates the interaction at mesoscopic and atomic scales. In LCP matrix, α-Syn proteins destabilized the cubic-Pn3m phase, whilst Cu^{2+} ions reverse the effect at a low stoichiometry. Cu^{2+} ions change the structure of α-Syn in *E.coli* cells (*in vivo*) by interacting with both its N- and C-terminus, with a more pronounced interaction observed in C-terminus compared with that in buffer (*in vitro*). The modulation of Cu^{2+} on α-Syn and lipid interaction could be essential for membrane-containing organelles to remain their functions, given the decreased levels of copper ions observed in the substantia nigra (SN) of PD patients.

Keywords: α-Syn; Cu^{2+} ions; LCP; SAXS; in-cell NMR

5.2 Introduction

Alpha-synuclein (α-Syn) is an intrinsically unfolded protein involved in neurotransmitter release from presynaptic terminals and a causative agent of Parkinson's disease (PD). Upon binding to lipid vesicles, the 95-residue N-terminus of α-Syn undergoes a structural transition from random coil to α-helix (1), and the N-terminal helical segment functions as the membrane anchor, with a central region acting as a sensor for lipids and determining the affinity of α-Syn membrane binding, while the disordered C-terminal region is weakly associated with lipid membranes (2), as shown in **Fig.1**. Membrane binding is considered to be crucial for the internalization, toxicity, and aggregation of α-Syn (1, 3) and influences the properties of both α-Syn and membranes. For instance, membrane curvature (4), membrane remodeling (5), the chain order and the thermotropic phase behavior of anionic lipid vesicles (6), membrane expansion (7), and aggregation behavior of α-Syn (8) are all affected by the interactions between α-Syn and the lipid membrane. The levels of copper ions in neurodegenerative diseases change considerably, so do the levels of zinc ions, in addition, whether the concentrations of copper ions and zinc ions increase or decrease is open to be determined, as shown in **Table.1**. It is

worth noting that the copper levels in PD brains are widely considered to be decreased. Copper ions play important roles in neurodegnerative diseases by interacting with both lipid membranes and amyloid proteins (9, 10). In addition, copper ions can catalyze protein oxidation, leading to subsequent denaturation (11). Given the fact that α-Syn and copper ions play essential roles in the pathology of PD, investigating the covariant effect of copper ions and lipid membranes on α-Syn can contribute to our understanding of the roles of α-Syn and copper ions in the pathology of PD, especially when it comes to membrane-containing organelles.

Lipid systems used in the field of α-Syn-lipid interaction are usually liposomes with constituting lipids varying in the nature of hydrophobic hydrocarbon chains and polar heads (7), resulting in hydrophobic environments, which are different from the amphiphilic and air-tight conditions in brains. Therefore, we used here not only liposomes but also two model membranes, the lipidic cubic phase (LCP) matrix and *Escherichia coli* (*E.coli*) whole-cell membrane. In membrane protein crystallization, LCP (Pn3m and Ia3d) is a three-dimensional lipidic array consisting of lipid and water in appropriate proportions that forms the transparent bicontinuous bilayer, pervaded by an intercommunicating aqueous channel (12). Besides, the LCP system can be manipulated by chemicals to change its property and curvature (13). α-Syn is a curvature-sensing protein and the curvature of lipid membranes can influence its lipid binding affinity (14, 15). Therefore, we used LCP to study the interaction of α-Syn with the lipidic bilayer and the phase changes effected from α-Syn. α-Syn can be produced in the periplasm of *E.coli* cells (16), where it spontaneously interact with both inner and outer membranes. Therefore, *E.coli* cell is an ideal lipid model for the in-cell NMR measurement.

Here, the small-angle X-ray scattering (SAXS) measurements show, at mesoscopic level, that α-Syn changed the mesoscopic structure of LCP matrix and Cu^{2+} ions were able to reverse the effect. Cu^{2+} ions modulated the secondary structure transition of α-Syn in the presence of lipid membranes, as indicated by circular dichroism spectroscopy (CD) assays. At the atomic level, nuclear magnetic resonance (NMR) experiments reveal that Cu^{2+} ions interacted with α-Syn within N- and C-terminus in both buffer solution and *E.coli* cells, with a more pronounced interaction with the C-terminus in the periplasma of *E.coli* cells. In summary, this study reports a covariant role of Cu^{2+} ions in the interaction of α-Syn with different lipid membranes at the atomic and mesoscopic levels, which may broaden our understanding of the pathology of PD.

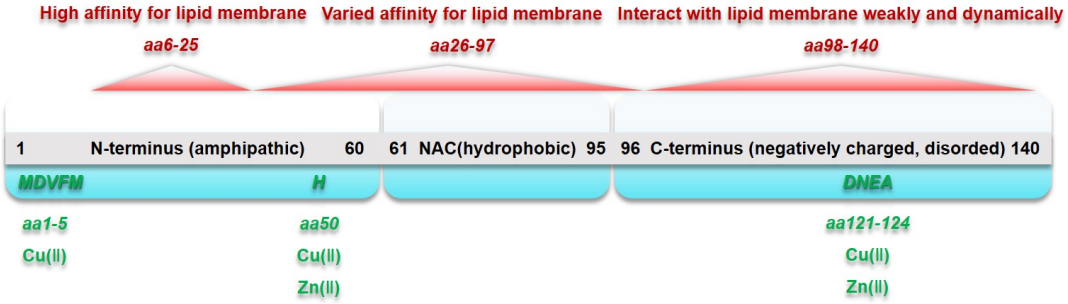

FIGURE 1: Interactions of α-Syn with lipid membranes. α-Syn consists of three domains including the N-teminal domain (aa 1-60), the NAC domain (aa 61-95), and the C-terminal domain (aa 96-140) (1). The N-terminus and the NAC domain (aa 1-95) consist of seven 11-amino acid imperfect repeats with a highly conserved hexamer motif (KTKEGV), predicted to form amphipathic α-helices and known to be responsible for lipid binding and membrane translation (17). The most N-terminus of α-Syn forms α-helix structure upon binding to lipid membranes with high affinity (aa 6-25), while the central part (aa 26-97) interacts with lipid membranes with variable affinity depending on the lipid composition (1). The C-terminus (aa 98-140) only interacts with lipid membranes weakly and dynamically (1). Cu^{2+} ions and Zn^{2+} ions have specific binding sites on α-Syn (amino acids in green) (9, 18, 19).

TABLE 1: Variation of copper ions and zinc ions in AD(D) and PD(D) patients.

Location	Cu			Zn		
	Change in AD(D) patients	Change in PD(D) patients	Reference(s)	Change in AD(D) patients	Change in PD(D) patients	Reference(s)
CSF	increased	increased	(20)	controversial	increased	(20, 21)
Blood	increased	decreased	(22, 23)	controversial	-	(21)
Brain (SN)	decreased	decreased	(24-27)	-	increased	(24)
Brain (HP)	decreased	decreased	(27)	increased	decreased	(27, 28)
Brain (CB)	decreased	-	(27)	decreased	-	(27)
Senile plaques	enriched	-	(29)	enriched	-	(29)

Note: AD(D), Alzheimer's disease dementia; PD(D), Parkinson's disease dimentia; CSF, cerebrospinal fluid; SN, substantia nigra; HP, hippocampus; CB, cerebellum. '-', no data.

5.3 Results

5.3.1 Cu^{2+} ions reverse the effect of α-Syn on the mesoscopic structure of LCP

Monoolein (MO) is a commonly used host lipid in in meso crystallization and produces a Pn3m cubic phase when mixed with water at a volume ratio of 3:2 at 20°C. MO is not a natural component of cell membranes, however, it forms a bilayer mimetic and a manipulable system for the addition of test lipids and chemicals. For crystallization of membrane proteins, natural lipids such as phosphatidylcholine (PC), phosphatidylserine (PS), and cholesterol are commonly added to the LCP system in order to achieve a more natural system to aid crystallization of the target protein (30, 31). PS is the major acidic phospholipids localized exclusively in the cytoplasmic leaflet in neural tissues, where it participates in forming protein docking sites that are crucial for the activation of signal pathways involved in neuronal survival, neurite growth, and synaptogenesis (32). In addition, PS is a lipid composition of synaptic vesicles that are responsible for the storage and exocytosis of neurotransmitters upon the arrival of an action potential (33) and related to PD (34). Besides, α-Syn selectively interacts with anionic lipids like PS (35). Therefore, to obtain a more physiologically relevant membrane, we prepared the lipidic matrix with 1-palmitoyl-2-oleoyl-sn-glycero-3-phospho-L-serine (POPS) and MO at molar ratios of 1%, 5%, and 10%, respectively, which were characterized by SAXS. In **Fig.2A-2D**, MO alone or MO supplemented with 1% or 5% POPS did not change the space group of the lipidic cubic phase and it was maintained as Pn3m, while MO supplemented with 10% POPS destabilized the Pn3m phase. Therefore, the lipidic matrix with MO and 5% supplemented POPS was selected as a physiologically relevant model to investigate the influence of α-Syn on the phase behavior of LCP. As shown in **Fig.2E**, α-Syn at a final concentration of 34 μM changed the Pn3m phase of MO+5% POPS that was prepared in 20 mM Tris-HCl buffer, pH 7.2. It suggests that α-Syn destabilizes the lipidic cubic system under experimental condition.

To study how Cu^{2+} ions influence the effect of α-Syn on the lipidic phase at mesoscopic scales, we prepared the lipidic matrix with 34 μM α-Syn, MO and supplemented with 5% POPS, in the presence of 17 or 83 μM Cu^{2+} ions. The addition of Cu^{2+} ions converted the phase back to the Pn3m phase compared to that with α-Syn alone, as shown in **Fig.2F-2G**, while Cu^{2+} ions alone can not considerably change the phase of LCP (**Fig.S1**). Taken together, Cu^{2+} ions counteracted the detrimental effect of α-Syn on the mesoscopic structure of LCP (similar results were obtained in the presence of zinc, as shown in **Fig.S2**).

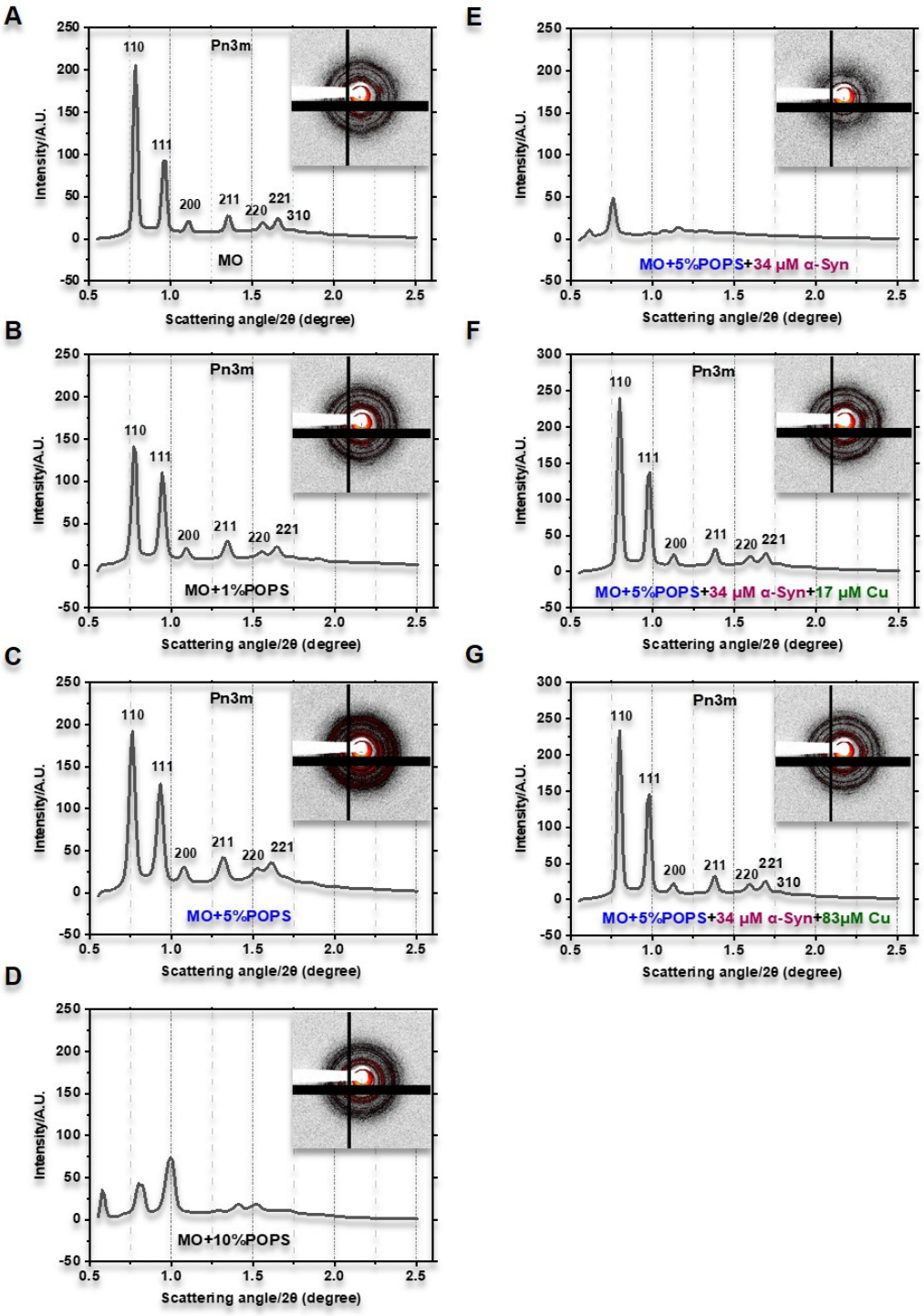

FIGURE 2: Effect of α-Syn and Cu^{2+} ions on the mesoscopic structure of LCP. (A-D) Effect of POPS on the phase behavior of lipidic cubic phase. SAXS experiments conducted with MO alone and MO supplemented with POPS at molar ratios of 1%, 5%, and 10%, respectively, show that POPS does not change the phase behavior of MO within the range of 5%, but modulates the phase behavior of MO when the molar ratio of POPS and MO reaches 10%. (E) SAXS experiments conducted with 34 μM α-Syn and LCP made of MO supplemented with 5% POPS indicate that α-Syn proteins destroy the Pn3m of LCP. (F-G) SAXS experiments performed with 34 μM α-Syn in the absence or presence of 17 or 83 μM Cu^{2+} ions in LCP made of MO supplemented with 5% POPS suggest that Cu^{2+} ions at used concentrations can eliminate the effect of α-Syn on the phase behavior of LCP and remain LCP as the Pn3m phase.

5.3.2 Cu^{2+} ions modulate the effect of liposomes on the secondary structure transition of α-Syn

To investigate how copper ions and DOPG liposomes influence the secondary structure of α-Syn, we continued our study by using CD spectroscopy. The effect of Cu^{2+} ions on the secondary structure transition of α-Syn was investigated by titrating Cu^{2+} ions into α-Syn solution to final concentrations of 0, 5, 25, 75, 150, 300 μM. The signal of the random coil structure of α-Syn gradually disappeared as the concentration of Cu^{2+} ions increased (data not shown here). DOPG liposomes were then titrated into α-Syn solution with or without 300 μM Cu^{2+} ions. The CD spectra were recorded immediately after sample preparation to quantify the secondary structure transition of α-Syn. The conformation transition of α-Syn in the presence or absence of DOPG with or without Cu^{2+} ions was monitored in the far-UV region from 190 to 260 nm at 37°C. It shows in **Fig.3A** and **3B** that the CD spectra of α-Syn alone showed a characteristic minimum at ˜198 nm, corresponding to the random structure of an intrinsically disordered protein. α-Syn gradually converts to a typical α-helical structure as DOPG liposomes are titrated in the absence and presence of Cu^{2+} ions, as indicated by the characteristic minima at ˜208 nm and ˜222 nm and a peak at ˜193 nm (**Fig.3**). The difference is that in the presence of Cu^{2+} ions, the signal intensity of α-helical structure of α-Syn is slightly stronger compared with those in the absence of Cu^{2+} ions (**Fig.3C**). Our CD data agree with the previous studies that α-Syn is an intrinsically disordered protein and that binding onto the surface of lipid membranes, DOPG liposomes in this case, then convert it to α-helical structure in the N-terminus and/or NAC domain and induce the aggregation of α-Syn. The presence of Cu^{2+} ions can also influence the structure of α-Syn to some extent, but cannot completely change its secondary structure. This may be explained by that α-Syn interacts with lipid membranes with high affinity to N-terminus and that Cu^{2+} ions can slightly induce the helical structure formation of the N-terminus or NAC domain of α-Syn in the presence of DOPG. Taken together, the results of CD experiments indicate that Cu^{2+} ions slightly enhanced the effect of liposomes on the secondary structure transition of α-Syn proteins. Likewise, zinc ions similarly modulated the liposome-induced change in the secondary structure of α-Syn (**Fig.S3**).

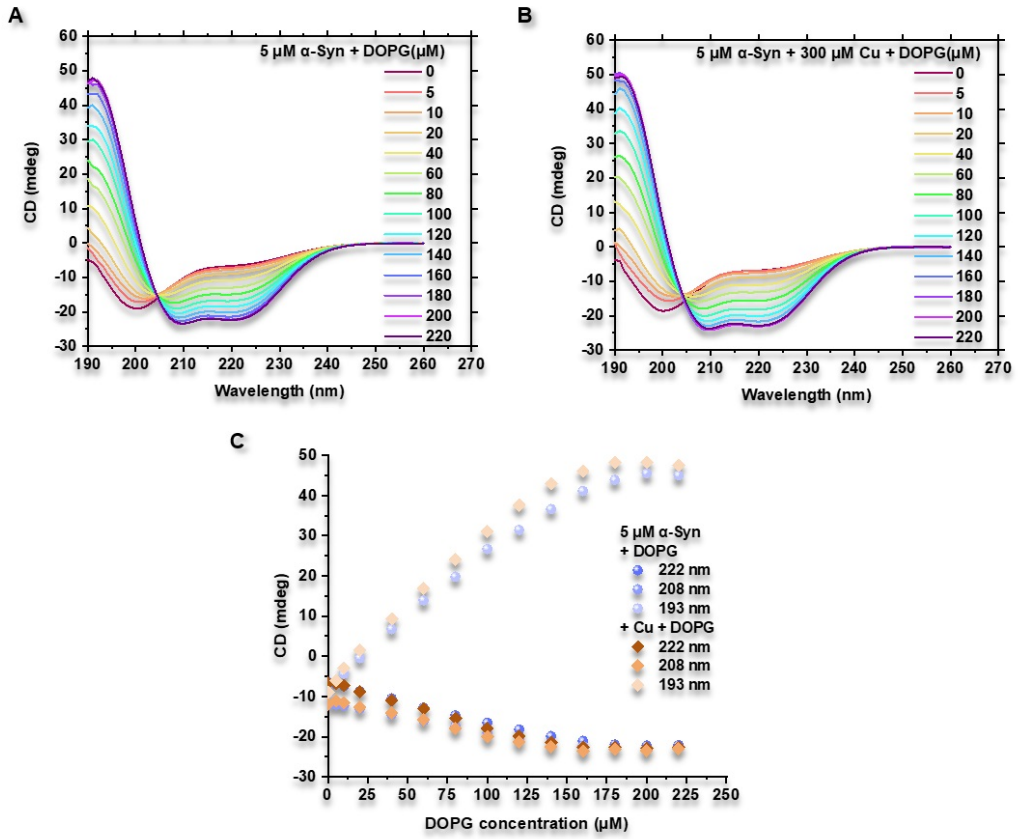

FIGURE 3: Covariant effect of Cu^{2+} ions and DOPG liposomes on the secondary structure of α-Syn. CD experiments were conducted by gradually titrating DOPG liposomes (at concentrations of 0, 5, 10, 20, 40, 60, 80, 100, 120, 140,160, 180, 200, 220 μM) into 5 μM α-Syn in the absence or presence 300 μM Cu^{2+} ions. The measurements were performed immediately after the addition of liposomes and Cu^{2+} ions. (A) CD experiments in the absence of Cu^{2+} ions indicate that lipid membranes induce the change of α-Syn from random coil structure to α-helical structure. (B) In the presence of Cu^{2+} ions, DOPG converted α-Syn from random coil structure into α-helical structure but with a slightly stronger signal intensity of α-helical structure. (C) CD signal intensities at 222 nm, 208 nm, and 193 nm of 5 μM α-Syn in the presence of DOPG liposomes with or without 300 μM Cu^{2+} ions, derived from (A) and (B).

5.3.3 Cu^{2+} ions interacts with α-Syn in both buffer solution and *E.coli* cells

In order to investigate the effect of Cu^{2+} ions on α-Syn in a lipidic environment, we took in-cell NMR measurements of α-Syn expressed in the periplasm of *E.coli* (16) where α-Syn proteins spontaneously interact with cellular membranes (**Fig.4**). To estimate the concentration of α-Syn in the *E.coli* cells we compared the amide crosspeak intensities in ^{1}H-^{15}N-HSQC spectra of α-Syn in the cells to the intensities of a known 100 μM concentration of α-Syn in buffer conditions (**Fig.4A**). The corresponding α-Syn concentration in the cells was determined to be approximately 60% of the one in buffer, corresponding a theoretical α-Syn concentration of 60 μM. Noteworthy, under buffer conditions α-Syn

is mainly unstructured, but in cellular conditions some of the crosspeaks show different chemical shifts which are indicative of a change in structure (**Fig.4A**). Especially residues of L8, T44, and V48 exhibit significant chemical shift changes ($\Delta\delta$).

To confirm the Cu^{2+} ion interaction in a simple model system, ^{1}H-^{15}N-HSQC spectra of 100 μM ^{15}N-α-Syn in 20 mM potassium phosphate buffer pH 7.4 with 150 mM NaCl in the absence and presence of 1 mM Cu^{2+} ions were recorded (**Fig.4B**). The amide crosspeak signal intensities were overall reduced by 40%-60%, and an especially significant reduction around residue H50 was observed. Histidine is a well-known metal ion interacting residue, and H50 as well as methionine located at the first amino acid position of α-Syn (Methionine 1) are typically important for the Cu^{2+} ion coordination (36, 37). Small chemical shift changes were also detected. Using a more complex model system, the Cu^{2+} interaction was studied in*E.coli* cells. *E.coli* cells with a theoretical α-Syn concentration of 60 μM were incubated with an increased concentration of Cu^{2+} ions (5 mM) administered to the extracellular environment of the cells, since only a proportion of Cu^{2+} ions applied extracellularly can translocate into the periplasm of *E.coli* cells. (**Fig.4C**). Even though the Cu^{2+} ions were administered from the outside of the cells, the effect of Cu^{2+} ions on α-Syn was similar to that of the Cu^{2+}-effect on α-Syn in buffer conditions, despite that a more pronounced C-terminal interaction effect in *E.coli* cells was observed compared to in buffer conditions, indicating that the Cu^{2+} ions are readily transported across the outer cell membrane and interacted with the periplasmic α-Syn proteins under the test conditions.

5.4 Discussion

PD-related α-Syn protein possesses various conformations under different conditions (38-40), for instance, the partially α-helical structure in the membrane-bound state (2), which is essentially important for both the physiological functions and pathological roles of α-Syn (41). Metal ions like Cu^{2+} act as crucial players in both the properties of lipid membranes and the states and functions of α-Syn, as well as in the normal activities of various enzymes (9), with decreased levels in the brains (SN) of PD patients (25). Therefore, investigating how Cu^{2+} ions modulate the intercommunication between α-Syn and lipid membranes will provide us with further insight into the pathogenesis.

Here, we report that α-Syn proteins destabilized the Pn3m phase of LCP (**Fig.2E**) and Cu^{2+} ions counteracted this effect (**Fig.2F-2G**). Cu^{2+} ions enhanced the secondary structure transition of α-Syn proteins (**Fig.3**). α-Syn proteins underwent structure changes upon interacting with lipid membranes of *E.coli* cells, and Cu^{2+} interacted with α-Syn in both buffer and *E.coli* cells by interfering with its N- and C-terminus,

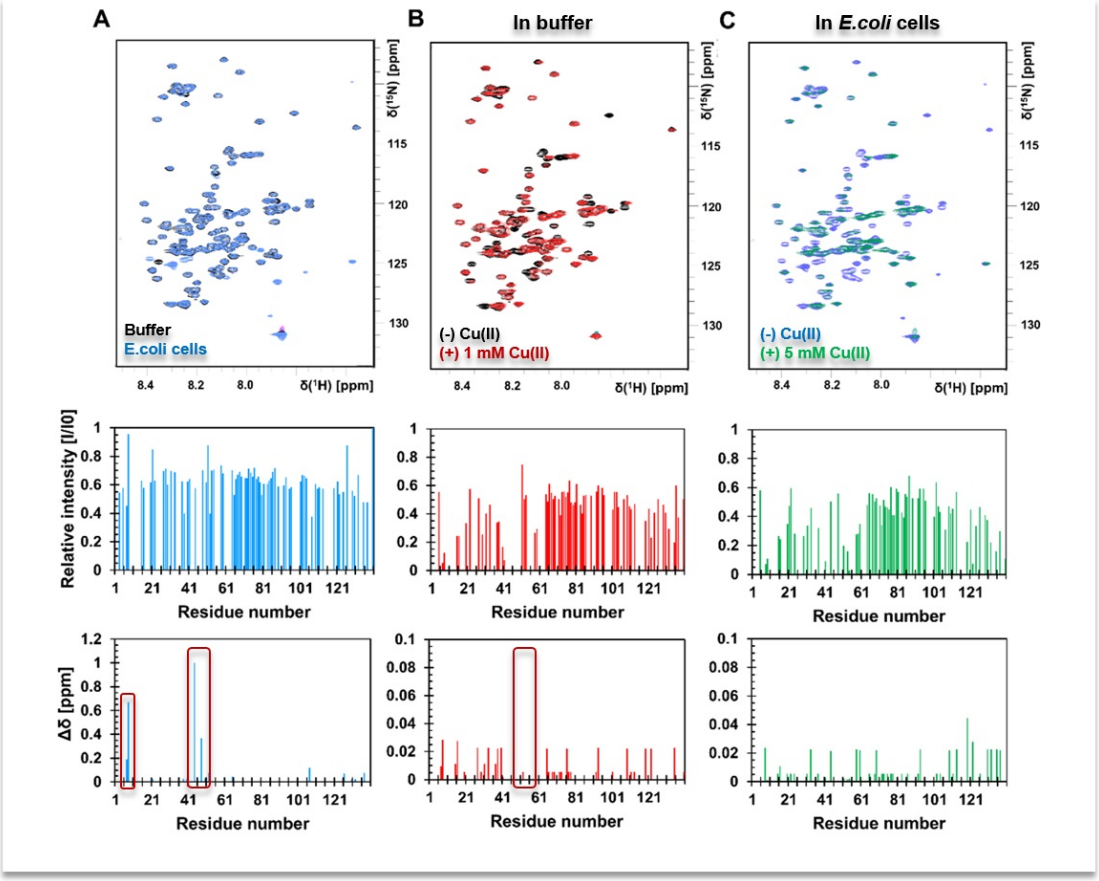

FIGURE 4: 2D NMR ^{1}H-^{15}N-HSQC spectra of ^{15}N-α-Syn in buffer and in *E.coli* cells in the absence and presence of Cu^{2+} ions. ^{1}H-^{15}N-HSQC spectra comparison of (A) ^{15}N-α-Syn in *E.coli* cells (blue spectrum) to 100 μM ^{15}N-α-Syn in 20 mM potassium phosphate buffer pH 7.4 with 150 mM NaCl (black spectrum). In (B) are 100 μM ^{15}N-α-Syn in 20 mM potassium phosphate buffer pH 7.4 with 150 mM NaCl in the absence of Cu^{2+} (black spectrum) compared to in the presence of 1 mM Cu^{2+} ions (red spectrum). (C) An estimated concentration of 60 μM ^{15}N-α-Syn in *E.coli* cells in the absence (blue spectrum) and in the presence of 5 mM Cu^{2+} ions (green spectrum). The relative amide crosspeak signal intensities are presented below the spectra. The chemical shift changes ($\Delta\delta$) are presented below the relative intensities.

despite that a more pronounced C-terminal interaction effect in *E.coli* cells was observed compared to in buffer conditions (**Fig.4**).

The effect of α-Syn proteins on the mesoscopic structure of LCP (**Fig.2E**), caused probably by the oligomerization and following pore-formation (41) of α-Syn, is in agreement with the detrimental effects of α-Syn on lipid membranes (41). It is supported by CD spectroscopy showing that DOPG liposomes induced the secondary structure transition of α-Syn from random coils to α-helix (**Fig.3A**). This transition may lead to the formation of partially folded intermediates which exposed the NAC domain and promoted oligomerization (1), resulting in the destruction of lipid membranes (**Fig.2E**). The reversion of the mesoscopic structure of LCP in the presence of α-Syn back to Pn3m phase by Cu^{2+} ions (**Fig.2F-2G**), may be due to the protective role of Cu^{2+}

ions on lipid membranes by competing with membrane-bound, NAC-exposing α-Syn for free α-Syn monomers. There is an equilibrium of α-Syn proteins between cytosolic and membrane-bound states in vivo (42, 43). Cu^{2+} ions possess two binding sites with strong affinity that locate within the N-terminus (coordinated around M1 and/or H50) and one with low affinity sitting in the C-terminus (coordinated around D121) (9, 18, 37). The binding of Cu^{2+} ions onto any of its three binding sites on α-Syn may lead to the formation of oligomers. As a result, the free monomers for oligomer formation on the lipid membranes decreased, and the damage of α-Syn to the lipid membranes was removed (**Fig.2F-2G**), meanwhile, the lipid-bound α-Syn monomers may convert into an extended α-helical structure, leading to the increase of the signal intensity of α-Syn helix in CD experiments (**Fig.3B**), which may also alleviate the detrimental effect of α-Syn on lipid membranes. Our observation supports that the presence of Cu^{2+} ions compromise the effect of Aβ42 on the lipid bilayers (44). α-Syn proteins coordinate Cu^{2+} ions both in its free state in buffer as well as bound to lipid membranes (45). The more noticeable effect in *E.coli* cells, and hence in possibly contact with biological membranes, may be explained by a more stabilized metal site on the C-terminus due to the proximity and simultaneously interaction with a membrane. It has been reported that the histidine residue (H50) in α-Syn located in a membrane is shielded from metal ion interactions, with the result of a more pronounced N-terminal interaction (37), and in this case in living*E.coli* cells the C-terminal might be compensating for the potential loss of H50 coordinating metal activity. On the other hand, the membrane bound α-Syn population of the sample might be in equilibrium (or co-existing) with "free" α-Syn in the periplasm.

The lipid systems used here including lipidic cubic phase matrix which is similar to cellular membrane-containing organelles, DOPG vesicles that mimic lipid membranes, and *E.coli* cells, in the periplasm of which α-Syn can be expressed. These lipid systems have different curvatures, which may lead to varied sensitivity.

The schematic model of how Cu^{2+} ions modulate the communication between α-Syn and lipid membranes is summarized in **Fig.5**. Briefly, in the lipid systems used in this study including LCP, DOPG liposomes, and *E.coli* cells, α-Syn monomers exist in equilibrium with membrane-bound forms. In the absence of Cu^{2+} ions, lipid-induced secondary structure transition of α-Syn promotes the formation of oligomers directly on lipid membranes, leading to the destructive effects of α-Syn on lipid membranes. However, Cu^{2+} can interact with α-Syn monomers and promote oligomer formation in aqueous solution, thus, the decrease in free α-Syn monomers available for oligomer formation on lipid membranes can be expected, meanwhile, membrane-bound α-Syn may adopt an extended α-helical structure, as a result, the damage to lipid membranes by α-Syn is counteracted by Cu^{2+} ions, which means that Cu^{2+} ions can, to some extent,

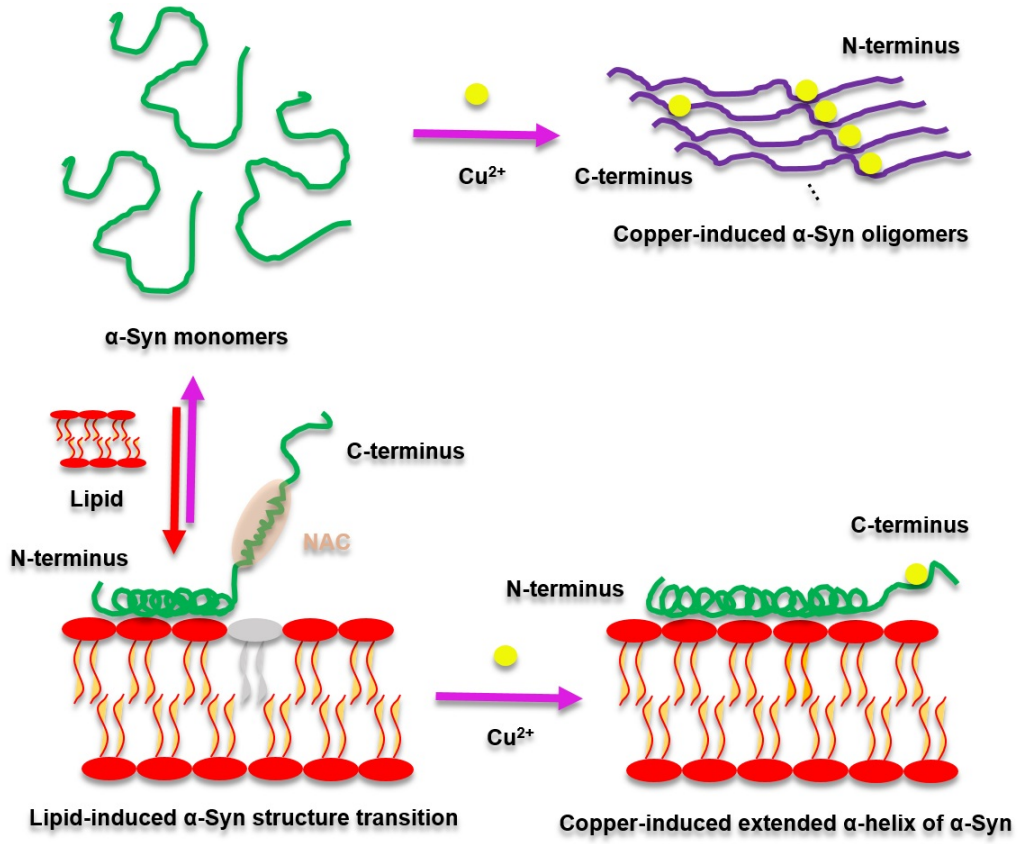

FIGURE 5: Illustration of how Cu^{2+} ions modulate the communication between α-Syn and lipid membrane. The presence of lipids induces the secondary structure transition of α-Syn from random coil to α-helix, leading to the oligomer formation directly on lipid membranes and subsequent damage to lipid membranes (shown as lipid in light grey). Meanwhile, free α-Syn monomers coexist with membrane-bound forms. Cu^{2+} interacts with α-Syn monomers more noticeably in N- terminus in buffer, leading to the oligomer formation in aqueous solution, followed by the inhibition of oligomer formation on lipid membranes and the reversion of the damage by α-Syn to lipid membranes. Besides, the membrane-bound form of α-Syn may adopt an extended α-helical structure and Cu^{2+} may interact with membrane-bound α-Syn within the C-terminus more pronouncedly compared with that in aqueous solution.

protects lipid membranes. α-Syn proteins can interfere with the structures and/or functions of membrane-containing organelles including mitochondria, by interacting with lipid membranes and components of these organelles, leading to the dysfunction or even death of cells (41). Considering the decreased levels of Cu^{2+} ions in the SNs of PD patients (24, 25), the protective role of Cu^{2+} in lipid membranes reported here provides further insight into our perception of the interplay between α-Syn, lipid membranes, and Cu^{2+} ions in the pathology of PD.

5.5 Experimental procedures

5.5.1 α-Syn expression and purification

Wild type α-Syn expression was conducted in phage-resistant *E.coli* BL21(DE3) cells grown on LB-Agar supplemented with 100 μg/mL Ampicillin. After overnight incubation at 37°C and 180 rpm, a single colony was transferred to a flask of 100 mL LB medium containing 100 μg/mL Ampicillin. After culturation in extended scale, IPTG (1.0 mM) was added into the cell culture when the OD600 reached 1.04. After incubation for 4 h at 37°C and 180 rpm, the pellets were harvested by spinning down the cell culture for 20 min at 5,000 rpm and 4°C. The purification was performed by referring to and modifying published methods (16, 46). Briefly, after Osmotic shock, the periplasm proteins were collected and dialyzed against buffer A (20 mM Tris-HCl, pH 8.0) overnight followed by Ion Exchange Chromatography (IEX) on a HiTrap Q-Sepharose Fast Flow column (GE Healthcare) and eluted with a 0-0.5 M NaCl gradient in buffer A. Fractions containing large amount of α-Syn were collected and α-Syn was precipitated by adding stepwise the saturated ammonium sulfate solution (4.3 M at room temperature) to 50% saturation (1:1). The precipitated α-Syn was dissolved in 3.5 ml of 20 mM Tris-HCl, pH 7.2 and subjected to size exclusion chromatography (SEC) on a GF Hiload Superdex 75 16/600 column (GE Healthcare), and eluted with 20 mM Tris-HCl, pH7.2. After the SDS-PAGE, fractions containing α-Syn were combined and stored at -80 °C.

5.5.2 Sample preparation

Lipid preparation 1-palmitoyl-2-oleoyl-sn-glycero-3-phospho-L-serine sodium salt (POPS, 783.99 g/mol) and monoolein (MO, 356,54 g/mol) were purchased from Sigma–Aldrich (St. Louis, MO, USA). POPS was dissolved in chloroform to a concentration of 100 mg/mL. Lipids used in sample preparation including MO, MO:POPS (99:1, 1% molar ratio), MO:POPS (95:5, 5% molar ratio), and MO:POPS (90:10, 10% molar ratio) were dried completely with nitrogen gas before usage.

Metal solution preparationn $CuCl_2$ and $ZnCl_2$ solutions were prepared by dissolving the $CuCl_2$ and $ZnCl_2$ powder into 20 mM Tris-HCl buffer, pH 7.2, to final concentrations of 25 μM and 125 μM, mixed completely and stored at 4°C.

Preparation of Small-Angle X-ray Synchrotron (SAXS) samples

The samples in this study include: 1) MO, MO+1% POPS, MO+5% POPS, and MO+10% POPS; 2) MO+5% POPS + 34 μM α-Syn; 3) MO+5% POPS + 34 μM α-Syn + Metal ions ($CuCl_2$ and $ZnCl_2$, 17 μM and 83 μM), mixed with 4 μL of control

buffer (20 mM Tris-HCl, pH 7.2). The lipidic cubic phases were prepared by referring to the published method (47). Briefly, molten (42°C for about 20 min) lipids including MO and MO+POPS were loaded into a pre-warmed 50 μL Hamilton gas-tight syringe with removable needle and Teflon ferrule (Hamilton, cat. no. 81030), and the buffers (20 mM Tris-HCl, pH 7.2, alone or α-Syn-laden) were loaded into another one, the two syringes were connected tightly with a coupler, and then the lipids : (protein-laden) buffers (3:2, volume ratio) were mixed with this coupled-syringe mixing device (48) gently until the mixture becomes transparent. The samples for diffraction were prepared by taking advantage of the in meso in situ serial crystallography (IMISX) (49). The prepared lipidic cubic phases were then dispersed manully into the wells of the plate at 20°C followed by the addition of 4 μL of 20 mM Tris-HCl buffer, pH 7.2, with or without metals. The wells were then sealed by overlaying the Mylar film stuck on the glass cover plate and rolling gently the double-sandwich plate with a brayer, this way, the plate was housed in the glass plate. The samples were prepared about 5 h before the diffraction and left at room temperature.

5.5.3 SAXS data collection

Immediately before the diffraction, the plate was separated from the glass bases, cut into sections (1*4 wells) and bonded onto the sample holder with the double-stick stape. Diffraction data collection was performed by referring to the published method (49) at room temperature (20°C) with 10*20 μm^2 X-ray beam size at 12.4 keV (1.0332 Å) on beamline PXII (X10SA, the Swiss Light Source, Villigen, Switzerland). The diffraction was carried out using a EIGER2 16 M detector with a sample-to-detector distance of 1200 mm and a sample-to-beamstop distance of 80 mm. Data corresponding to 2*50 grids were collected with a beam transmission of 100% and the exposure time of 0.2 s. In addition, as controls, the Mylar film alone and Mylar film+buffer were diffracted as well.

The control samples including MO and MO supplemented with Cu^{2+} ions were prepared with cyclic olefin copolymer (COC) film, aiming to check the influence of Cu^{2+} ions on the phase behavior of LCP. The data collection of control samples were performed at beamline PXI (X06SA, the Swiss Light Source, Villigen, Switzerland), and the results are shown in **Fig.S1**.

5.5.4 SAXS data analysis

The data were analyzed with the Albula software (DECTRIS, Switzerland) and then exported and saved as an Excel file, obtaining the intensity (I) vs scattering angle (2θ),

with around 15 repeats for each sample. The obtained intensities of each sample were averaged and the averaged background value was subtracted from each averaged intensity. The scattering angles were converted into radians. The d spaces and resolutions (q) of each sample were then calculated by using the Bragg's law

2dsinθ=nλ

where d = interplanar distance, θ= scattering angle, n = positive integer, λ = wavelength of the incident wave. The intensity vs scattering angle were plotted with the Origin software (Version 2018, OriginLab, USA).

5.5.5 Liposome preparation

10 mg/mL DOPG (1,2-Dioleoyl-sn-glycero-3-phospho-rac-(1-glycerol)) was dried with Argon gas, followed by vacuum drying overnight. The dried DOPG was sonicated and then dissolved in 25 mM potassium phosphate buffer, pH 7.4, obtaining the DOPG liposome at a concentration of 10 mg/mL.

5.5.6 Circular dichroism (CD) spectroscopy

In CD spectroscopy, the samples were prepared by titrating DOPG liposomes into 5 μM α-Syn with or without 300 μM metal ions in 25 mM potassium phosphate buffer, pH 7.4. The CD spectra were recorded in the far-UV region from 190 to 260 nm with a Chirascan plus CD spectrometer (Applied Photophysics Limited, U.K.). The samples were measured in a quartz cuvette with a pathlength of 10 mm at 37°C immediately after stirred manually with a pipette, using a step size of 1.0 nm, a bandwidth of 1.0 nm, and a time per point of 0.5 s. The spectra were recorded immediately after the preparation of 5 μM α-Syn solution, the addition of metal ions, and the titration of DOPG liposomes (final concentrations of 0, 5, 10, 20, 40, 60, 80, 100, 120, 140, 160, 180, 200, and 220 μM). The curves were smoothed with a window of 10 and replotted with the Origin (Version 2018, OriginLab, USA).

5.5.7 In-cell nuclear magnetic resonance (NMR)

In-cell NMR measurements of α-Syn proteins were prepared as described previously (50). A single colony (*E. coli* (BL21 (DE3) pLysS cells) with the α-Syn plasmid was cultured overnight in 15 ml LB medium. The overnight supernatant was discarded after the centrifugation at 3000 rpm for 15 min and the cell pellet was resuspended and grown in 250 ml M9 minimal medium (51) containing 100 μg/ml of $^{15}NH_4Cl$ (Sigma)

in a shaker at 180 rpm, 37°C. Until OD600 reaches 0.8, cell cultures were induced with 1 mM isopropyl β-d-thiogalactopyranoside for 4 h and then centrifuged for 20 min at 4°C, 3000 rpm. The pellet was resuspended by 1.5 ml supernatant for the in-cell NMR measurement. A sample of the resuspended cells: $^{2}H_2O$ at 90:10 (v/v ratio) was prepared to acquire the in-cell spectrum. The concentration of ^{15}N-labelled α-Syn was estimated by comparison to a known ^{15}N-labelled α-Syn concentration by comparing the amide signal intensities in ^{1}H-^{15}N-HSQC spectra. ^{1}H-^{15}N-HSQC spectra were recorded on a 700 MHz NMR spectrometer (Bruker AVIII 700) equipped with a cryogenic probe ^{1}H/^{13}C/^{15}N TCI cryoprobe (AV700). The spectra were recorded at 6°C. The assignment used for the ^{1}H-^{15}N-HSQC spectra has been published previously by other groups (52). Conformational properties of α-Syn in its free and lipid-associated states. The software Topspin v.4.0.7 was used to analyse the data.

5.6 References

1. M. Kiechle, V. Grozdanov, K. M. Danzer, The Role of Lipids in the Initiation of alpha-Synuclein Misfolding. Front Cell Dev Biol 8, 562241 (2020).
2. G. Fusco et al., Direct observation of the three regions in alpha-synuclein that determine its membrane-bound behaviour. Nature communications 5, 3827 (2014).
3. C. Masaracchia et al., Membrane binding, internalization, and sorting of alpha-synuclein in the cell. Acta Neuropathol Commun 6, 79 (2018).
4. J. Varkey et al., Membrane curvature induction and tubulation are common features of synucleins and apolipoproteins. The Journal of biological chemistry 285, 32486-32493 (2010).
5. M. M. Ouberai et al., alpha-Synuclein senses lipid packing defects and induces lateral expansion of lipids leading to membrane remodeling. The Journal of biological chemistry 288, 20883-20895 (2013).
6. M. Pantusa et al., Alpha-synuclein and familial variants affect the chain order and the thermotropic phase behavior of anionic lipid vesicles. Biochim Biophys Acta 1864, 1206-1214 (2016).
7. C. Galvagnion, The Role of Lipids Interacting with alpha-Synuclein in the Pathogenesis of Parkinson's Disease. Journal of Parkinson's disease 7, 433-450 (2017).
8. C. Galvagnion et al., Lipid vesicles trigger alpha-synuclein aggregation by stimulating primary nucleation. Nature chemical biology 11, 229-234 (2015).
9. E. Carboni, P. Lingor, Insights on the interaction of alpha-synuclein and metals in the pathophysiology of Parkinson's disease. Metallomics 7, 395-404 (2015).
10. G. Gromadzka, B. Tarnacka, A. Flaga, A. Adamczyk, Copper Dyshomeostasis in Neurodegenerative Diseases-Therapeutic Implications. Int J Mol Sci 21, (2020).
11. A. I. Bush, Metals and neuroscience. Current opinion in chemical biology 4, 184-191 (2000).
12. E. M. Landau, J. P. Rosenbusch, Lipidic cubic phases: a novel concept for the crystallization of membrane proteins. Proc Natl Acad Sci U S A 93, 14532-14535 (1996).
13. H. Qiu, M. Caffrey, The phase diagram of the monoolein/water system: metastability and equilibrium aspects. Biomaterials 21, 223-234 (2000).
14. E. R. Middleton, E. Rhoades, Effects of curvature and composition on alpha-synuclein binding to lipid vesicles. Biophys J 99, 2279-2288 (2010).
15. I. M. Pranke et al., alpha-Synuclein and ALPS motifs are membrane curvature sensors whose contrasting chemistry mediates selective vesicle binding. J Cell Biol 194, 89-103 (2011).
16. C. Huang, G. Ren, H. Zhou, C. C. Wang, A new method for purification of recombinant human alpha-synuclein in Escherichia coli. Protein Expr Purif 42, 173-177 (2005).
17. K. J. Ahn, S. R. Paik, K. C. Chung, J. Kim, Amino acid sequence motifs and

mechanistic features of the membrane translocation of alpha-synuclein. J Neurochem 97, 265-279 (2006).
18. R. M. Rasia et al., Structural characterization of copper(II) binding to alpha-synuclein: Insights into the bioinorganic chemistry of Parkinson's disease. Proc Natl Acad Sci U S A 102, 4294-4299 (2005).
19. A. A. Valiente-Gabioud et al., Structural basis behind the interaction of Zn^{2+} with the protein alpha-synuclein and the Abeta peptide: a comparative analysis. J Inorg Biochem 117, 334-341 (2012).
20. I. Hozumi et al., Patterns of levels of biological metals in CSF differ among neurodegenerative diseases. J Neurol Sci 303, 95-99 (2011).
21. S. Ayton, D. I. Finkelstein, R. A. Cherny, A. I. Bush, P. A. Adlard, in Encyclopedia of Metalloproteins, R. H. Kretsinger, V. N. Uversky, E. A. Permyakov, Eds. (Springer New York, New York, NY, 2013), pp. 2433-2441.
22. R. Squitti et al., Meta-analysis of serum non-ceruloplasmin copper in Alzheimer's disease. J Alzheimers Dis 38, 809-822 (2014).
23. E. Y. Ilyechova et al., A low blood copper concentration is a co-morbidity burden factor in Parkinson's disease development. Neurosci Res 135, 54-62 (2018).
24. D. T. Dexter et al., Increased nigral iron content and alterations in other metal ions occurring in brain in Parkinson's disease. J Neurochem 52, 1830-1836 (1989).
25. K. M. Davies et al., Copper pathology in vulnerable brain regions in Parkinson's disease. Neurobiol Aging 35, 858-866 (2014).
26. S. Genoud et al., Subcellular compartmentalisation of copper, iron, manganese, and zinc in the Parkinson's disease brain. Metallomics 9, 1447-1455 (2017).
27. M. Scholefield et al., Widespread Decreases in Cerebral Copper Are Common to Parkinson's Disease Dementia and Alzheimer's Disease Dementia. Front Aging Neurosci 13, 641222 (2021).
28. P. A. Adlard, A. I. Bush, Metals and Alzheimer's disease. J Alzheimers Dis 10, 145-163 (2006).
29. M. A. Lovell, J. D. Robertson, W. J. Teesdale, J. L. Campbell, W. R. Markesbery, Copper, iron and zinc in Alzheimer's disease senile plaques. J Neurol Sci 158, 47-52 (1998).
30. M. Caffrey, A comprehensive review of the lipid cubic phase or in meso method for crystallizing membrane and soluble proteins and complexes. Acta Crystallogr F Struct Biol Commun 71, 3-18 (2015).
31. V. Cherezov, J. Clogston, Y. Misquitta, W. Abdel-Gawad, M. Caffrey, Membrane protein crystallization in meso: lipid type-tailoring of the cubic phase. Biophys J 83, 3393-3407 (2002).
32. H. Y. Kim, B. X. Huang, A. A. Spector, Phosphatidylserine in the brain: metabolism and function. Prog Lipid Res 56, 1-18 (2014).

33. S. Takamori et al., Molecular anatomy of a trafficking organelle. Cell 127, 831-846 (2006).
34. H. Xicoy, B. Wieringa, G. J. M. Martens, The Role of Lipids in Parkinson's Disease. Cells 8, (2019).
35. M. Stockl, P. Fischer, E. Wanker, A. Herrmann, Alpha-synuclein selectively binds to anionic phospholipids embedded in liquid-disordered domains. J Mol Biol 375, 1394-1404 (2008).
36. C. G. Dudzik, E. D. Walter, B. S. Abrams, M. S. Jurica, G. L. Millhauser, Coordination of copper to the membrane-bound form of alpha-synuclein. Biochemistry 52, 53-60 (2013).
37. D. Valensin, S. Dell'Acqua, H. Kozlowski, L. Casella, Coordination and redox properties of copper interaction with alpha-synuclein. J Inorg Biochem 163, 292-300 (2016).
38. M. M. Dedmon, K. Lindorff-Larsen, J. Christodoulou, M. Vendruscolo, C. M. Dobson, Mapping long-range interactions in alpha-synuclein using spin-label NMR and ensemble molecular dynamics simulations. J Am Chem Soc 127, 476-477 (2005).
39. C. A. Waudby et al., In-cell NMR characterization of the secondary structure populations of a disordered conformation of alpha-synuclein within E. coli cells. PLoS One 8, e72286 (2013).
40. Y. Li et al., Amyloid fibril structure of alpha-synuclein determined by cryo-electron microscopy. Cell Res 28, 897-903 (2018).
41. L. D. Bernal-Conde et al., Alpha-Synuclein Physiology and Pathology: A Perspective on Cellular Structures and Organelles. Front Neurosci 13, 1399 (2019).
42. H. J. Lee, C. Choi, S. J. Lee, Membrane-bound alpha-synuclein has a high aggregation propensity and the ability to seed the aggregation of the cytosolic form. J Biol Chem 277, 671-678 (2002).
43. V. N. Uversky, D. Eliezer, Biophysics of Parkinson's disease: structure and aggregation of alpha-synuclein. Curr Protein Pept Sci 10, 483-499 (2009).
44. T. L. Lau et al., Amyloid-beta peptide disruption of lipid membranes and the effect of metal ions. J Mol Biol 356, 759-770 (2006).
45. Y. H. Sung, C. Rospigliosi, D. Eliezer, NMR mapping of copper binding sites in alpha-synuclein. Biochim Biophys Acta 1764, 5-12 (2006).
46. M. M. Wordehoff, W. Hoyer, alpha-Synuclein Aggregation Monitored by Thioflavin T Fluorescence Assay. Bio Protoc 8, (2018).
47. P. Ma et al., The cubicon method for concentrating membrane proteins in the cubic mesophase. Nature protocols 12, 1745-1762 (2017).
48. A. Cheng, B. Hummel, H. Qiu, M. Caffrey, A simple mechanical mixer for small viscous lipid-containing samples. Chemistry and Physics of Lipids 95, 11-21 (1998).
49. C. Y. Huang et al., In meso in situ serial X-ray crystallography of soluble and membrane proteins at cryogenic temperatures. Acta Crystallogr D Struct Biol 72, 93-112

(2016).

50. B. C. McNulty, G. B. Young, G. J. Pielak, Macromolecular crowding in the Escherichia coli periplasm maintains alpha-synuclein disorder. J Mol Biol 355, 893-897 (2006).

51. Z. Serber, R. Ledwidge, S. M. Miller, V. Dotsch, Evaluation of parameters critical to observing proteins inside living Escherichia coli by in-cell NMR spectroscopy. J Am Chem Soc 123, 8895-8901 (2001).

52. D. Eliezer, E. Kutluay, R. Bussell, Jr., G. Browne, Conformational properties of alpha-synuclein in its free and lipid-associated states. J Mol Biol 307, 1061-1073 (2001).

5.7 Supporting information

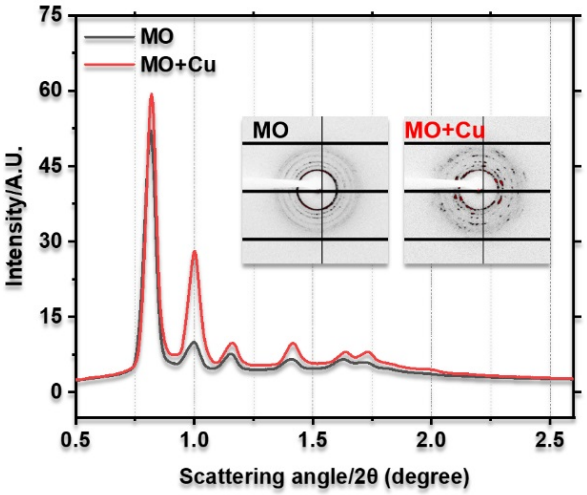

FIGURE S1: Effect of copper on the mesoscopic structure of LCP. SAXS experiments performed with MO alone and MO supplemented with Cu^{2+} ions indicate that the addition of copper does not change the phase behavior of LCP.

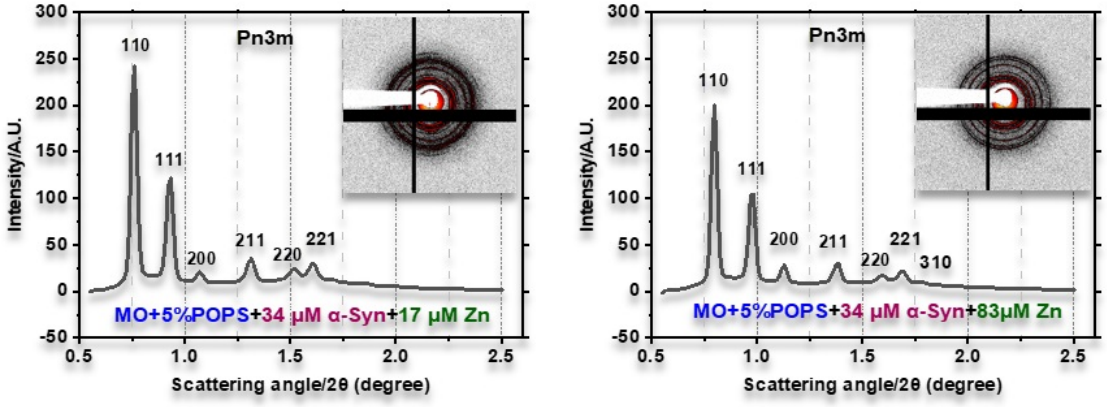

FIGURE S2: Zn^{2+} ions counteract the effect of α-Syn on the mesoscopic structure of LCP. SAXS experiments conducted with MO alone and MO supplemented with POPS at molar ratios of 5% show that POPS does not change the phase behavior of MO, which is Pn3m phase (Fig.2A-C). The addition of 34 μM α-Syn destroys the microscopic structure of LCP made of MO supplemented with 5% POPS (Fig.2E), while Zn^{2+} ions at used concentrtions counteract the effect of α-Syn on the phase behavior of LCP and recover the phase to Pn3m.

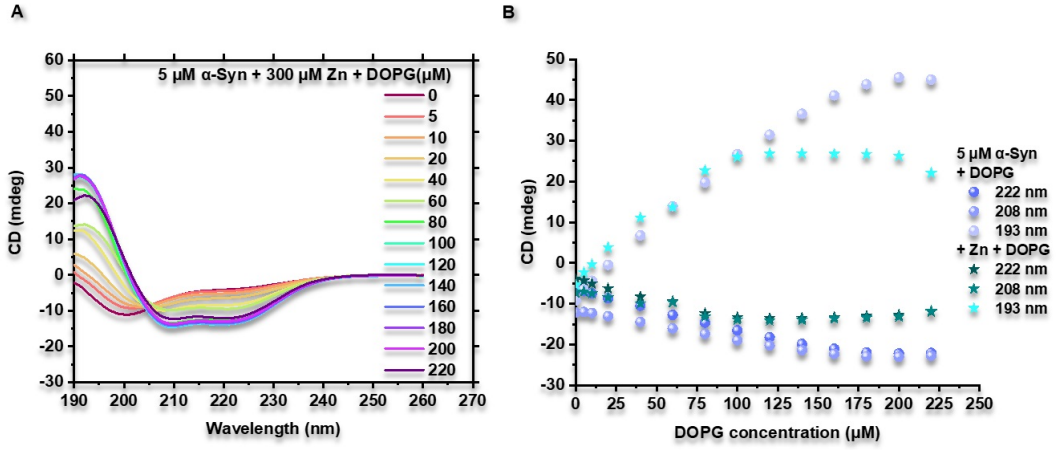

FIGURE S3: Zn^{2+} ions modulate the effect of DOPG liposomes on the secondary structure of α-Syn. (A) CD experiments conducted by titrating DOPG liposomes (at concentrations of 0, 5, 10, 20, 40, 60, 80, 100, 120, 140,160, 180, 200, 220 μM) into 5 μM α-Syn in the presence 300 μM Zn^{2+} ions. The measurements were performed immediately after the addition of liposomes and Zn^{2+} ions. The results indicate that lipid membrances induce the secondary struture transition of α-Syn from random coils to α-helices. (B) The change of CD signal intensities of 5 μM α-Syn in the presence of 300 μM Zn^{2+} ions with or without DOPG at 193 nm, 208 nm, and 222 nm, which are typical for α-helical structures.

Chapter 6

Conclusion

Amyloid protein aggregation is associated with neurodegenerative diseases, and considerably modulated by a variety of brain constitutes including proteins, pH, ionic strength (salt), metal ions, and lipids. This thesis aimed to clarify how these constitutes interact with amyloidosis-related proteins including Aβ, tau, α-Syn, prion, IAPP, SOD1, TDP-43 and others. To this end, the intercommunication between ApoE and various amyloid proteins was systematically reviewed and experiments on how Hsp90, ATP, pH, ionic strength (salt), and Zn^{2+} affect the aggregation of Aβ40 peptide and how copper ions interact with α-Syn and different lipid membrane models were conducted.

Based on my work, I propose the following conclusions. Firstly, ApoE cannot only influence the aggregation, but also the production, clearance, transcription, metabolism, and degradation of different amyloid proteins, focused mostly on Aβ, meanwhile, ApoE can also be influenced by amyloid proteins. Lipid membranes and phase-separated droplets could be the potential sites of the cross-interaction between ApoE and various amyloid proteins. Secondly, Hsp90 protein inhibits the fibrillation of Aβ40 peptide, while ATP impedes this effect of Hsp90, in which hydrophobic interactions among Aβ40 peptide and between Hsp90 and Aβ40 peptide, as well as the conformation dynamics of Hsp90 play crucial roles. Thirdly, the covariant effect of pH, ionic strength, and Zn^{2+} show that decreasing pH values from 8.0 to 6.5 can both promote and inhibit the aggregation of Aβ40 peptide, depending on the presence of Zn^{2+} ions. Besides, the increase in the concentrations of NaCl from 0 M to 0.1 M can enhance or impede the aggregation of Aβ40 peptide, depending on the pH values and the presence of Zn^{2+} ions. The effects of Zn^{2+} ions on the aggregation of Aβ40 peptide varies as the pH values change from 6.5 to 8.0, and this change can be influenced by the concentration of NaCl. Last but not least, Cu^{2+} ions counteract the damaging effect of α-Syn on the phase behavior of

LCP, probably by interacting with α-Syn within it N- and C-terminal domains, decreasing the oligomerization of α-Syn directly on the lipid membranes. In summary, these results indicate that the aggregation of amyloid proteins can be modulated by various micro-environmental factors, but not one specific factor.

In this thesis work, the results were obtained by performing ThT and ANS fluorescence assays, global fitting and sigmodial fitting, CD spectroscopy, AFM imaging in air and liquid, PICUP, LC-MS, FP, TEM, SAXS, and in-cell NMR experiments, preceded by the expression and purification of α-Syn and Hsp90 proteins and the preparation of ThT buffer with 96 different conditions with a robot named Formulator, which is designed for protein crystallization. These methods successfully enabled us to answer the questions raised in the beginning of the thesis, like how Hsp90, ATP, pH, ionic strength, and Zn^{2+} ions influence the aggregation of Aβ40 peptide, and how Cu^{2+} ions interplay with α-Syn and lipid membranes, even though limitations exist with specific methods. For example in Chapter 2, while the saturation of FP experiment was not achieved, this approach convinced us that the affinity between Aβ40 peptide and Hsp90 protein is pretty low, indicating that the interaction between them might be very weak or dynamic. Another limitation occurred in LC-MS experiments, in which the exact molecular weight of the samples has not been successfully figured out, due to the heterogeneity of samples, however, we can still confirm from these experiments the formation of complexes from Hsp90 protein and Aβ40 peptide.

In conclusion, the thesis systematically reviewed the cross-interactions of ApoE with various amyloid proteins, instead of a specific amyloid protein, the case in previous related reviews; explored the covariant effects of Hsp90/ATP and pH/ionic strength/Zn^{2+} ions on the aggregation of Aβ40 peptide, as well as the role of Cu^{2+} ions in modulating the interaction between α-Syn and lipid membranes. These results indicate that the aggregation of amyloid proteins is influenced by various micro-environmental factors, but not a single specific one. It is therefore of great importance to take other factors into consideration when design and perform experiments, as well as when interpret the obtained data in this field. This will most certainly enhance our understanding of the pathology of protein misfolding diseases under conditions closer to the physiological ones.

Appendix A

Acknowledgements

With the joy and pains comes the end of my three-year doctoral study, during which I grew professionally, and perhaps more importantly, it becomes clearer to me regarding the priorities of my life. That is why I value this experience a lot and would like to express my gratitude to my committee members and many others.

Firstly, I thank my supervisor, Dr.Jinghui Luo. He made it possible for me to perform studies at PSI by providing me with a PhD position and gathering funds. He tried his best to get me accustomed to the local circumstances regarding both research and life. Most importantly, I appreciate his patience in guiding me and supporting me through some hard days in the past three years. I also thank my thesis professor, Jan Peter Abrahams, who made me feel motivated and confident and provided me with constructive comments on each important presentation. My thanks also come to two other members of my committee, Prof. Roderick Lim and Prof. Raffaele Mezzenga, for their supervision through my doctoral study.

Excellent colleagues and collaborators, name only some of them, Jinming Wu, Rebecca Sternke-Hoffmann, Rolf Loch, Pik Yee Ma, Chia-Ying Huang, Andrea Prota, Natacha Olieric, Mara Wieser, Daniel Frey, Cecilia Wallin, Thorsten Hugel, Max Lallemang, Bianca Hermann, Bizan N. Balzer, Axel Abelein, and Huixin Xu, really deserve my gratitude for the valuable discussion, collaboration, and help regarding the thesis work, otherwise, the thesis cannot be accomplished. I also appreciate it that they made my life here colorful and meaningful.

Finally, I thank my families and friends, it is their deep love and understanding that encourage me to go on, no matter what happened.

Many thanks to all of many others, but not mentioned here, thank you for giving me a hand now and then, which warmed me and will warm me forever.